The study of polymers, minerals and their interactions by inverse gas chromatography

Ansari, Deeba M.

Award date:
2000

Awarding institution:
University of Bath

THE STUDY OF POLYMERS, MINERALS AND THEIR INTERACTIONS BY INVERSE GAS CHROMATOGRAPHY

Submitted by Deeba M. Ansari
for the degree of PhD of the University of Bath

2000

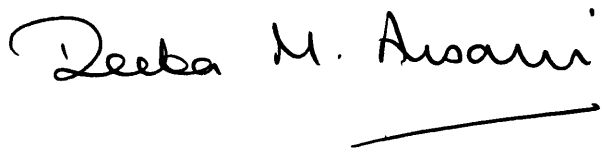

ProQuest LLC
789 East Eisenhower Parkway
P.O. Box 1346
Ann Arbor, MI 48106-1346

SUMMARY

The aim of this study was to use inverse gas chromatography (IGC) to characterise the surface thermodynamic properties of some industrially significant polymers and additives. A commercial GC system was modified to allow accurate recording of the necessary data and this was validated using a polystyrene stationary phase by measuring free energies of adsorption and phase transitions. Results were in good agreement with literature values.

Three polymer-filler composites systems were identified for detailed analyses. The first was a polypropylene /calcium carbonate system. A precipitated calcium carbonate (PCC) was prepared and treated with sodium polyacrylate and stearic acid. Specific and non-specific enthalpies of adsorption for a range of probes were measured, as well as the dispersive component of the surface free energy. These properties varied significantly with surface treatment. The PCCs were then incorporated into polypropylene mouldings and their physical properties measured. The IGC data were used to explain strength differences of the composites. This extended the scope of all previous IGC studies of calcium carbonates.

The second system, used to study the effect of surface chemistry on polymer stability, was based on heat-treated (calcined) kaolinite in polyethylene. Calcination of kaolinite was found to reduce the enthalpy of adsorption and the dispersive component of surface free energy. Polyethylene films containing two calcined clays were then produced and their photodegradation studied. In the first recorded use of IGC for this application, differences in film stability were related to high-energy sites on the surface of the clays.

The calcined clays were then modified with an aminosilane and incorporated into polyamide composites. The polyamide was also studied, and found to interact strongly with alcoholic probes. The physical properties of the composites were measured, and compared with those for unmodified calcined clay. In this previously unpublished use of IGC, improved impact strength was shown to be related to improved wetting and stability of the modified filler by the polymer.

INDEX

ACKNOWLEDGEMENTS

I gratefully acknowledge the help, patience and guidance of Dr. G.J. Price of the University of Bath. I would like to thank Dr. D.A. Taylor, Dr. M. Hancock and Mr. C.D. Paynter of IMERYS Minerals Ltd. for their scientific contributions, and Ms. J. Manclus for her administrative support.

I also thank IMERYS Minerals Ltd. for financially supporting this research.

1 INTRODUCTION

1.1 Justification for the work

Minerals are often used in conjunction with polymers for the production of materials for common household or automotive applications. Classically, the mineral component was considered a simple filler, giving cost reduction, but little else. With the ability to tailor-make composites, the emphasis has changed, with the mineral component providing additional benefits in terms of processing and end properties[1]. To achieve such benefits, the surface properties of each component must be selected or modified to ensure bonding or compatibility between them. In particular, the surface energetics of the mineral and polymer require characterisation to predict their interactions.

Surface interactions depend on the thermodynamic nature of the components. They can be quantified by calorimetric methods or adsorption studies. Conventional methods are often laborious and inaccurate. Contact angle measurements between non-wetting liquids and the substrate are often used, but have many disadvantages[2]. Interpretation is given in terms of critical surface tension or the surface free energy. Fine particulate samples are prepared by powder pressing or thin layer coating onto glass plates. Preparation can cause heterogeneity and hysteresis of the solvent front, and results are often inaccurate and irreproducible. The problem is exacerbated by the small mean size and surface curvature of particles studied. Inverse gas chromatography (IGC), in contrast, is a robust and well-known method for the study of surface characteristics[3]. IGC was therefore chosen for the thermodynamic study of polymers, minerals and their interactions.

The aim of the study was to apply IGC to a number of filled polymer systems and relate the surface chemistry to their physical and material properties. The objective was to set up and validate an IGC instrument for published and novel systems. This included modification of a standard GC instrument, and validation with a known polymer. The technique was used to analyse each component of a composite. The study was then extended to look at the matrix, across a broad temperature range.

Surface properties were characterised in terms of both bulk and specific components. This allowed surface modifications, both chemical and environmental, to be monitored. The composites were tested for key properties, such as mechanical strength, or weather resistance, and the results were related to thermodynamic differences. From these, the effects of surface properties on the composite could be predicted, and used to design products with improved performance.

The thesis contains an introduction to the two types of industrial polymers under consideration, namely thermoplastics and thermosets (section 1.2). Additives, fillers and reinforcing agents used in these polymers are then discussed. Composites of the two systems are detailed by application and their physical properties are listed. In section 1.3 some methods available for surface characterisation are given, and their uses for studying composites are considered. IGC theory is detailed in section 1.4, with calculations given for key thermodynamic data.

Literature, published up to April 2000, is reviewed in section 1.5. This begins with a critique of other summaries and reviews and is then subdivided by application. After listing the aims and objectives of the study in section 1.6, sections 2 to 7 give full experimental details. Potential further work is suggested in section 8 and a summary of conclusions is provided in section 9.

1.2 **Polymers, fillers and composites**

1.2.0 *Introduction*

Polymer composites are defined as "multiphase materials of two or more components in which the polymer forms the continuous phase". Typically, additive concentrations of greater than five percent are necessary to influence mechanical properties significantly. Composites can be categorised broadly into two groups: those comprising continuous fibres that are laminated with the polymer; and those made up of discontinuous fillers, either particulate or fibrous. Geometrical arrangements are illustrated in Figure 1.1.

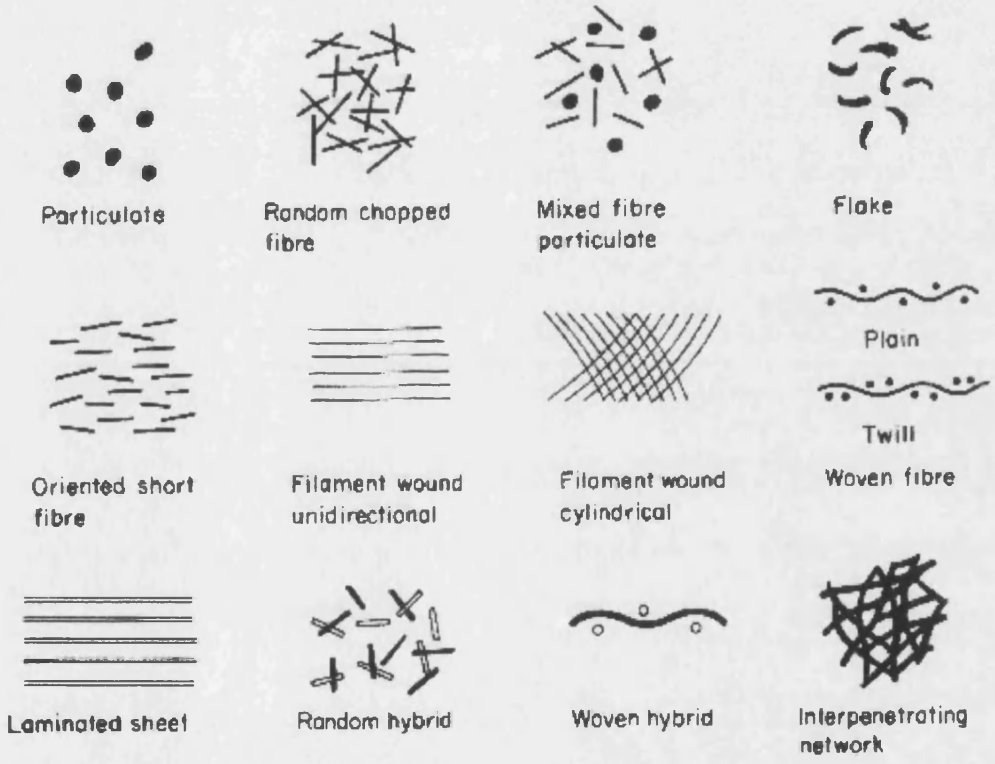

Figure 1.1 Types of composites, showing different geometrical arrangements[4].

Simple laminates are made from alternating layers of resin and sheet filler. Each layer is usually anisotropic, and this is exploited in construction to give the required mechanical properties. Layers may also have different porosities. For example, a continuous sheet may have little resin penetration, whereas woven fibres may be loosely or tightly woven to accept lesser or greater resin volumes.

Particulate fillers are divided into three basic classes, namely spherical, cubic and platey. Discontinuous fibres are usually described in terms of fibre length, length distribution and orientation.

Discontinuous fibres are described by their specific dimensions. Particulate fillers will also have specific size distributions. So, for example, glass beads will be monodistributed, whereas a mineral filler will have a particle size range depending on its processing history. Particle size will affect composite properties either by altering rheology during fabrication or by changing the interfacial contact between the resin and the filler. Knowledge of size distribution is important when considering high filler concentrations. In these systems, the distribution influences the maximum packing fraction[5]. For equal-sized spheres, the theoretical maximum packing fraction is 0.63. Smaller spheres can occupy the interstitial space, with even smaller ones fitting in between these, and so on. By tailoring size distribution, packing fractions of up to 0.95 can be achieved. Packing is important not only in terms of flow during fabrication but also because of subsequent interfacial effects. Depending on the surface forces between filler particles and the distances between them during processing, aggregation may occur. Thus knowledge of interaction forces is essential when determining volume additions and their effect on final properties.

The shape, size and packing of the filler therefore influence polymer composites either as continuous fibres, as short fibres or particles. In addition to more intrinsic parameters a further, profoundly influential property is that of the polymer-filler interface.

Interfaces may be formed between two distinct, immiscible phases in equilibrium. They may also occur between two essentially miscible components that have not yet reached equilibrium. Kinetic influences should not, of course, be overlooked. Processing conditions, such as shear energy and cooling rates will influence dispersion and crystallinity. The work described in this thesis was, however, restricted to analyses under equilibrium conditions.

Composite behaviour reflects interactions between the various phases. If no binding occurs between them, then, under low strain rates, the matrix alone contributes to the flexural and tensile strength of the whole. At higher strain rates, a rigid and/or isotropic filler can exert some influence on this behaviour. The region between the polymer and filler (the interphase) affects these properties[6]. For a particular application, therefore, the interface may be tailored by altering the surface of one or both components.

The interface may be described in terms of wetting or adhesion and polymer adsorption. The theoretical concept of surface tension is described in section 1.3.5 and will not be detailed further here. In terms of filler-polymer composites the polymer is considered as the liquid component and the filler as the solid. To attain low stress between them, the surface tensions of each component should be similar. In order for this to hold true, there must be intimate surface contact. Within all systems there will be surface irregularities such as flaws, undulations and microcracks. The ability to fill these will depend on a number of parameters, as described in Poiseuille's equation for capillary flow[7].

Surface modification of the filler is often used to alter the interface. By changing the filler surface tension, the matrix may wet out more readily. This is often termed "compatibilising". If a chemical bond is desired between the two phases, then a coupling agent is used. Of these, the most widely used are silanes. Silanes may be added to a variety of polymer-filler composites to give significant improvements in mechanical properties. Specific uses include applications with glass fibres, glass beads, mica and calcined clays.

Perhaps the most commonly used method for ensuring good adhesion and filler dispersion within a composite is the careful choice of compatible components. To ensure compatibility, a thorough knowledge of the intrinsic thermodynamics of each component is necessary.

1.2.1 *Synthetic Polymers*

Polymers can be divided into two distinct groups – thermosets and thermoplastics. Thermosets, as the name implies, will set or cure irreversibly on heating by chemical cross-linkage. Thermoplastics will melt on heating and set when cooled. The process is reversible. Historically the thermosets preceded the thermoplastics in terms of large-scale industrial production. This situation has now reversed, with thermoplastic polymer production now six times greater than that of thermosets.

Thermosets

The phenolics comprise the most important class of thermosets. They are condensation products of phenols and aldehydes. Low molecular weight reaction products are first produced. These are then compounded with fillers or laminated sheets before final cure. If an amine or amide replaces the phenol then aminoplasts are formed. Of these, the two most important are urea formaldehyde and melamine formaldehyde resins (Figures 1.2 to 1.4).

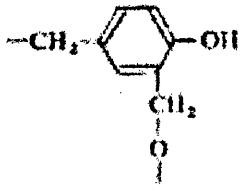

Figure 1.2 Phenolic resin.

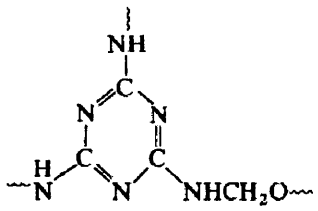

Figure 1.3 Melamine formaldehyde resin.

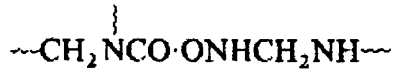

Figure 1.4 Urea formaldehyde resin.

Probably the most versatile class of thermosets is that of the unsaturated polyesters. They are prepared by heating a diol with a mixture of di-acids and curing with a peroxide initiator. One example is given in Figure 1.5.

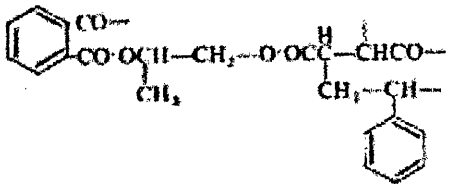

Figure 1.5 Styrenated polyester resin.

Epoxy resins are based upon bisphenol A and epichlorohydrin, as in Figure 1.6. Cure is most often initiated with aliphatic amines and organic acids and anhydrides.

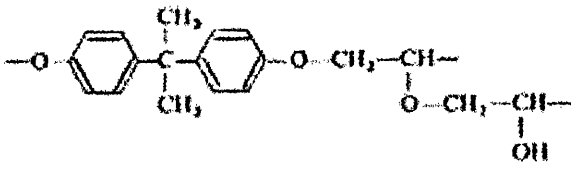

Figure 1.6 Epoxide resin.

The polyurethanes (PU) are another, versatile class of thermoset resins (although some are thermoplastics). PUs (Figure 1.7) are formed by reacting a di-isocyanate with a diol. Due to the wide availability of a range of precursors and their susceptibility to secondary reactions, they can be tailored to provide a wide range of properties.

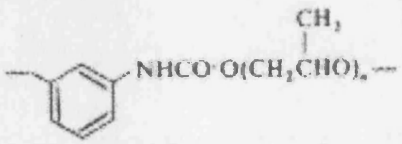

Figure 1.7 A polyurethane.

Other cross-linked elastomeric polymers include natural and synthetic rubbers.

Thermoplastics

Thermoplastic production in 1990 totalled over 90 million tonnes[8]. This is predicted to more than double to 195 million tonnes by 2001. Of these, five classes account for the bulk of this consumption (Figure 1.8). In addition, a number of niche engineering thermoplastics are of commercial significance.

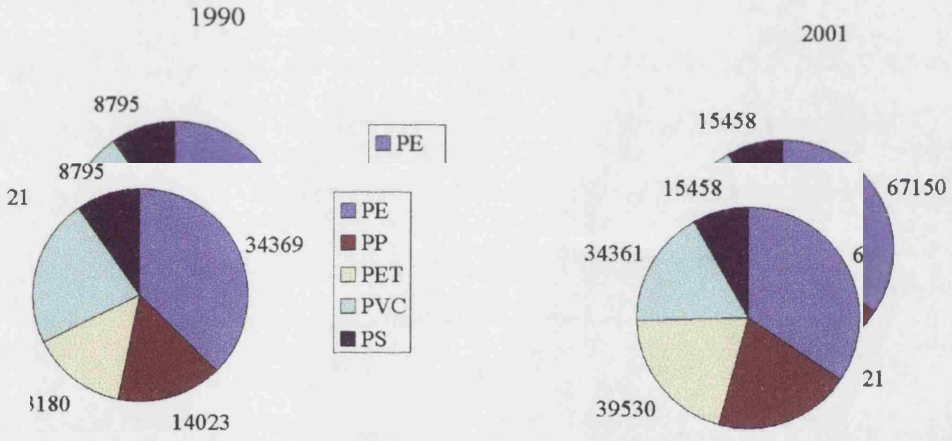

Figure 1.8 Worldwide thermoplastic capacities in kT, 1990 and 2001[8].

Polyethylenes (PEs) are supplied in the greatest tonnage worldwide, due to their low production costs and versatility. They are distinguished from each other by density, reflecting the degree of chain branching, crystallinity and (indirectly) their method of synthesis. High density (and some low density) PEs (Figure 1.9) are prepared using Ziegler-Natta catalysts. Low-pressure and high-pressure gas phase processes are also common. Of increasing importance is the use of metallocene catalysts for linear and low molecular weight distribution polymers.

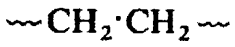

Figure 1.9 Polyethylene.

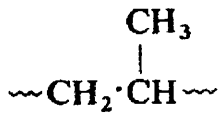

Figure 1.10 Polypropylene.

The second largest volume polyolefin is polypropylene (PP) (Figure 1.10). This is made by catalysis of propylene monomers using Ziegler-Natta catalysts. Copolymers can also be produced by polymerisation of two or more different monomers.

Another important addition polymer is polyvinyl chloride (PVC) (Figure 1.11). PVC is prepared by free radical polymerisation mainly through emulsions and suspensions. The vinyl acetate copolymers (Figure 1.12) are also made by these routes.

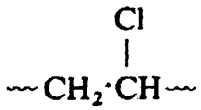

Figure 1.11 PVC.

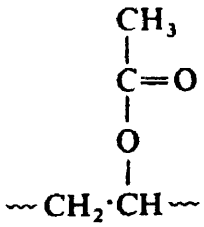

Figure 1.12 Polyvinyl acetate.

Acrylics, of which polymethyl methacrylate (PMMA) is the most important, cover a wide range of applications (Figure 1.13). MMA is polymerised by free radical methods.

Polystyrene (Figure 1.14) was one of the earliest commercial addition polymers. It is polymerised by a free radical process from styrene using one of four major processes of bulk, solution, emulsion and suspension polymerisation. An important variant of rigid polystyrene is foamed polystyrene in which suspension polymer beads are mixed with a blowing agent and heat initiated.

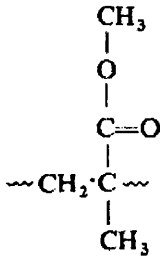

Figure 1.13 PMMA.

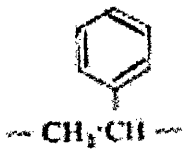

Figure 1.14 Polystyrene.

The aforementioned thermoplastics are all produced by continuous addition processes. The bulk or step-growth class of polymers includes many important engineering thermoplastics. The most widely known examples are the nylons or polyamides. These can be prepared by the condensation of a diamine with a diacid or by ring opening of cyclic lactams. Commercial examples include nylon 6 (Figure 1.15), nylons 6,6; 6,10; 7, 9, 11 and 12. They tend to be crystalline and are often used in fibre formation.

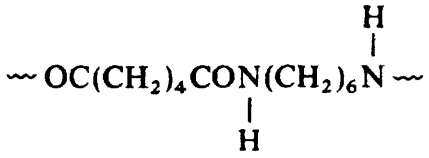

Figure 1.15 Nylon 6.

Polyesters include polyethylene terephthalate (PET). PET (Figure 1.16) is important industrially due to its relatively high melting point. Prepared by the ester interchange of dimethyl terephthalate and ethylene glycol, it can be melt spun or used for biaxially-orientated high-clarity films. Other important thermoplastics include polycarbonates (Figure 1.17) and polyacetals (Figure 1.18).

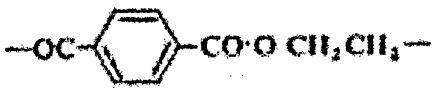

Figure 1.16 Linear polyester.

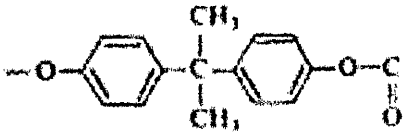

Figure 1.17 Polycarbonate.

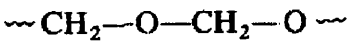

Figure 1.18 Polyacetal.

1.2.2 *Filler+s and reinforcing agents*

The list of fillers, additives and reinforcing agents can never be exhaustive. However, a summary is given in Table 1.1, which includes those most commonly used. They can be subdivided into fibres and particulates.

Table 1.1 Fillers for polymers[4].

Particulate		**Fibrous**	
Organic	**Inorganic**	**Organic**	**Inorganic**
Woodflour	Glass	Cellulose	Whiskers
Cork	Calcium carbonate	Wool	Asbestos
Nutshell	Alumina	Carbon/graphite	Glass
Starch	Beryllium oxide	Aramid fibre	Mineral wool
Polymers	Iron Oxide	Nylons	Calcium sulphate
Carbon	Magnesia	Polyester	Potassium titanate
Protein	Magnesium carbonate		Boron
	Titanium dioxide		Alumina
	Zinc oxide		Metals
	Zirconia		Sodium aluminium hydroxy carbonate
	Hydrated alumina		
	Antimony oxide		
	Metal powder		
	Silica		
	Silicates [a]		
	Barium sulphate		
	Molybdenum disulphide		
	Silicon carbide		
	Potassium titanate		
	Clays		
	[a] talc, mica, calcium silicate		

Organic fibres

These form a minor class of fillers and extenders for composites due to their low thermal stability and variability. Cellulose fibres are the most important, and are woven for use in lamination processes. Ligno-cellulosic fibres, such as jute and sisal have found limited application in phenolic and polyester systems. Their propensity for water absorption also restricts their use.

Synthetic fibres are industrially significant. Many types are produced from nylons, aromatic polyesters, acrylics, polyolefins, polyurethane and PVC. Manufacturing processes vary, but those most commonly employed are spinning from the melt, solution spinning and dry spinning. Continuous filaments are produced which may be used directly or chopped to form fibres. Increasing draw ratios up to 40:1, under elevated pressure, can produce ultra- high stiffness fibres, with modulus values of greater than 100 GPa (Figure 1.19).

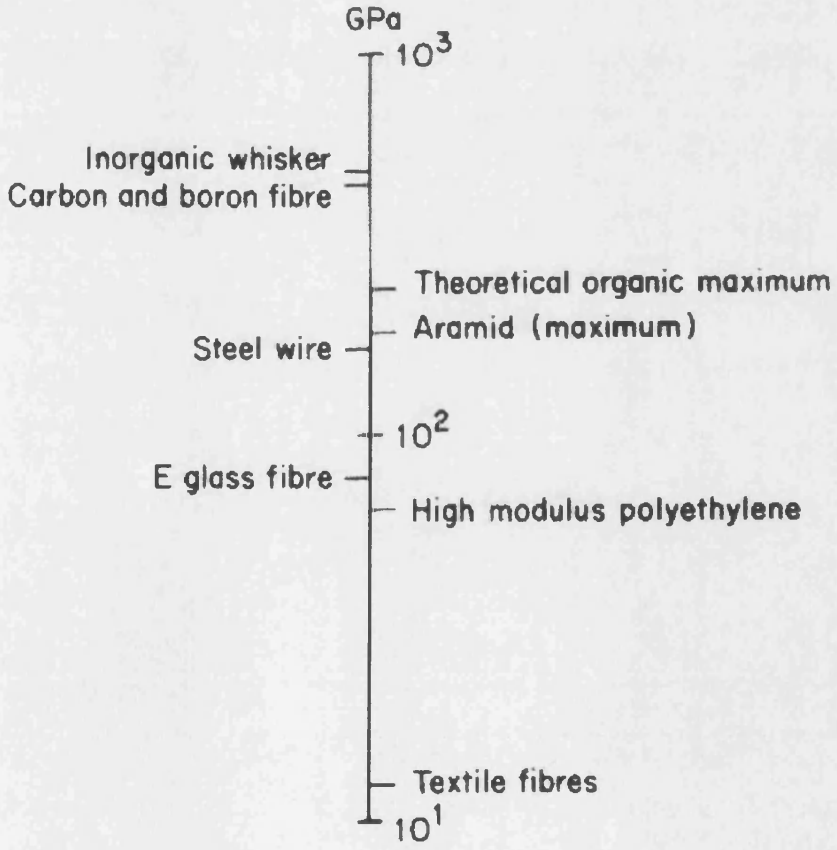

Figure 1.19 Moduli (stiffness) of fibrous fillers.

These fibres offer high stiffness and low weight in composite systems. Nylon fibres are used in phenols and polypropylene fibres in inorganic cements.

One class of well-known organic fibres is the aramids. These include Kevlars®, such as Kevlar® 29 and 49. They are available as woven and non-woven fabrics, fibres and rovings. Composites are produced with high modulus and very high impact resistance. A further class of high-strength specialist fibres is the carbon fibres. These are lightweight, high performance materials. They find application in specialist composite areas such as those used in the aerospace and high performance automotive industries.

Inorganic fibres

Both natural and synthetic forms occur, although natural fibres were primarily prepared from asbestos. Their use is now severely limited due to health and safety concerns. Glass is, without doubt, the most important inorganic fibre, although a number of specialist fibres are also in use. Glass fibres are usually produced in a direct melt process (Figure 1.20).

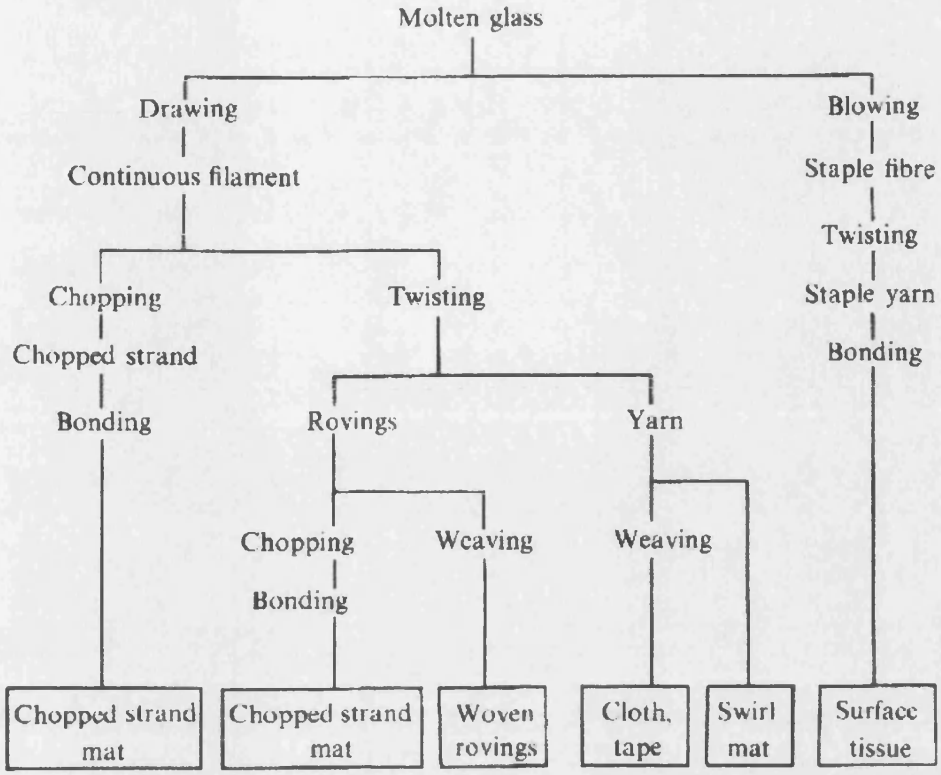

Figure 1.20 Glass fibre manufacture[4].

The molten glass is extruded through several hundred spinneret holes to produce continuous filament. The filament strands are converted to roving or cut to make chopped strand. Types are given designation letters, depending on the glass origin and use. Examples include: 'A' (soda glass); 'E' (electrical grade); 'C' (chemical resistant); and 'S' (high strength). Glass fibres are often 'sized' with latex emulsions or silanes to improve processing or polymer compatibility.

Other specialist fibres include boron fibres, giving high strength and low density. They are used as reinforcers in epoxy resins. Ceramic fibres, particularly alumina, have found niche applications due to their polycrystalline nature. Metal filaments and silicon nitride whiskers also find limited use.

Organic particulates

Many organic particulates are cellulose-based, derived as bi-products from the wood and paper industries. These include lignins and cellulose-based materials from wood dust, nutshell flour and ground bark. Other protein-based fillers have been obtained from soya beans and feathers. Additionally, powdered rubber, plastic and particularly carbon black are used. Organic fillers are low density and many are used as cheap extenders for relatively expensive polymers, as well as being used to reduce mould shrinkage.

Powdered cellulose has high whiteness and has a microscopic fibrous structure. It is used particularly in phenolic acid and related resin systems. Woodflour is used in similar applications, as is nutshell flour. In some applications the two are mixed to improve gloss and processability. The bulk of nutshell flour is derived from walnut and coconut.

A wide variety of natural starches are used as fillers, these being derived from rice, wheat, maize and potato. Much has been made in the use of starch-based polymers for biodegradable polymers, although their use is limited currently.

Particulate carbon finds extensive use as a reinforcing agent, processing aid and as a pigment. Over 90 % of carbon blacks are used in tyres, where they improve mechanical and wear properties for synthetic and natural rubbers. Carbon is naturally conductive and is used in insulating polymers to provide an electroconductive pathway. These composites are particularly useful in antistatic areas.

Carbon blacks have been studied extensively especially with respect to their surface properties. They are produced from the combustion of aromatic oils in a gas or oil flame. The carbon black particles formed are quenched in a water spray. They are agglomerated by electrostatic precipitation, followed by milling to reduce aggregation. Carbon types are classified according to their particle size and use, as defined by ASTM D3192-89 and are listed in Table 1.2.

Table 1.2 Examples of particulate carbons[9].

ASTM first digit	Particle size (nm)	Example on ASTM designation	Type of carbon black
0	1 – 10		
1	11 – 19	N110	Super abrasion furnace
2	20 – 25	N220	Intermediate super abrasion furnace
3	26 – 30	N330	Channel and high abrasion furnace
4	31 – 19	N440	Fine furnace
5	40 – 48	N550	Fast extruded furnace
6	49 – 60	N660	General purpose furnace
7	61 – 100	N770	Semi-reinforcing furnace
8	101 – 200	N880	Fine thermal
9	201 – 500	N990	Medium thermal

Carbon blacks typically have very high surface areas (> 100 $m^2 g^{-1}$), and their use is determined by their particle size distribution and surface activity. Porosity and irregularity as well as unsaturation and oxidisation dictate surface activity.

Inorganic particulates

Many fillers are added to reduce the flammability of polymers. Aluminium hydroxide is, by far, the most widely used flame-retardant filler. Often referred to as ATH (aluminia trihydrate) it has several crystalline forms including gibbsite. ATH is manufactured from the aluminium-based ore bauxite. Magnesium hydroxide, usually as the mineral brucite, is another such flame-retardant, but has superior thermal stability to ATH. Commercial production is by the precipitation of magnesium salts in seawater and the addition of lime or dolomitic lime. Other synthetic flame retardants include basic magnesium carbonate and antimony oxides. The latter are used in conjunction with halogen compounds.

Silica has up to twenty two distinct phases. Some occur naturally, whilst others can be synthesised. Pyrogenic amorphous silica is colloidal and has a high surface area of up to 380 m^2g^{-1}. It is manufactured by the hydrolysis of silicon tetrachloride in an oxygen-hydrogen flame[10]. Precipitated amorphous silica is also colloidal and is produced from an aqueous solution. Silica gel is formed from the reaction of sodium silicate with a mineral acid. Precipitated silicas have surface areas of up to 140 m^2g^{-1}, whilst silica gels are significantly finer and more porous, with surface areas of 175-800 m^2g^{-1}.

Fused or vitreous silica is manufactured from high purity coarse sand by fusing in an arc furnace using graphite electrodes. A fused block or ingot is formed that is ground to the desired particle size. Fused silica is a high-performance filler used especially in applications with extreme temperature requirements. It has a negligible thermal expansion from – 225 ° to 1650 °C.

Naturally occurring silica is found in many forms. Of these, the two of greatest commercial importance are crystalline silica, found as quartzite, and diatomaceous earth. Commercial quartzite is chemically inert, very hard, with good heat resistance and electrical insulation properties. The paint market uses the majority of crystalline silica, with some used as functional extenders for thermosets and silicone elastomers. Diatomaceous earth is a product of fossilised siliceous remains of small organisms known as diatoms.

Precipitated calcium carbonate, or PCC, is manufactured by three processes, with naturally occurring calcium carbonate as the raw material. In the ammonia process calcium carbonate is a by-product of sodium carbonate production[11]. The PCC is washed to remove soluble salts, then dried and micropulverized. The particle size is controlled by conditions of precipitation: temperature; concentration, rate and order of reagent addition; and degree of agitation.

The lime-soda process uses calcium carbonate in sodium hydroxide production. Calcium carbonate is heated to form calcium oxide and reacted with water to form calcium hydroxide.

This is reacted with sodium carbonate to form calcium carbonate and sodium hydroxide. The PCC settles out, is removed and then washed free of residual sodium hydroxide.

The recarbonation process has largely superseded both of these methods. Limestone is calcined to form calcium oxide, as with the lime-soda process. The bi-product, carbon dioxide, is also collected. Calcium oxide is slurried in water to form calcium hydroxide, which is then recombined with carbon dioxide by carbonation to precipitate calcium carbonate. Median particle sizes are between 0.2 μm – 2.0 μm.

Naturally occurring calcium carbonates are categorised into three forms; chalk, limestone and marble. All three are used in polymer composites. Chalks are a specific limestone-type, formed from coccoliths during the Cretaceous Period. Limestone was usually formed from decomposed shells and skeletons of marine organisms. These were consolidated by overlaying rocks or by recrystallisation from leached water. Marble was formed from recrystallised limestone, altered by extreme temperatures and pressures. Marble is harder and more dense than the parent rock. Calcium carbonates are highly ordered, although impurities in the lattice may alter this significantly. In their natural state they absorb water readily and have a hydrated surface layer (Figure 1.21).

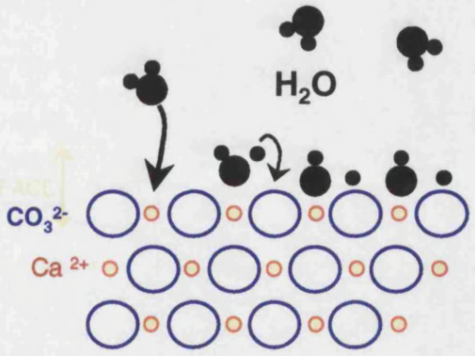

Figure 1.21 Structure of calcite, showing hydrated layer at the interface[12].

Calcium carbonates are ground either by wet or dry milling into individual calcite crystals of around 3-5 μm. If finer products are required, more severe processing is necessary to break down the primary calcite crystals[13].

Many calcium carbonates, either natural or precipitated, are surface modified with carboxylic acids, especially stearic acid. The coating assists mineral wetting and reduces dispersion energy requirements in many polymer systems.

Kaolin, or china clay, is found in many parts of the world. The most important commercial deposits are located in the South Eastern United States, Cornwall, UK, and the Amazon region of Brazil and the former USSR. Clay deposits are usually classified into primary, secondary and tertiary. Clay is formed by the weathering of feldspatic igneous and metamorphic rock (especially granite) and classification is dependent on post-metamorphic history. Primary deposits are a mixture of clay and granite, occurring within the same metamorphic region. Secondary deposits occur when the fine clay particles are transported by water to a new location. These will be deposited along the watercourse where flow is disrupted. Tertiary deposits are re-suspended secondary clays, typically moved by changes in shoreline with tidal flows. Kaolin is an aluminosilicate, $Al_2O_3.2SiO_2.2H_2O$. Two structural units comprise the kaolinite lattice[14]. One unit consists of two sheets of closely packed oxygens or hydroxyls in which aluminium is embedded equidistantly from six oxygen atoms or hydroxyl groups (Figure 1.22).

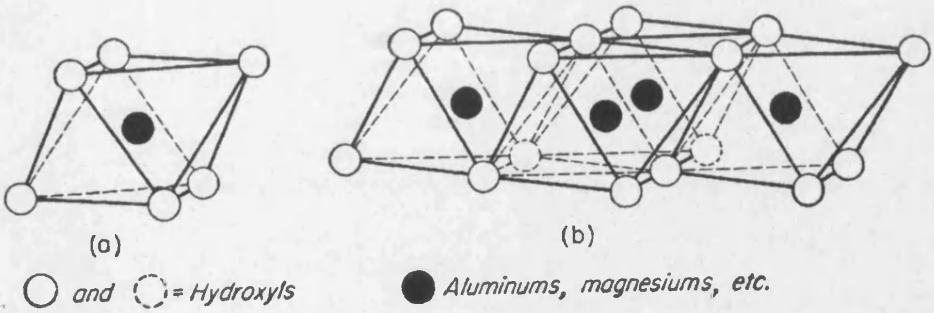

Figure 1.22 Diagrammatic sketch showing (a) a single octahedral unit and (b) the sheet structure of the octahedral units[11].

The aluminium atoms are arranged in hexagons in a plane. The second unit is built from a sheet of silicon tetrahedrons in which the silicon atom is equidistant from the four oxygen atoms or hydroxyl groups, and the silicon atoms are arranged in hexagonal planes (Figure 1.23).

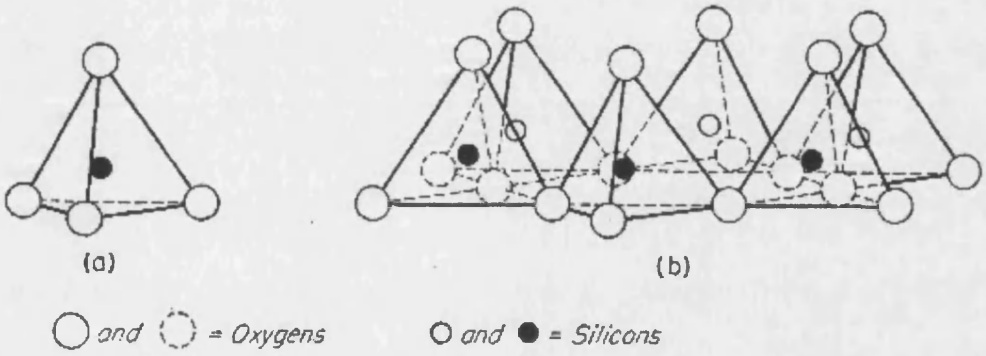

Figure 1.23 Diagrammatic sketch showing (a) a single silica tetrahedron and (b) the sheet structure of silica tetrahedrons arranged in a hexagonal network.

The two sheets interlink with the tips of the tetrahedra facing the bases of the octahedra in a distorted state (Figure 1.24).

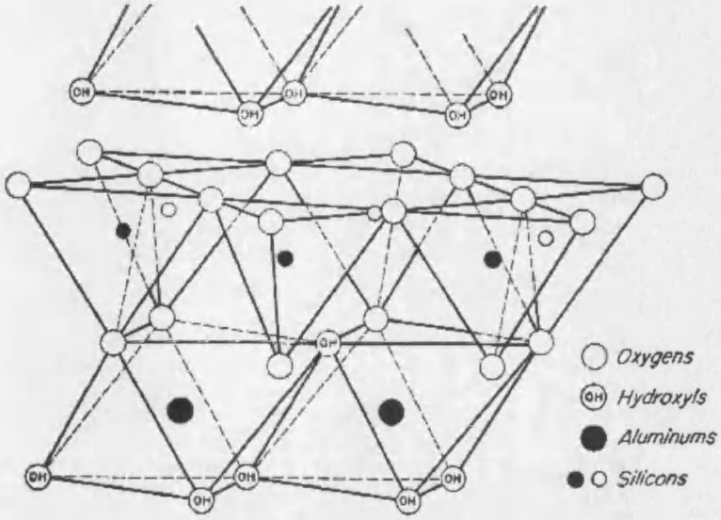

Figure 1.24 Tetrahedral and octahedral configurations in kaolin minerals.

Kaolinite plates have negatively charged faces and positively charged edges. These structures undergo rearrangement on heating to form two further widely used mineral fillers. Above 500 °C, kaolinite dehydroxylates endothermically to form metakaolin. By 650 °C, approximately 90 % of the dehydroxylation is complete. The aluminium octahedra rearrange to four and five-fold sites. On further heating, to above 980 °C, a defect spinel structure arises forming calcined clay (Figure 1.25). Metakaolin has a highly reactive surface, probably due to an increase in the number of Lewis sites, with reduction in the co-ordination of aluminium. Calcined clay is much less reactive than metakaolin, but isolated hydroxyl groups are retained on the surface and may undergo coupling reactions[15].

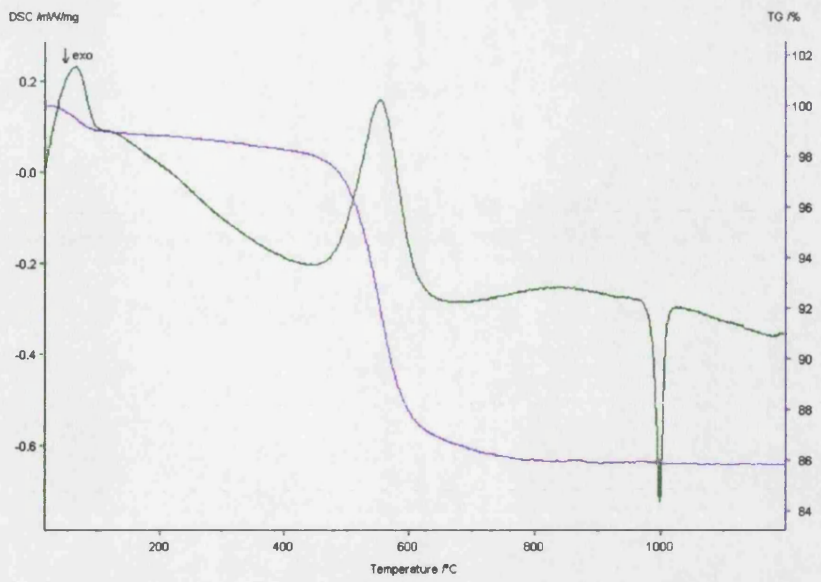

Figure 1.25 Thermogram illustrating the dehydroxylation of kaolinite.

Mica occurs in several crystalline forms including phlogopite, muscovite and sericite, is a complex mineral comprising a mixture of silicates, typically hydrous potassium, aluminium and magnesium silicate. Deposits are found worldwide, with commercial operations in the South East and South West US, Canada, India and Brazil. Its use is governed by its high aspect ratio, and consequent platey particle shape. This is claimed to engender stiffness in plastics at a lower volume fraction than other platey minerals.

Talc is a secondary mineral found in metamorphic rock. Main production sites are found in the US, Norway, France and Italy. Also known commercially as soapstone, pure talc has the chemical composition Mg_3 (Si_4O_{10}) $(OH)_2$. Its trioctahedral structure comprises octahedral $Mg(OH)_2$ sheets sandwiched between two tetrahedral siloxane sheets. The sheets are bound only by van der Waals forces and will cleave readily to reveal face layers with exposed oxygen atoms. This cleavage produces a platey structure, with aspect ratios said to match those of some grades of mica, hence their similar usage. Talc is used as a semi-reinforcing filler in rubber and as a partitioning agent. Thermoplastic applications include those where high modulus is paramount.

Barite or barytes ($BaSO_4$) is a widespread mineral often associated with metallic ores. Deposits are found in the US, Canada and Russia. Low purity ores are often iron-stained, although some white deposits are exploited.

A high purity, precipitated form of barite is known commercially as "blanc fixe". Barite has a unique combination of two properties: chemical inertness; and high specific gravity. Its low surface area and high specific gravity allow high loading and assist heat transfer. Hence its use as an alternative to asbestos in brake linings. The high density of barite provides excellent sound deadening.

Having considered polymers and fillers separately, a summary of the composites is given below. These can be classified, as with the polymer systems, into thermosets and thermoplastics.

1.2.3 *Composite systems*

Thermosetting composites

As discussed earlier, thermosets are chemically cross-linked prior to their use. Compounding must therefore be carried out either before or during polymerisation. Woodflour provides a cheap filler for phenolic resin, improving impact resistance and reducing shrinkage. Fibrous fillers, such as cotton flock, chopped fabric or paper pulp, give impact strength increases of up to five times that of the unfilled resin. Synthetic fibres, such as nylon, increase this further, by up to twenty times the unfilled system. Mica is added to electrical grade phenolics, where insulation properties are required. Organic fillers are typically used in 1:1 ratios, whereas inorganic fillers are used often at around 1.5:1 ratios. Phenolics are used widely in the electrical industry as casings, machine parts and handles. Heat and electrical grades, including fillers such as kaolin and metakaolin, are used in electronic and electrical engineering and in the automotive industry. Laminates find application in high voltage insulation, gear wheels and bearings.

Urea-formaldehyde and melamine-formaldehyde composites have lower impact resistance than phenolics. However, they have greater optical clarity and lower density. Particulate fillers are restricted to wood pulps. Fibrous-filled composites are used where heat and stain resistance is required, with good surface finish. Such applications include decorative laminates and tableware.

Unsaturated polyesters are used widely due to their excellent balance of mechanical and chemical properties, combined with ease of production. Particulate fillers are added to increase viscosity or thixotropy and influence cure rate. Fibrous fillers will increase rigidity, impact strength, reduce shrinkage and alter electrical behaviour. Some forty to fifty different particulate fillers are used commonly in polyester composites. Glass is the main fibrous filler, although carbon fibre composites are becoming increasingly common. Production techniques are diverse, including hand and spray lay-up, vacuum moulding, injection moulding and casting. Their main use is in large section components for the transportation, marine and construction industries.

Epoxy resins may also be used in similar applications. They have advantages in terms of durability, low shrinkage and high heat and chemical resistance. Few organic particulates are used. Inorganic materials are added to give rigidity and dimensional stability. These include calcium carbonates, mica, zircon and alumina. Epoxies are also combined with some of the specialist additives, such as boron and aramid fibres. Applications include the electrical, nuclear, mechanical and aerospace industries.

Silicone composites are expensive and find limited, specialist applications. Mineral and short length fibres are added for reinforcement with high-temperature applications in aircraft and missile parts. Glass cloth is used as a laminate for electric applications. As stated previously, many elastomers also contain fillers. Of these, carbon black is the most important, not only in natural rubber, but also in synthetic elastomers like styrene-butadiene rubber (SBR).

Thermoplastic composites

Composite fillers may be either particulate or fibrous, with choice of filler governed by the physical property requirements. As with thermosetting polymers, fillers may be added simply to reduce costs, but are more commonly added to give specific functionalities. Particulate composites can have improved toughness and dimensional stability, compared with the polymer alone. Fibres can add strength and stiffness along the direction of fibre alignment.

Polyolefin composites usually contain particulates. Calcium carbonate is probably used in greatest volumes, where it is added to PE and PP to produce materials with improved toughness and rigidity. Examples include heavy-duty sacks and garden furniture. Carbon black is used extensively in both polymers. In PE agricultural films, for example, it acts as a pigment and an UV stabiliser. These films are used for silage wrap and mulching. Titanium dioxide is also used to produce pigmented PE films. These films are white, and have a high opacity due to the refractive index differences between the particles and the polymer. Titanium dioxide films also have good UV stability.

Finely divided silica can produce composites with improved heat distortion temperature and modulus. This is important in applications exposed to heat and stress. Talc-polyolefin composites are often highly loaded (up to 40 wt.%). Stiffness may be increased up to 300 % compared with an unfilled PE, for example, but this is offset, to a certain extent, by a reduction in impact strength.

Plasticised PVC contains calcium carbonate primarily to reduce the overall cost. As these materials require high levels of stabilisers and other additives, the filler can be added without additional expense. Polystyrene is most commonly used in high clarity applications, and true composites are seldom found. One exception is a calcium carbonate-PS system used for video cassette casings.

Engineering thermoplastic composites often comprise a mixture of particulates and fibres, to give the best balance of stiffness, toughness and dimensional stability. PA composites may contain mica, quartz or finely divided graphite to improve dimensional and thermal stability. Amine-treated calcined clays and wollastonite are also added as reinforcing agents. These are materials are used typically for automotive applications, such as wheel trims and small components. Specialist PA composites may include molybdenum disulphide to improve bearing properties under abrasive, high load conditions.

Glass reinforced engineering thermoplastics have been in common use since the 1960s. These composites have increased toughness; abrasion resistance and tensile strength compared with the unfilled polymer. Their main weakness lies in the natural tendency of the fibres to debond from the matrix. Treatment with silanes and other coupling agents can reduce this significantly. Polyesters, such as PET and PBT may also be glass reinforced, and are used in water pipelines due to their superior water absorption resistance compared with PA composites.

By careful choice of polymer, filler and their surface modification composites are selected by end-use requirements. For high temperature applications, thermosetting composites must be used. For the majority of applications, thermoplastic composites find wide use. Although the incorporation of fillers to the base polymer affects all properties, the composition is chosen primarily because of its mechanical properties.

1.2.4 *Physical properties of composites*

The influence of filler type on composite properties can be summarised (Tables 1.3 and 1.4).

Table 1.3 The influence of fillers on physical properties of composites[16].

	MAXIMUM IMPROVEMENT BY FILLER		FILLER			RELATIVE [d] FILLER EFFECT ON MATRIX TYPE	
Physical property of composite	**at**	**when V_f/P_f is**	**Bond/ matrix [b]**	**Type**	**Size range [c]**	**Rigid**	**Flexible**
Modulus, M [a]	P_f	high	max	solid max M	broad	Least	most
Tensile strength	V_f/P_f	low	max	fibre	narrow	Least	most
Flexural strength	V_f/P_f	medium	max	fibre	narrow	Least	most
Elongation	V_f/P_f	low	min	sphere	narrow, fine	Least	most
Tear strength	V_f/P_f	low	max	fibre	narrow		
Impact strength	V_f/P_f	low	min	fibre	narrow, fine	Most	least
Compressive strength	P_f	high	max	solid max M	broad	Least	most
Creep	P_f	high	max	fibre	broad	Least	most
Hardness	P_f	high	max	Solid, hi Mohs	broad	Least	most
Coefficient/friction	P_f	high	max	solid	broad	Least	most
Abrasion resistance	P_f	high	max	solid, hi Mohs	broad	Most	least
Density	P_f	high		sphere, low density	broad		

a Young's, shear or bulk.

b Surface modification of filler may be necessary to maximise bonding.

c Broad size range produces highest P_f.

d At a testing temperature below Tg of matrix for rigid, and above Tg for flexible.

where V_f is volume fraction and P_f is packing fraction.

Table 1.4 General guide to filler use[16].

Improvement	Matrix Type [a]	Without loss of	Matrix should be [b]	Best filler type [c]	Concentration
Thermoplastics					
Modulus	high Tg	impact	ductile	fine, narrow range	low
Modulus	high Tg	tensile	ductile, tough	fine, fibre or flake, max bonding	low-moderate
Modulus	high Tg	flexural	tough	high P_f, max bonding	moderate-high
Abrasion resistance	high Tg	compressive strength	ductile, tough	high hardness, high P_f	high
Lower density	high Tg	compressive strength	hard, tough	glass micro-balloons	moderate-high
Modulus	low Tg	low viscosity	low melt viscosity	high P_f, wide range	low
Tensile	low Tg	impact	high elongation type	fine, narrow range, moderate bonding	low
Creep	low Tg	tensile	moderate elongation type	fine, wide range, max bonding	low-moderate
Tear resistance	low Tg	impact	moderate-high elongation type	fine, narrow range, moderate bonding	low
Thermosets					
Modulus	high Tg	impact	ductile	fine, narrow range	low-moderate
Modulus	high Tg	tensile	moderate ductile	fibre or flake	moderate
Flexural	high Tg	-	moderate ductile	fibre or flake	moderate
Compressive strength	high Tg	impact	moderate ductile	fine or flake	moderate
Tear resistance	low Tg	abrasion resistance	tough	fine, hard, max bonding	low-moderate

[a] Versus temperature of testing.

[b] Matrix may require modification to obtain indicated property.

[c] Compare with Table 2-14; best choice may not be the most efficient filler type.

[d] Compare top relative filler volume; V_f/P_f, where high is in excess of 0.5, moderate is 0.25 – 0.5 and low is below 0.25.

Elastic modulus or "stiffness" will be increased with filler addition and is affected by filler shape. If very high modulus is required, fibre composites are used. Flexural modulus is often measured by a three-point bend technique, in which a sample bar is subjected to a single downward force, whilst supported at either end[17]. A load cell is used to record a load-extension, or stress-strain curves (Figure 1.24).

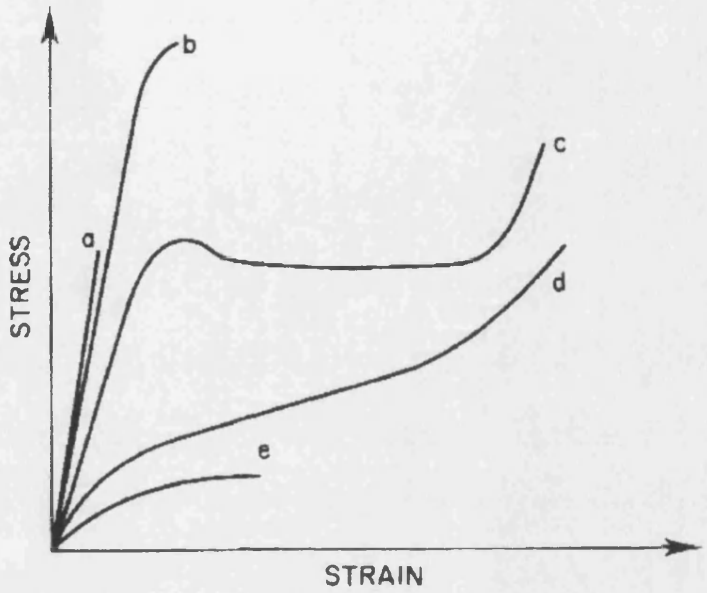

Figure 1.24 Stress-strain behaviour (a) rigid, brittle; (b) rigid, strong; (c) rigid, tough; d) flexible, tough; (e) flexible, weak[4].

Fillers affect tensile properties of composites according to their particle size and interfacial bonding. A uniform extension is applied to a clamped test specimen. The peak and breaking tensile load is measured, as well as dimensional extension, related to cross sectional area. At the maximum volume packing fraction of the filler the particles are separated by at least the thickness of the matrix coating. All interparticulate spaces are assumed to be filled with the matrix, with no interstitial voids. Under these conditions, when a tensile load is applied, these matrix segments stretch, pulling away from the particles. Tensile strength of these systems will therefore be very low. If the filler packing volume is reduced, the matrix contribution becomes more significant, and the tensile strength increases. Where coupling agents are used, interfacial bonding reduces the mobility of the polymer chains. Tensile strength will increase, but elongation is reduced.

Impact strength measurement is also dependent on specimen geometry. Fundamentally, impact strength is proportional to the area under the stress-strain curve of a specimen subjected to an impacting force[18]. Both strength and flexibility will contribute to the total energy[19]. Inclusions in the matrix can act as stress concentrations. Fillers will tend to embrittle composites. However, if a filler contributes to the cohesive strength, compared with the matrix alone, or if the particulate filler distributes the impact stress over a larger area than the impaction area, improved impact strength may occur. Fibres and fillers with improved matrix adhesion show this behaviour.

Tear resistance is measured by a number of standard techniques, depending on the type of moulding or test specimen. Again, the filler-matrix bonding is predominant in determining ultimate tear strength. As with impact resistance testing, tear resistance is a measure of crack or slit propagation. Tear strength is a function of particle size or surface area. With coupling agents, tear strength may be increased considerably in specific composites.

The colour of a fabricated compound is most frequently altered by pigmentation. The natural composite colour will, however, affect pigmentation, and often limits use of certain fillers, such as carbon blacks. The colour of the composite cannot be predicted by measuring the components in isolation, as relative refractive indices and birefringence have a significant effect. Colour is usually expressed in terms of whiteness (L), red and green (+ a and – a) and yellow or blue (+ b and – b). Composite gloss is dependent on fabrication method, and filler concentration.

Gloss is measured by light reflectance at a specified angle from the normal (for plastics, commonly 20 ° and 65 °)[20]. For particulate-filled composites, gloss will be determined by particle size for an equal concentration with finer particles resulting in relatively higher gloss.

Other surface sensitive properties are of specific importance in plastic film applications (films are defined as thin sheets typically less than 100 μm in thickness). These include anti-blocking, which is the ability to separate two films; and slip or coefficient of friction, which is the force required to slide one film over another.

Composite materials cover a vast range of polymers, fillers, additives and surface modifiers. Interactions in these systems are diverse and complex. To choose the most suitable technique for measuring surface thermodynamic properties of such matrices background knowledge of the methods available is essential. The most widely used methods are detailed in section 1.3.

1.3 **Surface Characterisation**

Methods in the fields of spectroscopy, chromatography and solution and surface chemistry have developed giving insights into the surface activities of many solids. Although a wide range of techniques exist, few are suitable for the systems studied, namely organic and inorganic solids and mixtures. Of the methods suitable for analysing such a broad range, two distinct fields emerge – those employing spectroscopic techniques, and those using reactive methods.

Three of the four spectroscopic techniques are based on ultra-high vacuum (UHV) technology, namely X-ray photoelectron spectroscopy (XPS or ESCA), Auger electron spectroscopy (AES) and secondary ion mass spectroscopy (SIMS). The fourth is rooted in the older, but nevertheless valuable principle of infrared absorption, that is Fourier Transform Infrared spectroscopy (FTIR).

The reactive techniques for surface characterisation are based on classical chemistry. Surface tension, for example, has been used to predict reactivity for almost two hundred years. The techniques have been refined and modified, and three emerge as suitable for describing surface, and near surface, thermodynamics, namely contact angle measurement, flow microcalorimetry (FMC) and IGC. The last is described in detail in section 1.4.

1.3.1 *XPS*

XPS or ESCA (electron spectroscopy for chemical analysis) measures core electron binding energies[21]. A molecule or atom in UHV is bombarded with high-energy X-rays, which cause the emission from inner-level electrons. All electrons with binding energies less than the energy of the exciting X-rays are ejected with characteristic kinetic energies. These energies define a specific atom unambiguously. Incident X-ray photons may penetrate and excite photoelectrons to a depth of several hundred nanometres.

Only the outmost photoelectrons, however, will have sufficient energy to escape from the material environment. Most XPS measurements from solids generate information from up to 2 nm below the surface layer.

Relative binding energies, or chemical shifts, are used in chemical studies. For example, the chemical shift of a metal oxide relative to the metal is calculated from the measured kinetic energies. The surrounding electrons and thus the atomic chemical environment influences the binding energies of the core electrons. Chemical shift measured by XPS is inherent to the chemical species and thus provides a means of chemical analysis. In general, any parameter, such as oxidation state, ligand electronegativity or co-ordination that affects electron density will result in a chemical shift.

Thus XPS can be used to determine surface elements, and some structural information. Peak intensities are proportional to the number of atoms sampled, so that atomic composition may be calculated with accuracies of ± 2 %.

1.3.2 *AES*

Electronic bombardment of a sample under UHV gives rise not only to photoemission of core electrons but also a relaxation leading to emission of a photon, or more commonly, an electron (the non-radiative Auger process). The electron energy is a function of the atomic energy levels involved in Auger transition, and is characteristic of the atom. All elements except hydrogen and helium produce Auger peaks. The spectrum produced, when compared with known spectra of pure elements, enables a chemical analysis to be made.

XPS and AES are complementary. In the lighter elements ($Z < 30$) Auger emissions dominate, making AES more sensitive. For heavier elements XPS is more useful. As with XPS, Auger electrons are emitted from the first few atomic layers, with a similar sampling depth of 2 nm.

The electron beam can be focussed to a small diameter (50 nm) and both spatial resolution and surface mapping are possible. AES usually employs a high-intensity electron gun and a low resolution analyser, giving fast analysis. This produces primary elemental information, but little information on chemical bonding, such as that obtained by XPS.

The strength of AES lies in the fast qualitative and quantitative non-destructive analysis of elements in the surface layers, with a very small sampling size. When combined with a controlled removal of surface layers by ion spluttering AES proves useful for analysing atomic layers, such as corrosion on metals. Its use is limited for polymers and composites because of charging problems with highly insulating powders and beam damage to polymeric samples.

1.3.3 *SIMS*

In SIMS an energetic primary ion bombards the sample surface releasing secondary ions. The ion beam (such as Ar^+, O_2^+, Ga^+ or Cs^+) has an energy of 1 – 30 keV. If the secondary ions are of atomic origin they are analysed and detected as such. Molecular ions, however, will fragment to give positive and negative mass spectra.

Two types of experimentation are possible – these being dynamic and static. In dynamic SIMS the primary ion current is high ($\geq 10\ \mu A\ cm^{-2}$) so that the surface is rapidly eroded. Elemental ion intensity is a function of time (and therefore erosion depth), providing compositional depth profiles. This technique is very sensitive, with trace element detection in the ppm – ppb range. In static SIMS the primary ion current is much lower (around 1 nA cm^{-2}), so the spectrum represents the relatively undamaged surface layer. The aim is to optimise the collection of large ion fragments (cluster ions) representing the surface molecular structure corresponding to only 1 nm sampling depth. The technique is particularly valuable for identifying surface contaminants

Dynamic SIMS gives only elemental information, therefore static SIMS is used for structural elucidation. Static SIMS instruments usually combine a noble gas ion source, such as Ar^+ or Xe^+ with a quadruopole mass spectrometer (QMS). The beam is focussed on 50 μm diameter and is scanned over an area of several square millimetres. Time of flight (TOF) mass analysers have more recently been introduced, and give much greater transmissions. Secondary ions are detected in parallel, unlike QMS, increasing sensitivity tenfold[22]. Despite the sensitivity of both instruments, quantitative evaluation is limited.

1.3.4 *FTIR*

IR spectroscopy is a means of detecting chemical bonds. The spectral range covers between 14,000 and 20 cm^{-1}, although the range most used is the mid-IR range from 4000 to 200 cm^{-1}. Upon interaction with IR radiation, portions of the incident radiation are absorbed at specific wavelengths. A highly complex absorption spectrum is produced due to molecular vibrations from individual chemical bonds. These are uniquely characteristic of the functional groups, and their position within the molecule.

Older instrumentation is based on the dispersive spectrometer. These are usually double-beamed instruments in which two equivalent beams of radiant energy are taken from the surface. Most instruments now employ Fourier transformation of the data (FTIR). This takes the background and sample spectra as interferograms and reconstructs the sample spectrum, subtracting the background by a mathematical transformation.

Sampling techniques will depend on the nature of the material. For polymers, thin films are produced, either by deposition from solution or melt pressing. These may then be analysed in transmission. Powders or solids can be examined as a thin paste or mull in an IR transparent medium. A pelletising preparation is often used for ground samples. The sample is mixed with potassium bromide powder (transparent to IR in the detection range) and pressed in an evacuable die to form a transparent disc.

A further adaptation of FTIR has been the advance of diffuse reflectance (DRIFT). This allows powders to be analysed without the need for grinding or mulling. DRIFT employs an additional cell replacing the conventional sample holder. The incident beam is focussed onto the sample surface using the mirrors and optics. Reflected radiation is scattered from the powder surface and captured by an elliptical output mirror. The mirror refocuses the radiation back into a single beam, which is further refined before detection. This technique has been used widely to study surface coatings, such as silane coupling agents on powdered silica[23].

Reflection-absorption IR (RAIR) and photoacoustic spectroscopy (PAS) have also been used to study surface modifications. With RAIR, a beam polarised parallel to the plane of incidence is reflected from a polished metal mirror at about 80 °. The sampling method has been useful for metal surfaces. PAS is another IR method of increasing importance. The solid sample is contained in a chamber filled with a coupling gas such as helium, air or argon. The sample surface is heated by about 0.001 °C causing a small increase in gas pressure. The IR beam, temperature rise and gas pressure are all modulated and the modulation of gas pressure is detected by a microphone. With this method, a sampling depth of 10 to 30 μm can be achieved.

1.3.5 *Contact angle measurement*

Contact angle studies have been used to determine wetting, and surface tension for polymers, composites and powder fillers. Four methods are in common use, namely: direct geometric measurement; calculation from capillary shape; measurement of force balance and comparison with surface tension and calculation from intermolecular forces[24]. The contact angle (θ) is measured within an advancing liquid phase. As the liquid is prone to hysteresis both advancing and receding angles are measured.

Direct geometric measurement uses a liquid contacting a surface, the image of which is captured, usually, on video or camera (Figure 1.25).

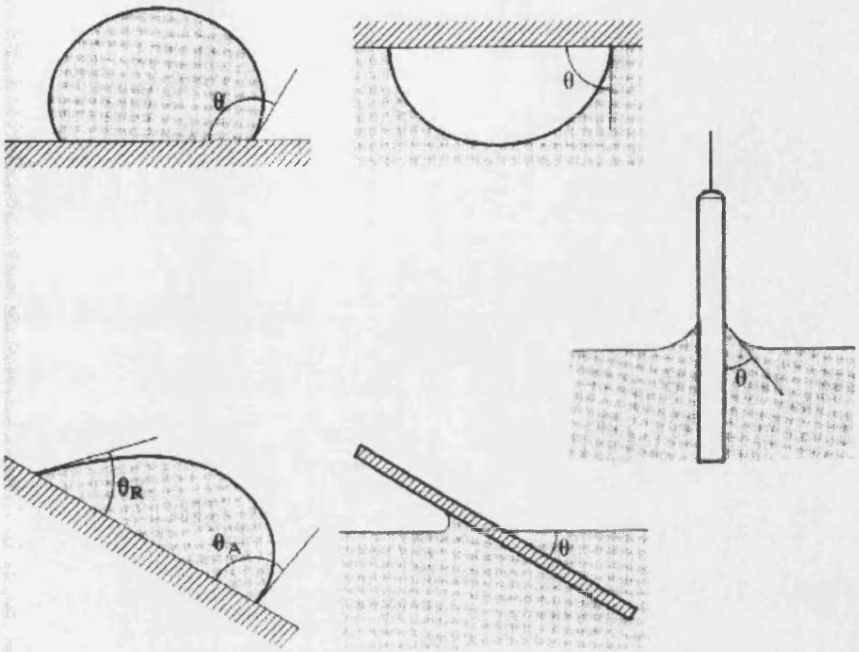

Figure 1.25 Methods of contact angle measurement[21].

Capillary shape methods can be calculated indirectly from geometric measurement. However, these are only suitable if the capillary constant is known. One example is the determination of the radius and height of a sessile drop followed by estimation of best-fit contact angle from published tables. A simpler method is to determine the spreading coefficient from the limiting height of a large sessile drop.

$$S_{c123} = -\rho g h^{2}/2$$
$$= \gamma_{23} (\cos\theta - 1) \qquad (1.1)$$

where S_{c123} is the spreading coefficient, ρ is the liquid density, g is the gravitational acceleration, h is the limited height and γ_{23} is the surface tension. The contact angle can be derived from the spreading coefficient with a knowledge of the liquid's surface tension.

Using a Wilhelmy plate to measure the forces involved in wetting, the force balance may be used to find contact angle. Surface tension is measured firstly using a clean platinum plate. Next the force, F, is determined for the experimental surface before the surface tension is again measured. θ can be calculated from

$$F = \gamma_{23} L \cos \theta \qquad (1.2)$$

where L is the perimeter of the plate and F the force determined.

Calculation of indirect contact angle is more commonly used. In this, the wetting of a solid is determined using reference liquids. For a drop of liquid L, at a surface S in the presence of a fluid, F (where the second vapour or liquid is immiscible within the first) the surface tension (γ_{SF}) can be calculated from Young's equation (1.3). The interfacial tension of the liquid/fluid (γ_{LF}) must be known, and the equilibrium contact angle found.

$$\gamma_{SF} - \gamma_{SL} = \gamma_{LF} \cos \theta \qquad (1.3)$$

where the difference between solid/fluid and solid/liquid tensions is $\gamma_{SF} - \gamma_{SL}$. These two terms cannot be separated unless certain assumptions are made.

In the case of polymers, Zisman made detailed studies[25]. Contact angles (θ_o) were measured using a series of liquids of decreasing surface tension (γ) on the polymer surface. θ_o decreases with γ, while $\cos \theta_o$ increases. By plotting $\cos \theta_o$ versus γ, extrapolations can be made to $\cos \theta_o = 1$.

The value of γ for $\cos \theta = 1$ is the critical surface tension of the solid (γ_c) and corresponds to the value at which the liquid just spreads spontaneously. It is not exact, because, by Young's equation

$\gamma_{SF} - \gamma_{SL} = \gamma_c$

However, because interfacial tension between a polymer and an organic liquid is generally low, an approximation is made where

$$\gamma_c \sim \gamma_{SF} \sim \gamma_S \qquad (1.4)$$

Using this assumption a relatively simple "wipe test" has been developed[26]. Cotton wool is dipped in solutions of different surface tensions and wiped over the polymer surface. Critical surface tension is assumed when liquid film break occurs.

Young's equation is over-simplified for most applications. Even in a vapour atmosphere γ_{SF} does not correspond necessarily to the surface tension of the solid γ_S. γ_S actually corresponds to a pure solid, whereas γ_{SF} refers to the same quantity after any potential absorption of the liquid vapour. The difference due to the spreading pressure is π_e where

$$\pi_e = \gamma_S - \gamma_{SF} \qquad (1.5)$$

Additionally, the interfacial tension must be lower than the sum of the two individual surface tensions, or no interface would form. The difference, given as the Good-Girifalco interaction parameter, Ø, can be expressed as in (1.6)[27],

$$\gamma_{SL} = \gamma_S + \gamma - 2\,\text{Ø}\,(\gamma_S\,\gamma)^{1/2} \qquad (1.6)$$

Fowkes refined this further, taking into account acid and base components[28].

$$\gamma_{SL} = \gamma_S + \gamma - 2\,(\gamma_S^D\,\gamma^D)^{1/2} - I^{ND}_{SL} \qquad (1.7)$$

where D refers to the dispersive components of γ and γ_S and I^{ND}_{SL} represents the non-dispersive interactions.

Contact angles of a series of liquids are measured and a graph of θ_o versus $(\gamma^D)/\gamma$ plotted. Alternatively, a two-liquid mixture may be used[29].

Powders and fillers have also been analysed by similar techniques. In these cases, the preparative method has a profound effect on the data. Powders may be deposited onto glass from solutions or slurries. Alternatively they may be presented as compacted tablets. Using liquid penetration, the Washburn equation is applied (1.8)[30] .

$$H_2 = \frac{t.R.\gamma_L \cos\theta}{2\eta} \qquad (1.8)$$

where H is the height to which the liquid has risen in time t, R is the effective interstitial pore radius between packed particles, γ_L is the liquid's surface tension and η is the liquid viscosity.

The equation was originally derived for penetration in a cylindrical capillary. Rate of penetration can be measured. One assumption is that the powder comprises a series of parallel capillary tubes of uniform radius. Clearly, this has limited value when applied to non-uniform, porous fillers, and a number of corrections have been proposed[31]. Using apolar liquid wicking data on thin films, the average interstitial pore radius can firstly be determined. Although most suited to spherical, or near spherical particles, the method has been applied to anisotropic materials with some success.

1.3.6 *Flow microcalorimetry*

Both static and flow calorimetry are used to measure enthalpy changes. Static calorimetry may use one of two techniques. In the first, the adsorbent and the adsorbate are placed in a calorimeter isolated from each other. The two are then brought into contact and the heat of reaction measured. In the second method, the adsorbent is held within the calorimeter and an adsorbate solution added. These methods do not take into account any interacting equilibria merely giving an enthalpy change for a batch system.

Using flow microcalorimetry (FMC) the enthalpy change is that which occurs as the adsorbate changes from being in equilibrium with a known fluid to that of a second known fluid[32]. The initial and final states are relatively well defined and enthalpy can be more readily attributed to known adsorption-desorption processes.

The instrument can be adapted from a standard calorimeter cell, or obtained as a dedicated system (Figure 1.26).

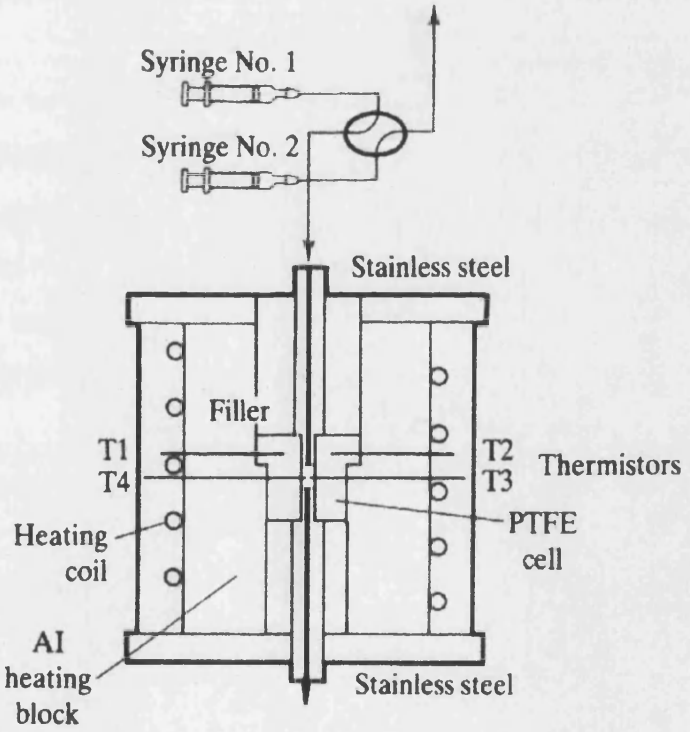

Figure 1.26 Schematic diagram of a flow microcalorimeter[29].

The cell comprises four highly sensitive thermistors. Two sampling thermistors protrude into the cell and are referenced to two thermistors in the PTFE cell walls using a Wheatstone bridge. The circuit is sensitive to temperature changes of 10^{-5} °C.

The substrate or filler is placed in the cell and pre-conditioned by heating or equilibrating in a pure solvent flow (fluid A). Fluid B is usually a mixture of fluid A and an interacting liquid or probe. Syringe 1 contains fluid A, and syringe 2 contains fluid B. A steady flow of fluid A is maintained until equilibrium is achieved. Fluid B is then introduced at a constant rate. Flow continues until a second equilibrium is attained. The flow may then be switched back to fluid A to test for reversibility.

Adsorption of the probe onto the surface causes a temperature increase, which is detected by the thermistors. This is amplified and plotted against time with the area under the peak representing adsorption (or desorption). The solvent is typically non-polar, such as n-heptane. The probes are chosen, as with IGC, depending on this acceptor-donor characteristics. Alternatively, a surface modifying agent such as a silane coupling agent or dispersant may be used.

To enhance the use of FMC, the cell is often linked in tandem with high pressure liquid chromatography (HLPC). Eluent from the FMC is passed through the HLPC. Differences in retention time result in changes in HPLC response curves. Standard solutions are run, and a calibration curve constructed. From these, the molar heat of adsorption can be calculated as a function of time[33]. This will give an indication of the heterogeneity of acidic or basic surface sites.

1.3.7 *Conclusions*

The techniques for surface characteristics fall into two distinct regimes. Spectroscopic techniques can be used to determine the chemical composition of the surface, and may be quantitative. Structural elucidation is possible, with FTIR often being used to demonstrate bonding and surface modification. SIMS is highly surface sensitive, and reference spectra are available. XPS may give insights into functionality by the interpretation of chemical shifts.

To measure reactivity, contact angle, FMC or IGC can be used. As stated in 1.3.5, contact angle data are severely restricted due to assumptions and preparative techniques. Both FMC and IGC use site-specific probe molecules to determine surface energies and adsorption enthalpies. FMC can be used to measure surface modification directly.

IGC is a more versatile and robust technique than FMC. Using IGC, various interaction energies associated with the bulk surface tension are calculated. Molecules in the surface region of the liquid are subject to attractive forces from adjacent molecules, resulting in a net attraction into the bulk phase in the direction normal to the surface. The attraction reduces the quantity of surface molecules, and results in an increase in intermolecular distance. The force associated with these attractions is the surface tension. Surface tension data are of limited use in understanding intermolecular interactions between materials. To characterise materials in thermodynamic terms, specific properties, such as surface free energies, entropies and enthalpies of adsorption and work of adhesion are required.

Using IGC, the retention behaviours of pure vapours are studied when passed through a column packed with the material under investigation. The vapours, known as probes, interact by various retention mechanisms. The major mechanisms are surface adsorption, and bulk solubilisation with diffusion. Thus IGC can be used not only as a surface technique, but also to study bulk diffusion for certain materials. The mechanisms are relevant to real systems, and can be used to describe interfacial bonding in composites, wetting of fibres and particulates, polymer-polymer miscibility and other polymer properties such as phase transitions.

The versatility and sensitivity of the technique makes it a powerful tool for studying physisorption and chemisorption in a wide variety of materials. The background theory is described below in section 1.4.

1.4 **IGC theory and background**

A standard GC system, modified as shown in Figure 1.27, is used to obtain the necessary data for IGC calculations, these being: the retention time, t_r, of the probe through the column; oven temperature; pressure drop across the column; and carrier gas flow rate.

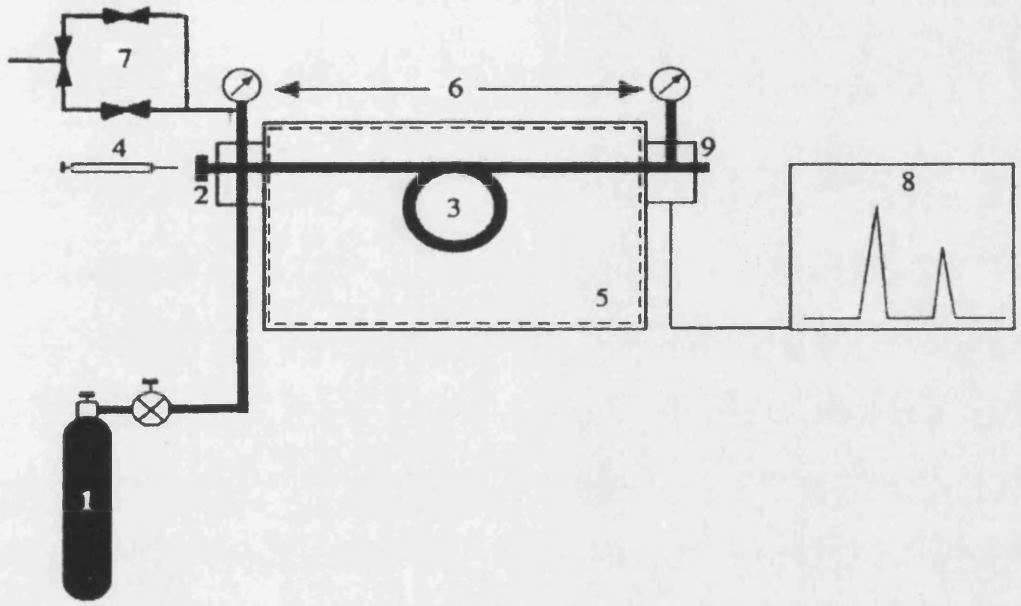

Legend

1. Carrier gas supply.
2. Injection port.
3. Column.
4. Micro-syringe.
5. Oven.
6. Pressure drop (measured by GC).
7. Outlet to pressure/flow meter.
8. PC interface and printer.
9. Detectors (tandem TCD and FID).

Figure 1.27 IGC instrumentation.

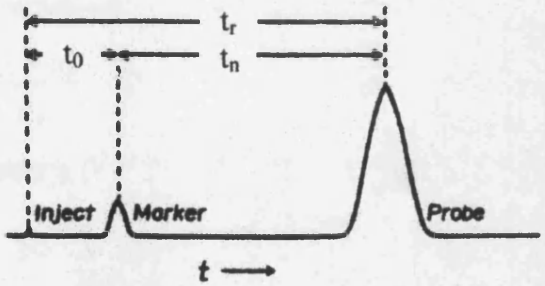

Figure 1.28 A typical chromatograph obtained from a single probe injected onto a polymer-coated stationary support[34].

1.4.1 *Calculating the retention volume*

The net retention volume, V_n, can be calculated by

$$V_n = Jf\,(t_r - t_0) \qquad = Jft_n \qquad (1.9)$$

where: f is the carrier gas flow rate; t_r is time taken for the probe to travel through the column; t_0 is time taken for a non-interacting marker, such as methane or air, to pass through the column; t_n is the net retention time; and J is the correction factor for pressure drop across the column giving rise to gas compressibility.

$$J = \frac{3\left[(p_i / p_0)^2 - 1\right]}{2\left[(p_i / p_0)^3 - 1\right]} \qquad (1.10)$$

where p_i is the column inlet pressure and p_0 is atmospheric pressure. Inlet pressure is measured both by the instrument and an independent thermal flow meter. It is checked at the beginning and end of each run[35]. Under usual operating conditions

$$\Delta p = p_i - p_0 \qquad (1.11).$$

The relative pressure across the column (P) is a more useful expression, which is defined by (1.12),

$$P = \frac{p_i}{p_0} \qquad (1.12).$$

If p_i is unknown, P can be rewritten as

$$P = \frac{\Delta p + p_0}{p_0} \qquad (1.13)$$

Substituting (1.12) into (1.10) gives J in terms of relative pressure.

$$J = \frac{3\left[(P)^2 - 1\right]}{2\left[(P)^3 - 1\right]} \qquad (1.14).$$

Calculation of the flow rate of the gas, f, through the column will depend on the measuring device used. For a soap bubble flow meter, flow can be determined from

$$f = \frac{V}{\Delta t}\frac{p_a - p_w}{p_{ref}}\frac{T_{ref}}{T_a} \qquad (1.15)$$

where $V/\Delta t$ is the measured flow rate; p_a is the ambient pressure, measured in the room with a calibrated anaeroid barometer; p_w is the partial vapour pressure of water at ambient temperature (obtained from literature); p_{ref} is the pressure at reference conditions, taken as 1 atmosphere, or 101.325 kPa; T_{ref} is 0 °C, taken as 273.15 K; and T_a is ambient temperature, measured in the room with a calibrated thermometer.

If flow readings are taken directly from the instrument, or a calibrated mass flow meter is used, no compensation is required for water vapour effects.

The net retention volume, V_n, is a factor of bulk and surface sorption processes, assumed to be independent of each other, as defined by

$$V_n = K_s A + K_l V_l \qquad (1.16),$$

where A is the total surface area of stationary phase; V_l is the total volume of the stationary phase; K_s is the surface partition coefficient; and K_l is the bulk partition coefficient.

Where adsorption into the bulk is negligible, (1.16) can be reduced to

$$V_n = K_s A \quad = K_s W_s S_a \qquad (1.17)$$

where S_a is the specific surface area of adsorbent; and W_s is the weight of sample in the column.

1.4.2 *Calculating the free energy of adsorption*

For isothermal adsorption of one mole from the standard gaseous state to a standard adsorption state (assuming no bulk absorption), the change in Gibbs free energy is

$$\Delta G_a^{\,0} = -\Delta G_d^{\,0} = -RT \ln \left(\frac{p_{s,s}}{p_{s,g}} \right) \qquad (1.18)$$

where $\Delta G_a^{\,0}$ is the standard free energy change of adsorption; $\Delta G_d^{\,0}$ is the standard free energy of desorption; and R is the universal gas constant. $p_{s,s}$ is the vapour pressure of the adsorbate (in its solid state) in equilibrium with the vapour; and $p_{s,g}$ is the equilibrium vapour pressure of the adsorbate (in the bulk gas) in the gaseous standard state.

K_s, the partition coefficient of the solute between the mobile and stationary phase, can be defined as

$$K_s = \frac{\Gamma}{c} \qquad (1.19)$$

where Γ is the surface concentration of adsorbate and c is the adsorbate concentration in the gas phase. Under ideal conditions

$$c = \frac{p}{RT} \qquad (1.20)$$

where p is the partial pressure of adsorbate. By substituting this into equation (1.19) the partition coefficient can be expressed as

$$K_s = \frac{\Gamma RT}{p} \qquad (1.21).$$

Surface concentration can be related to the two dimensional surface pressure of the gas, π, by the Gibbs equation

$$\Gamma = \left(\frac{1}{RT}\right)\left(\frac{d\pi}{d\ln p}\right) \qquad (1.22)$$

$$\Gamma = \left(\frac{p}{RT}\right)\left(\frac{d\pi}{dp}\right) \qquad (1.23).$$

In the infinite dilution region $d\pi / dp$ approaches π / p

$$\text{Thus } \frac{\Gamma RT}{p} = \frac{\pi}{p} \qquad (1.24),$$

and substituting into equation (1.21) gives

$$\frac{\pi}{p} = K_s \qquad (1.25).$$

In the standard adsorption state

$$p_{s,s} = \frac{\pi}{K_s} \qquad (1.26)$$

Substituting the above into equation (1.18) yields

$$\Delta G_a^{\,0} = -RT\ln\left(\frac{K_s p_{s,g}}{\pi}\right) \qquad (1.27).$$

as stated in (1.17), $K_s = V_n / W_s S_a$. By substituting this into the above, a useful expression of $\Delta G_a^{\,0}$ can be derived,

$$\Delta G_a^{\,0} = -RT\ln\left(\frac{V_n p_{s,g}}{\pi W_s S_a}\right)$$

$$\text{or } \Delta G_a^0 = -RT\left[\ln(Vn) + \ln\left(\frac{p_{s,g}}{\pi W_s S_a}\right)\right] \qquad (1.28)$$

To determine ΔG_a^0, $p_{s,g}$ and π must be known. De Boer[36] first proposed that the standard surface pressure was that where the distance of separation between molecules in the adsorbed state was equal to that in the liquid at the standard state (1 atmosphere, 273 K). $p_{s,g}$ was thus determined as

$p_{s,g} = 1.013 \times 10^5$ Pa ,

and $\pi = 3.38 \times 10^{-4}$ Nm^{-1}.

If V_n is found at various temperatures, ΔG_a^0 can be calculated for specific probes.

All the bracketed components in (1.28) with the exception of V_n, are constants and can be reduced to k.

1.4.3 *Calculating the enthalpy of adsorption*

$$\Delta G_a^0 = -RT \ln V_n + k \qquad (1.29), \text{ and}$$

$$\Delta G_a^0 = \Delta H_a^0 - T\Delta S_a^0 \qquad (1.30).$$

If ΔG_a^0 (calculated from equation 1.28) is plotted against T, a straight line plot is produced, where ΔH_a^0 (the enthalpy of adsorption) is seen graphically as the intercept and ΔS_a^0 (the entropy of adsorption) is determined from the slope.

1.4.4 *Calculating the non-specific surface free energy*

The non-specific or dispersive component of the substrate's surface energy, γ_s^d can be calculated from the elution data for hydrocarbon vapours. The free energy change for the adsorption of a methylene group in an alkane series is $\Delta G_a^{0CH_2}$ and is found as the difference in free energies of adsorption for succeeding alkanes in an homologous series. γ_s^d is calculated from

$$\gamma_s^d = \frac{1-\left(\Delta G_a{}^{0CH_2}\right)^2}{\gamma_{CH_2}\left(2N.a_{CH_2}\right)} \qquad (1.31)$$

where N is Avogadro's number; γ_{CH2} is the surface tension of hypothetical surface of polyethylene containing only methylene groups[37], calculated from:

$$\gamma_{CH2} = 35.6 + 0.058\ (293.13 - T) \qquad (1.32)$$

and a_{CH2} is the cross-sectional area of a methylene group ($\approx 0.06\ nm^2$).

Thus if T is constant, and a mixture of probes is injected onto the column, a plot of number of carbon atoms versus $RTlnV_n$ should give a straight line graph where ΔG^{0CH_2} can be found from the slope. This is then inserted into equation (1.31) to give a value for the surface free energy.

1.4.5 *Calculating specific interactions*

Much of the work in this area is founded on the thermodynamic studies of Fowkes, and useful background information can be obtained from a monograph[38] dedicated to his work. Saint Flour and Papirer were the first to apply IGC to acid-base characterisation[39],[40]. Adsorption data for a range of acidic, basic and neutral probes can be used to determine specific adsorption components ($\Delta G^0_{specific}$), where the total free energy is the sum of the specific components:

$$\Delta G_a^0 = \Delta G^0_{\text{non-polar}} + \Delta G^0_{\text{specific}} \quad (1.33)$$

For non-polar interactions, the work of adhesion, W_a, between an adsorbate and an adsorbent is related to ΔG_a^0 by

$$\Delta G_a^0 = -Na\, W_a \quad (1.34)$$

where a = surface area of the adsorbed molecule and N is Avogadro's number.

W_a (for non-polar molecules) was found by Fowkes to be described by

$$W_a = 2 (\gamma_s^d \gamma_L^d)^{1/2} \quad (1.35)$$

where γ_s^d and γ_L^d are the dispersive components of the surface tension for the solid and liquid components respectively. By substituting equations (1.35) and (1.31) into (1.30) equation (1.36) is derived,

$$RT ln V_n = 2N (\gamma_s^d)^{½}.\, a(\gamma_L^d)^{½} + k \quad (1.36)$$

By plotting $RT ln V_n$ as a function of $a(\gamma_L^d)^{½}$ a straight line graph is produced with a slope of $2N (\gamma_s^d)^{½}$. The slope corresponds to the response of a non-polar (alkane) probe. If a polar probe is used, with an equivalent $a(\gamma_L^d)^{½}$, the deviation from the slope on the $RT ln V_n$ axis results in the determination of $\Delta G^0_{\text{specific}}$

$$\text{where } \Delta G^0_{\text{specific}} = \frac{-RT \ln[V_n]}{V_n^{ref}} \quad (1.37)$$

To quantify differences related to probe of specific polarity, the acid-base strengths must be known. Gutmann[41] expressed the acceptor-donor characteristics of acids and bases in terms of acceptor and donor numbers.

The acceptor number (measure of acidic strength) is found by measuring the electron shift in the P-O bond of triethylene phosphoric oxide when interacting with the material in 1,2 dichloroethane. As a reference, the acceptor number of hexane is 0, and $SbCl_5$ is 100. The donor number (measure of basic strength) is characterised by measuring the heat of reaction with $SbCl_5$ in 1,2 dichloroethane. Donor and acceptor numbers are given by

$$-\Delta H_{A\text{-}B} = AN_A \,.\, DN_B \qquad (1.38)$$

where $-\Delta H_{A\text{-}B}$ is the enthalpy of formation for acid-base pairs, AN is the acceptor number and DN is the donor number.

To apply this to solid surfaces the specific enthalpy of adsorption, $-\Delta H^0_{specific}$, is related to acid-base properties by

$$-\Delta H^0_{specific} = K_A.DN_B + K_B.\, AN_A \qquad (1.39)$$

where K_A and K_B are two constants which characterise the solid's acid and base properties. The variation of $\Delta G^0_{specific}$ with temperature can be used to determine $\Delta H^0_{specific}$ as shown previously. Acceptor and donor numbers can then be assigned to the substrate.

1.5 **Literature review**

1.5.1 *Scope of the review*

This review is limited to publications in the main areas of interest, that is polymers, filler and additives and their interactions. Several papers overlap these divisions, and have been included in the field most pertinent to the main topic. IGC can also be used to characterise a wide variety of materials outside the main areas, some of which have been considered under a miscellaneous heading. These include surfactants[42,43], raw petrochemicals[44,45] pharmaceuticals[46] and adhesives[47].

The early work of Conder and Young[48] has not been included. It is often quoted as the standard reference for any physicochemical study by GC, and should not be overlooked. This review includes all papers up to and including April 2000. Within this period, IGC has already been reviewed a number of times. Russian researchers pioneered the use of IGC for the study of inorganic powders and catalytic surfaces[49]. Papers from an ACS symposium dedicated to IGC in 1988[3] reveal the range of its use for interfacial and bulk characterisation. Many of the papers have been considered in greater detail. Further reviews by Williams[50] and Voelkel[51] demonstrate the diversity of current applications.

1.5.2 *General papers and reviews*

A number of reviews and general application papers have been written relating specifically to IGC. Of these, the most accessible is by Schreiber and Lloyd[52]. The growth of the technique is stated as increasing from only 3 % of total published papers (in the field of gas chromatography) in the years 1967 to 1977 to some 30 % in the decade to 1987. Indeed a recent survey on the use of IGC for polymer-related subjects cited 197 published papers between 1993 and 1999[53]. Schreiber and Lloyd consider its versatility and ease of use for determining various thermodynamic data relating to polymers, composites, particulate fillers and their surface modifications. The review is detailed and sub-divided for easy reference. Over fifty papers are cited from the early work of Kiselev to contemporary work, under submission at time of publication.

Although somewhat dated, having been published in 1988, it undoubtedly stands as the primary reference for those new to the technique.

An exhaustive critique by Voelkel is perhaps the most comprehensive study written to date[51]. One hundred and forty five references are reviewed and discussed in detail. The theoretical bases for determining key characteristics by IGC are considered. These include: retention mechanisms, singular and mixed; thermodynamic and Flory-Huggins interaction parameters; solubility parameters; acceptor-donor characteristics and data interpretation for fibres. The experimental section gives examples of common probe molecules and methods for column preparation. Difficulties arising from data reduction are mentioned. In particular, errors inherent in measuring the specific retention volume are discussed. Reported results for the parameters listed above are compared. The use of IGC in determining the degree of crystallinity of polymers is also included. By exemplifying modified silicas, the general effects of surface modification are reviewed. Other materials considered include fibres and surfactants, the latter being tabulated to reveal trends in thermodynamic and polarity data.

In conclusion, Voelkel is critical of the correction factors used for adsorption effects and the influence of carrier gas flow rate. He notes the inconsistencies when quoting retention volumes. Net retention volume is often used rather than specific. In affirming the benefits of the method he sounds a note of caution as to the accuracy of the absolute values so obtained. It is perhaps unfortunate that such a review does not conclude on a more positive note. Words of caution could have been balanced with recommendations for method improvement. Voelkel has published a number of thorough papers based on IGC and a summary of his findings to assist in more rigorous experimental techniques would have been useful.

A more succinct, but nevertheless useful, review is that by Williams[50]. The evolution of IGC, driven by the need to determine basic thermodynamic information is charted. A comparison versus classical adsorption methods emphasises its speed and versatility. A discussion on the underlying principles of IGC is illustrated by the work of Gray and co-workers and Williams' study on polyamides and carbon fibres.

The work also contains data on adsorption in the "infinite dilution" region. This is a useful comparative study, particularly for those interested in the surface chemistry of synthetic fibres.

A more recent review by Schreiber[54] concentrates on the use of IGC for polymer characterisation. Following a discussion on the derivation of surface free energy and the acid-base contribution to the free energy of adsorption, a table listing acid-base constants for some polymers and additives is given. Schreiber goes on to consider the nature of common additives in polymers and the effect of surface modifications and stabilisers. The acid-base pair interaction parameter I_{sp} , is stated as being directly related to the mechanical properties of composites. A recent study on polyurethane adhesives serves to illustrate this statement. The importance of IGC for predicting the performance of polymer systems is stressed, as is its future as a fundamentally important experimental method.

The review seeks to cover a broad range of applications in a brief and largely non-specific manner. In doing so, the absence of detail leaves the reader without a clear understanding of the technique. Its usefulness is therefore considered to be limited by its lack of specificity. The paper is perhaps more suitable as an introduction to IGC for those in the field of polymer science rather than surface chemistry.

Al-Saigh reviewed IGC for characterising polymer blends in terms of polymer-polymer and polymer-solute interaction parameters, melting point and contact energy[55]. A complete treatment of the theories of polymer blend solution and IGC is illustrated and the general use of the IGC method is reviewed. The paper also includes information on column preparation and data acquisition, both of which require careful consideration before meaningful results can be obtained. This work is comprehensive and is considered essential reading for anyone wishing to characterise polymers or polymer blends. Nearly two hundred and fifty references are given, together with a glossary of symbols which provides an easy reference when reading other literature.

1.5.3 *Polymers*

Basic Principles

Interest in IGC for surface characterisation has grown alongside the development of polymers and composites. Following the work of Kieslev and co-workers[49], Gray et al. published works concerning GC studies of cellulose and natural fibres[56,57] and cotton paper[58]. The results were considered somewhat inaccurate, probably due to the surface roughness of the substrates. Returning to first principles, Katz and Gray looked at cellophane packed in a GC column, using straight chain alkane vapours as the probe molecules. From this work two definitive papers were published, concerning adsorption in the infinite dilution region[59] and at finite dilution[60]. At infinite dilution the retention volumes of a series of n-alkanes on cellophane were obtained using the eluted pulse technique (EPT). The corresponding partition coefficients were calculated.

Varying the column temperature permitted the thermodynamics of adsorption to be studied, with linear adsorption isotherms, characterised by corresponding equilibrium partition coefficients, being obtained. The investigation was extended to measuring finite coverages with the same alkane series and mesitylene on cellophane. Elution peaks at several temperatures were obtained and analysed using the BET theoretical model[61]. From this, monolayer capacities and molecular areas of the hydrocarbons were calculated. The variation of thermodynamic adsorption quantities with surface coverage was measured.

Poly (ethylene terephthalate) (PET) film was characterised similarly by Anhang and Gray[62]. The dispersive component of surface energy was obtained by adsorption of n-alkanes at infinite dilution and compared with data from contact angle measurements. Adsorption isotherms and spreading pressures for n-decane were also measured in the finite adsorption region. Al-Saigh obtained similar thermodynamic properties for another semi-crystalline polymer (polyethylene oxide)[63]. Guillet et al.[37] considered various aspects of IGC and proposed an automated system for providing more reliable data. The sources of inaccuracies within a conventional set up were discussed, such as measurement of polymer mass in the column and data acquisition.

The parameters determined by IGC were reviewed, including glass and melt transition temperatures, degree of crystallinity, solubility and interaction parameters, surface area and adsorption isotherms. A plot of *ln* Vg versus 1/T illustrates the phase transitions of a semi-crystalline polymer (Figure 1.29).

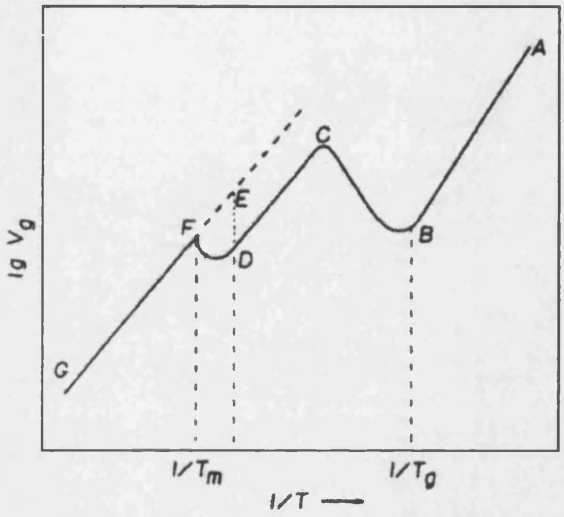

Figure 1.29 Retention diagram for a semi-crystalline polymer.

Segment AB represents the polymer below the glass transition temperature (T_g). Retention is due to condensation and adsorption onto the polymer surface, as the probe is unable to diffuse into the bulk polymer. The first deviation from linearity is interpreted as the T_g. Theoretically this represents the first detectable contribution from bulk sorption to the total retention volume. Region BC represents non-equilibrium absorption of the probe into the bulk phase. Diffusion is slow, with bulk contributions increasing up to point C. The maximum is reached when the increase in bulk sorption due to the increase in probe diffusion constant is balanced by the decrease in retention time due to increased probe volatility. Section CD represents equilibrium absorption of the probe molecules in the amorphous phase. Contributions to retention volume arise from surface adsorption, bulk absorption and surface condensation. Region DF represents melting, with the final linear portion of the plot attributed to sorption in the amorphous polymer.

Copolymers have been studied extensively. These include ethylene vinyl acetate (EVA)[64], ethylene vinyl alcohol (EVOH)[65], ethylene-propylene dienes[66] and chloroprene with methyl methacrylate and methacrylic acid[67]. Changes in surface properties of dimethacrylates with annealing have been measured[68].

The use of IGC in determining solubility of polymers extends back to the work of Smidsrod and Guillet in 1969. Since that time it has been refined and updated enabling its use in the measurement of interaction parameters. Di-Paola-Baranyi and Guillet applied the method to polystyrene and polybutyl methacrylate[69]. The solubility of a host of other polymers has since been measured by IGC. These include polydimethylsiloxane (PDMS) and rubber[37], PDMS and organic solvents[70], polyelectrolytes[71], poly (p-naphthalene-2 (β) sulphonyl styrene)[72], PVC- PMMA blends[73] PVAC and PS-toluene systems[74] and surfactants[75],[76].

Munk and Tian[77] measured interaction parameters and their components for a large number of polymer systems by IGC at infinite dilution. The results serve as a useful data source for future work.

Shiyao et al. used IGC for the assessment of gas and vapour permeation through polymeric membranes[78] for filtration and separation. Permeability of rigid PVC was considered by a similar technique[79]. The degree of fusion of PVC is dependent upon processing history. The relative degree of fusion, assessed by degree of permeability, was quantified by the retention volumes of alkane probes.

Interactions within polymer composites, based on coated glass fibres in a cured epoxy resin matrix, were assessed by measurement of both the Flory-Huggins and solubility parameters. The method was applied to amine[80] and anhydride cured epoxy resins[81] and polydimethysiloxane-methyl ethyl ketone systems[82]. Estimations were found to be in good agreement with other methods. The same thermodynamic parameters may be used to determine the degree of cross-linking in a polymer network[83]. Solubility parameters have also been measured for PMMA and polymethylstyrene[84] and styrene butadiene[85].

Having assured the accuracy of interaction measurements for two-component systems over a wide temperature range, the technique was extended to more complex systems. Numerous systems have been studied including polystyrene blends[86,87,88,89,90,91,92,93] polydimethyl phenylene oxide blends[94], PVC blends[95], polymethacrylate blends[96], polyethylene with oligoesters[97] and conducting polymer blends[98]. The diffusion coefficients of several polar probes in polyisobutylene were measured by Seong et al.[99].

These results were compared with data from gravimetric and spectroscopic analysis and found to agree well. Diffusion coefficients have also been measured for polybutadiene[100] and alcohols in EVOH copolymers[101]. A comparative method between characteristic energy interaction density (CEID) and IGC has been developed, exemplified by polyether mixtures[102]. CEID was found to be temperature dependent and the dominant role of CEID in mixture miscibility was demonstrated.

El-Himbri et al.[103] found that the retention volumes were not related solely to adsorption effects, but were also influenced by probe polarity. Thus for example, the retention volumes of alkanes were found to be independent of probe concentration, but polar probes were strongly dependent. This behaviour was considered to be due to retention on the "inert" support. The investigation included twenty-five different probes. Suggestions for experimental modifications are given, some of which have since been adopted. The most significant change was in the mode of coating the polymer onto an inert packing. Traditionally the polymer sample is deposited onto the support in solution using slow solvent evaporation. The revised technique, known as the "partial soaking method"[104] allows the exact mass of the polymer coating to be determined. Improvements were also made to the flow rate measurement and data acquisition system.

Vapour probe variability was also addressed by Shi and Schreiber[105,106]. They suggested that probe dependence for solubility parameters was due to differences between the bulk and surface compositions of the stationary phase. They developed a method of estimating the effective composition of the surface region, dramatically reducing this dependence. Temperature related variations in polypropylene and a fluorochemical processing aid were also considered.

Fluoropolymers were studied further in non-olefinic polymers systems[107]. Differences in apparent melt viscosity were correlated with acid-base characteristics of the polymers.

Several authors have used IGC to monitor the phase changes and kinetics of polymerisation. Tripathy et al. studied the polymerisation of bismaleimidodiphenyl methane and compared data with those obtained from DSC[108]. Aromatic polyesters, prepared by high temperature solution polycondensation were analysed by Dieckmann et al.[109]. Panda and coworkers determined the glass transition temperatures of a number of industrial polymers, including PMMA and polycarbonate[110]. Several different methods for the exact determination of T_g were investigated, and two new methods proposed.

Acid/Base Characteristics

The work of Fowkes on acid/base characterisation can be linked directly with the study of adhesive forces in multiphase systems. When polar adsorbates are used, dispersive and acid/base interactions contribute independently to the total interaction between adsorbent and adsorbate. In evaluating specific interactions, the dispersive forces may be determined from retention of n-alkanes. The introduction of polar probes onto the chromatographic column gives rise to higher retention volumes due to dual adsorption contributions. The donor/acceptor characteristics of strongly acidic and strongly basic probes may be found from published data[41]. By finding the specific enthalpy of adsorption, $\Delta H_{specific}$, the acid/base nature of the substrate may be determined using the method defined by Saint-Flour and Papirer[39, 40].

The method has been used widely to describe adhesion in multicomponent systems. Schultz and Lavielle[111] equated carbon-fibre-matrix adhesion to acid/base interactions. Similarly, Bolvari and Ward[112] considered the surface modifications of carbon fibres with coupling agents. The acid-base interaction parameters of two polybenzoxazines have been studied[113]. These properties were found to influence the adsorption of the polymers onto substrates such as alumina and fumed silica.

Schreiber et al. used the technique extensively for polycarbonates[114], styrene/maleic anhydride[115], and styrene/vinyl pyridine copolymers[116]. The latter were considered above and below the T_g[117] and extended to similar studies for styrene-butadiene rubber[118]. Other rubbers have been analysed by IGC, including polyisoprene/polybutadiene[119] and cis-butadiene[120]. Using IGC, three copolymers with different emulsification efficiencies were characterised[121]. Acid-base data for an immiscible blend of PE and PVC were used to predict the modifying potential of emulsifying agents. A useful review from Schreiber et al. summarises these and earlier findings, taking into account polymer system formulations[122].

Polypyrrole was used as an example for a novel empirical GC method by Chehimi and Pigois-Landreau[123]. The method was based on the determination of ΔH^d_{vap}, the dispersive contribution to the enthalpy of vaporisation of the probes, to assess acid/base and gas/solid interactions. Data were compared with published works of Papirer, Sawyer and Schultz and found to be in good agreement. The study was later extended to other intrinsically conducting polymer powders and nanocomposites[124]. Acid-base parameters have also been reported for polyethers[125] and other polypyrroles[126].

1.5.4 *Other polymer applications*

Although emphasis for IGC evaluations has been on blends and composites, the method has also been applied to a number of novel polymers. Thomas and Williams[127] considered thin polymeric films of PMMA, PS and PVC on Kevlar fibres. Using finite probe concentrations, Kevlar fibres have also been studied by Rebouillat et al.[128].

Liquid crystals with varying side-chains were analysed by Price and Shillcock[129] amongst others. Phase transitions in liquid crystals determined by DSC were correlated with chromatographic results. The method could be extended to calculate the enthalpy and entropy of mixing for these transitions. Liquid crystals have since been analysed by Tovar et al.[130]. Tan and Vansco studied the microstructure of amorphous polymers by using different molecular probes at finite dilution[131].

1.5.5 *Minerals*

Following polymer characterisation by IGC, interest was raised in the interaction of additives within these, and other matrices. Additives may be either naturally occurring minerals such as calcium carbonate or talc, or synthetics such as glass and carbon fibres. Inorganic fillers are commonly incorporated into thermoplastics to bulk out the polymer, and, in some cases, as functional additives to enhance certain physical properties such as stiffness and impact strength (as detailed in section 1.2).

Calcium Carbonate

By far the greatest number of papers have come from the research base of Eugine Papirer at the Centre de Recherches sur la Physico-Chimie des Surface Solid, Mulhouse, France. Papirer, Schultz and Turchi evaluated the surface modification of calcium carbonate by stearic acid[132]. Surface energy values for varying stearate coverage were determined by contact angle techniques and compared with chromatographic data. They found that IGC at infinite dilution could be used to accurately measure the dispersive component of the mineral and its reduction in the presence of stearic acid. By using polar probes the acidic and basic sites were also identified.

The surface properties of calcium carbonate were also analysed in greater detail by Schmitt and co-workers[133]. The procedure of Papirer was followed, with the calcium carbonate being firstly agglomerated under pressure before being sieved and packed into a stainless steel column. The total adsorption behaviour of n-alkanes was found to be quite similar for stearic acid and non-treated minerals. However, the entropy contributions were different. The affinity of the treated sample was believed to be due to gas-solid adsorption and gas-liquid interactions for the modified sample. Where long-chain probes having eight or more carbon atoms were used, the loss of entropy was smaller than for the shorter chains. This was explained in terms of the insertion of the chains in between the stearyl grafts. Longer chains were believed to only partially insert, maintaining a higher degree of freedom.

Similar results were obtained by Okonkwo et al. for precipitated calcium carbonate (PCC)[134], although the surface modification required for monolayer coverage was found to be much higher due to increased surface area. Ahsan and Taylor measured surface energetics of calcium carbonates, also modified with stearic acid[135], and in a preliminary study found some correlation with impact data in polypropylene systems.

Various forms of calcium carbonate were studied by Keller and Luner[136]. The surface energies of chalk, marble and PCC were determined in terms of the dispersive component of the surface free energy, and the differential enthalpy of adsorption. The results were equated to physisorbed and chemisorbed water bound at the surface and within the pore structure. By elevating the temperature, the surface free energies were increased due to the removal of bound water. Differences in the surface energetics of the three calcium carbonate forms were also observed. The chalk samples interacted most strongly with the alkane probes, with PCCs interacting the least. These differences were suggested to be due to the presence of impurities in the chalks.

The modifying agents for calcium carbonate were scrutinised by Balard, Papirer et al [137]. Calcite was treated with stearic, undecylenic and linoleic acids and a carboxylated polybutadiene (PB) before surface evaluation by IGC. The influence of temperatures was also noted. They found the dispersive component of the surface free energy for stearic acid-treated calcite was strongly dependent upon surface coverage, whereas undecylenic and linoleic acids were less dependent, due to steric hindrance of the more bulky molecules. Additionally, results for the higher acids were unaffected by elevated temperatures whereas the chemisorption of stearic acid was decreased significantly. Zaborski et al. considered calcium carbonate modified with monomaleates, along with other fillers including silica and zinc oxide[138].

Soils

An experimental variation of IGC, known as the elution of characteristic points (ECP) was used by Steinberg and Kreamer to measure the sorption of a vapour probe on calcareous soils from Southern Nevada[139].

The dried soil was treated with a number of volatile organic compounds (VOCs) and the vapour phase sorption measured. Sorption isotherms were found to be non-linear, with finite desorption kinetics contributing to tailing chromatographic peaks. Competitive sorption between VOCs and water was examined by adding water to the carrier gas via an in-line reservoir. Steinberg and Kreamer found this dramatically decreased the sorption of non-hydrogen bonded VOCs in the soil and eliminated the effect of finite sorption kinetics. Those compounds, which exhibited hydrogen bonding, still exhibited non-linear sorption isotherms.

The method was also employed in the determination of vapour adsorption of trichloroethylene on quartz sands[140]. Static equilibrium sorption measurements were compared with IGC results and found to be similar. Static methods were less precise, but were more usable over a range of porosities and moisture contents.

Clays

Clay minerals have been studied, using IGC, with an emphasis on determining the effect of chemical modification. Smectites are layered clay minerals, which expand with specific interlayer spacings. They may be intercalated with ionic species. Bandosz et al.[141] introduced large metal polycations into the interlayer space of clay minerals using ion exchange. After calcination the cationic spacers or "pillars" were oxidised. The products were considered useful for catalysts, adsorbents or molecular sieves. Alkane and alkene probes were used to define the acidic properties of smectites before and after intercalation. After calcination, the Lewis acid sites were reduced, decreasing π-bonding interactions. The study was extended to include polymerisation and carbonisation[142]. The modifications could be monitored at each stage. Montmorillonite and hydrotalcite matrices were also modified by a similar technique and the sorption properties characterised [143],[144].

The application of IGC in surface area determination has been described in detail[145]. Data were compared with BET measurements and found to be in excellent agreement. Illites and kaolinites are important in the petrochemical industry. The clays comprise the majority of subsoils in oilfields, and their wettability is considered to be related to the retention of heavy oils.

Saada et al. used IGC to determine surface energy characteristics for minerals of various origins and differing water adsorptions[146],[147]. Other minerals which have been included in studies are ground mica[148], talcs[149] and titanium dioxide[150],[151],[152],[153],[154].

1.5.6 *Synthetic Fillers*

In a series of papers Saint-Flour and Papirer described their ground-breaking work on the measurement of the surface free energy of short glass fibres[39],[40]. The difficulties of packing a column with such fibres are considered and a stainless steel was proposed for future work. Adsorption isotherms, using retention theory at infinite and finite dilution showed good reproducibility. The study was extended to polar probes for the first time in this area and equated to the donor/acceptor character of the fibres. Following on from this work, glass and carbon fibres were analysed by Schreiber and co-workers[155],[156], Papirer and Balard[157] and others [158],[159],[160],[161],[162],[163],[164]. The latter by Allington et al. is an interesting comparison between IGC measurement and simulated atomic adsorption of small molecules onto functionalised carbon fibres.

Silicas

Silicas have been studied extensively. In a paper by Hadjar, Balard and Papirer[165] amorphous and crystalline silicas were evaluated. Interestingly, branched and linear alkane retention data were compared and used to produce an index of morphology (I_m). The index represented the percentage of solid surface accessible by branched alkane probes. The reference was a fumed silica known to have a flat surface profile at a molecular level.

Synthetic silicas, modified by heat or chemical treatment, have been analysed[166],[167],[168]. The use of very small molecular probes such as argon, carbon monoxide and methane at sub-ambient temperatures permitted investigation of the molecular motions of alkyl grafts on the silica surface. At the lowest temperature, movement was found to be due to the methyl end group. As the temperature increased, the main chain became partially mobile, and eventually obtained complete mobility. Silicas surface-treated with chlorosilanes, amines and esters have been considered [169] and molecular modelling has been used to compliment the technique[170].

Applying the finite concentration method Jagiello et al. characterised silicas in terms of the adsorption energy distribution function[171]. Two important procedures are described, the multiple injection and the single peak method. The multiple injection technique assumes the system is in equilibrium, that is: the temperature of the whole column; the volume and rate of carrier gas; and the volume of solute are all equal at any point in the column. Having established a linear response, a single peak may be analysed. Once the peak is obtained it may be divided into *i* number of sections, corresponding to *i* pressures and volumes. From these sections, an adsorption isotherm may be constructed.

Both of the above methods were applied, with mathematical treatments, to obtain adsorption energy distributions for a number of treated silicas. Bimodal distributions were observed, and considered to correspond to two types of energy sites at the surface. Treatment with methanol and hexadecanol shifted and sharpened the distribution peaks. This was believed to reflect increasing homogeneity and steric hindrance. The technique was thus proved capable of describing interactions on a surface and their associated physicochemical modifications.

Adsorption energy distributions of silicas were also determined from their chromatographic retention data by Putyera et al.[172]. In this case, capillary columns were used in tandem. Samples were prepared in a dimethylsulphoxide suspension and forced, under pressure, through a capillary column. The probe was split between a calibration column and a test column. The split was constant, and found from the ratio of the gas flow rates through the two columns. The use of capillary columns was believed to minimise the effects of dispersion and mass transfer kinetics. Data matched well with theoretical models of the silicas studied.

Other Synthetic Materials

Carbon blacks and activated carbons have been studied extensively, a small selection of which is included in this review. A few papers were found to be of interest, most notably that of Lopez-Garzon et al., describing the effect of porosity upon the calculated surface free energy of active carbons[173]. Data obtained by IGC were found to be consistently higher than those obtained by other methods.

They reasoned that surface curvature of the pores was having a marked effect on the retention of probe molecules. Corrections for the free energy of a methyl group adsorbed into a pore, compared with the free energy of the methyl group adsorbed onto a flat surface were applied. The surface free energy results obtained were significantly reduced, but in good agreement with data from other techniques. The study highlighted the limitations of the method when applied to highly porous systems.

Other materials studied include those used in the paper industry, notably polysaccharides and lignins[174], amorphous cellulose[175] and pulp fibre[176].

The acid/base characteristics of synthetic materials can be used to predict their interactions in multi-phase systems. These interactions are of primary importance in polymer-filler interactions. Literature relating specifically to acid/base interactions for these materials includes studies of glass fibres[177], glass beads[178], microcrystalline cellulose and wood pulp fibre[179] and graphite[180]. The latter by Donnet, Park and Balard takes into account the deformation polarizability of the molecule. Again, inaccuracies of measuring surface energies of high surface area particles were emphasised.

Graphite exhibits a relatively high dispersive component of surface energy. A number of workers observed both weak and strong polar probes as lying below the reference line for n-alkanes. Returning to first principles, the contribution for polarizability was considered.

Many of the inaccuracies during calculation of interaction parameters are derived from the elevated temperatures at which experiments are carried out. Deformation polarizibility is independent of temperature. Thus, using equations derived from polarizibility, more accurate measurements were obtained. The method was proven using graphite substrates and polar probes.

A study of wood fibres and polymers by Shen et al. compares IGC acid-base characterisation results with those obtained from contact angle measurement using the Good-van Oss theory[181]. The two methods both had limitations, and reservations were expressed as to the suitability of acid-base estimation by contact angle measurement.

1.5.7 *Polymer-filler interactions*

Having discussed polymers and fillers in isolation, the interactions between the two have also been studied using IGC. In the forefront of this area is Henry Schreiber, whose review[182] underlines the fundamental aspects of the method. He illustrates the technique with multi-component polymer systems. The interaction effects were related to end properties of pigmented epoxy resins.

Polymer-filler interactions for calcium carbonate-filled polyvinyl chloride (PVC) and polyethylene (PE) systems have been measured by Schreiber et al.[183].

They found the ease of dispersion of fillers in the polymer matrices was related to acid/base interactions in the polymer-filler pairs. These were equated to mechanical properties of the end products. The method was considered useful for optimising surface modification of fillers for specific polymers.

Similar studies followed this work. Surface-treated calcium carbonate in a PVC matrix was irradiated with gamma rays under different atmospheres[184]. The mechanical properties of test pieces were determined and compared with interactions deduced chromatographically. The adsorption of styrene/vinyl pyridine co-polymer onto rutile (TiO_2) is another such example[185].

Further works include interactions in: sepiolite-filled PVF-PS (polyvinyl fluoride-polystyrene) blends[186]; silica gel in PMMA (polymethyl methacrylate)[187, 188]; silica in acrylonitrile-butadiene rubber[189] and polydimethylsiloxane[190]; metals in polyesters[191]; cellulose[192],[193],[194] and carbon fibres in epoxy resins[109],[195],[196],[197].

The methods used for determining polymer-filler interactions have been scrutinised by Farfard et al.[198]. Pigments of rutile and Parylene blue used in polycarbonate and polystyrene were subjected to surface analysis at infinite and finite dilutions. Varying polymer concentrations were coated onto inert, solid supports. The study demonstrated that conventional quantities of polymer gave data comparable with previous work. Thin layers (< 0.1μm) however, possessed different surface properties.

In this case, interactions at the polymer-support interface strongly affected the characteristics of the exposed polymer surface. The heterogeneities of both pigment and polymer surface were seen to vary with injection volume. The finite volume technique was thus considered suitable for heterogeneic studies and polar sites.

1.5.8 *Miscellaneous applications*

The majority of investigations using IGC have related to polymer and/or filler systems. However, the technique has been applied to more novel areas. Although too many to be considered individually, a few papers are detailed.

In an interesting variation, interactions relating to polymer-paper adhesion were considered[199]. A review, by Borch, studied the bond strength of polymers on uncoated paper surfaces. Adhesion is classically measured by paper laminate or tape peel testing. Borch describes the factors affecting adhesion and the role of thermodynamic parameters.

By comparing data derived from mechanical tests with data acquired by chromatographic means, the two were shown to be interdependent, just as those of polymer-inorganic filler systems. In another paper application, the influence of latex binders on paper pulp and filler interactions was studied[200].

Balard and Papirer have considered thermodynamic investigations of fillers for paints and coatings[201]. By dividing the surface energy into dispersive and specific components, the acid-base interactions were measured. Various inorganic fillers were characterised by IGC and treatments by heat and chemical modifiers were considered. Results were equated to the use of minerals in paint.

Surface coatings of, for example, titanium dioxide with silica, aluminium and zinc oxides are commonly used to prevent chalking of paints. IGC was used to measure the degree and type of coating on titania, and optimise treatments for cost-effective products. Although touched upon, details of interactions in real paint systems were not included.

In contrast, IGC at high dilution and finite probe concentrations was used to study real paint formulations by Ziani et al.[202]. The fundamental thermodynamic interaction data were used to optimise performance aspects of protective coatings. Paint formulations have also been studied by other authors[203].

Pharmaceutical powders are manufactured to very rigorous standards. Contact angle measurement has been used to determine surface variability. IGC was applied to the determination of surface energetics of salbutamol sulphate[46].

Two batches were compared and found to vary considerably in terms of dispersive and specific components of surface energy. These differences were not highlighted by conventional means. Following the study, IGC was suggested as an effective quality control technique for pharmaceutical products.

Other surface modifications have been considered. One such example is the use of silane adhesion promoters in polyurethane adhesives[204]. Thermodynamic data were related to initial and residual bond strengths on different substrates.

Surface-treated aluminium is used in a large number of applications. The oxide surface of aluminium, conditioned at two different temperatures, has been studied[205].
The values obtained by IGC for specific interaction energies were related to the anodising conditions needed for good surface coverage. Again, the method was used to optimise substrate treatment conditions by methodical rather than empirical means.

1.5.9 *Conclusions*

From the rapidly expanding application of IGC, the technique has been demonstrated as invaluable in the repertoire of physicochemical methods. In isolation, it can be used to quantify thermodynamic components, both apolar and polar. In conjunction with other spectroscopic methods, IGC becomes a vital tool in structural elucidation.

For polymer applications, interaction enthalpies can be measured at concentrations far greater than conventional methods. Temperature dependent parameters can be determined directly, rather than extrapolated. Diffusion of liquids in single and multi-phase polymer systems can be investigated with relative ease across a broad temperature range, and solubility parameters can be measured as composition is varied.

In more complex polymer systems, such as those containing reinforcing fibres or particulates, each component may be studied individually or in combination. IGC data can then be related to the mechanical properties of the composites and used to predict the behaviour of new combinations. The compatibility of coupling aids and surface modifiers can also be quantified, by considering polar interactions and steric alignment of molecules.

Mineral studies have highlighted differences due to processing and environmental effects. Minor additives or impurities are known to have considerable impact on certain key properties when the minerals are used as fillers and, binders or on substrates such as paper.

The limitations of absolute data have been discussed by a number of workers and the caution they sound must be heeded. Its use in polymer-related fields has been emphasised in this review. One should not, however, overlook its usefulness in other areas.

IGC has been used successfully in determining the surface characteristics of a wide range of materials, from polymers to silicas and soils. These data have then been applied to modify and improve surface treatments and optimise coatings and coupling agents. The method has been applied for quality control, especially in high-specification applications such as the pharmaceutical and electro-coatings industries. IGC has been used to predict the compatibility of polymer blends and mixtures, and thus their physical properties.

In all of these cases, the method has been applied to quantify thermophysical properties, that could not be measured easily, or accurately by other means. IGC was thus considered ideal for studying the thermodynamics of polymer composites, in relation to industrial applications, the aims and objectives of which are given in section 1.6.

1.6 **Aims and objectives**

The aim of the study was to apply IGC to polymers, minerals and their composites in order to predict physical properties for selected applications. After initial studies on model systems, the method was applied to those of industrial significance. Key physical properties were measured. The surface chemistry measurements were then considered in the context of the composite properties.

The objective was to set up and validate an IGC instrument, confirming its suitability by studying materials already documented in the literature and then to study novel applications. The detailed objectives were

1. To modify a GC instrument for use as an IGC system in the laboratory.

2. To validate the instrument with a known polymer (polystyrene).

3. To measure the thermodynamic data of a pure inorganic filler (calcium carbonate) and a polymer (polypropylene) and compare these with literature values, to confirm the accuracy of the instrumentation.

4. To measure key physical properties of a composite (calcium carbonate/polypropylene) and correlate these with the thermodynamic data.

5. To study mineral systems, including kaolinite and calcined kaolinite, not previously studied by IGC.

6. To assess the suitability of calculation methods to determine specific surface interactions and make recommendations for future use.

7. To study calcined clays with minor differences in composition and relate these to key physical property differences in a polymer system (polyethylene).

8. To assess the suitability of IGC for measuring surface modifications of silane-treated calcined clays and related these to the physical properties of a composite matrix (polyamide).

2 EXPERIMENTAL TECHNIQUES

2.1 Instrumentation and Construction

2.1.0 Introduction

IGC is carried out using a modified conventional gas chromatograph (Figure 1.27, section 1.4). These modifications are necessary for accurate data acquisition. Measurement of gas flow rates, pressure drops across the column and temperatures all require external calibration to minimise errors.

The choice of detector is dependent on the nature of the probes. Flame Ionisation Detectors (FIDs) are most commonly used, as these are capable of detecting most organic compounds. Their response is over seven orders of magnitude, down to around 4 pg sec^{-1}. A FID may be used in tandem with a Thermal Conductivity Detector (TCD), placed before it in the effluent stream. The TCD is non-destructive and non-discriminating and can detect compounds such as water, undetectable by the FID.

The carrier gas is usually helium, hydrogen or nitrogen. Pressure at the inlet has classically been measured by a mercury manometer, although a digital pressure transducer is also suitable. The outlet is open to the atmosphere.

An accurate barometric reading, by mercury or precision aneroid barometer, is used to calculate the pressure drop along the column. Gas flow rates are measured by means of a flowmeter at the column outlet, purged with carrier gas prior to readings being taken. This prevents inaccuracies due to the diffusion of gas at low flow rates.

The oven temperature, although maintained within 0.5 °C by the thermostatic control of the GC, should be checked independently with a calibrated thermometer, such as a platinum resistance thermometer.

The chromatographic column is the heart of the equipment. Packed columns are most commonly used, although capillary columns have also been used for polymer applications. Packed columns are usually made of stainless steel or copper, varying in length from 300 to 1600 mm with a 0.2 to 6 mm internal diameter.

Injection of the probes has typically been through standard microsyringes. However, with advancements in GC equipment, programmable injectors and autosamplers have reduced sampling time and errors in the injection process. An inlet splitter or split injector is used with capillary columns. This is necessary to prevent excessive peak broadening.

Data may be collected either manually or fed directly into some form of processor. Modern GCs are controlled through a computer interface, and are capable of recording experimental conditions and results simultaneously.

As with conventional GC, IGC columns must be packed uniformly, without air pockets. A comprehensive review of column preparation is given by Voekel[51]. For polymers, the material under investigation is dissolved in a high vapour pressure solvent and deposited onto an inert medium such as glass beads or a traditional chromatographic support. An acid-washed, dimethylchlorosilane treated support, such as Chromasorb W is widely used, at a loading of 15 wt.% on the stationary phase. The weight of polymer on the support is determined by ashing in a thermogravimetric analyser (TGA) or by Soxhlet extraction.

Fine minerals can be packed into columns without support, but require agglomeration to produce sufficiently large particles for reasonable gas flow. Typically, minerals are compressed in a high pressure die (such as that used for preparation of potassium bromide discs for Infrared analysis). The cake is then crumbled and sieved to a size fraction suitable for column packing[206],[207]. Any large agglomerates or fines not removed in this process reduce packing efficiency, and cause peak tailing. Fibres, such as glass or carbon can be chopped, sieved and poured into the column or whole lengths may be threaded through the tubing, and trimmed to size[208],[39],[40].

Capillary columns have limited use in IGC and are restricted principally to studies of polymers. Fused silica tubing is coated with the polymer either by forcing a volatile solution through the column under inert positive pressure which consequently dries the material onto the wall (the "dynamic" technique) or by filling the column with a coating solution of the required concentration (the "static" technique). After sealing one end of the tube, the solvent is gradually removed by evaporation over several days. Once packed and installed, the column should be conditioned before use, typically at elevated temperatures of 100 to 150 °C for 4 to 24 hours. This ensures that all lower temperature volatiles are removed, although care must be taken to prevent modification of the substrate.

Probe choice is governed by the thermodynamic properties under investigation. Linear alkanes have been used extensively for the determination of fundamental surface energy components. By introducing probes with varying acidity or basicity, the acid-base interactions of the substrate are found[122]. For studying polymer blends and determining polymer-polymer interactions, a much wider range of probes with varying polarities is used[103]. Polar probes must, however, be chosen with care, as excessive retention times or peak tailing may give erroneous results.

The oven is maintained at a predetermined temperature and an unreactive probe (often methane) is injected as a marker (Figure 2.1). This allows the determination of the column "dead time" (t_n, the length of time taken for a non-adsorbing species to pass through the column). The probes are then introduced individually in very small quantities (between 10 to 100 nmol).

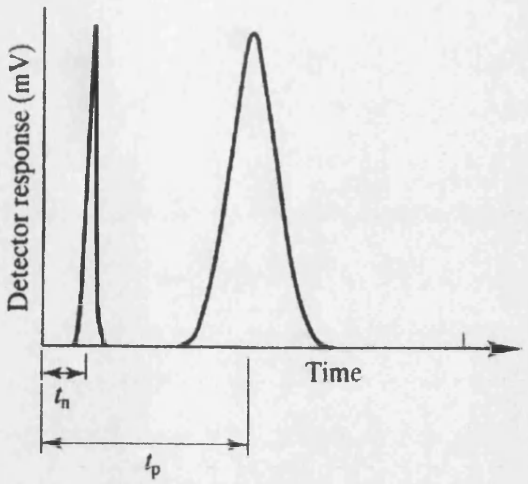

Figure 2.1 Plot of GC detector response versus retention time of a linear alkane and an inert marker (methane).

The specific retention time, t_p, is recorded and corrected for "dead time". Adjustments must also be made for compressibility of the carrier gas. Data are usually extrapolated to zero flow rate, although the validity of this method has been questioned[209],[210]. Correction of specific retention volumes for solute-column wall interactions has been found to be beneficial[211].

2.1.1 *Instrument modification and calibration*

A Perkin-Elmer Autosystem XL was used in all the studies (Figure 2.2). The instrument was fitted with an autosampler, and a tandem TCD/FID. The FID was used in all studies. Instrumental readouts included the direct pressure drop across the column, the carrier gas flow rate and the oven temperature. The instrument was modified to allow independent gas flow and pressure (Figure 2.3), and oven temperature (Figure 2.4) readings. Looped-valve tubing before the column inlet permitted inlet pressure and flow to be measured with a solid state dual flow and pressure meter (an FP-407 from Chrompack International). This was calibrated at the factory, and the certified data used.

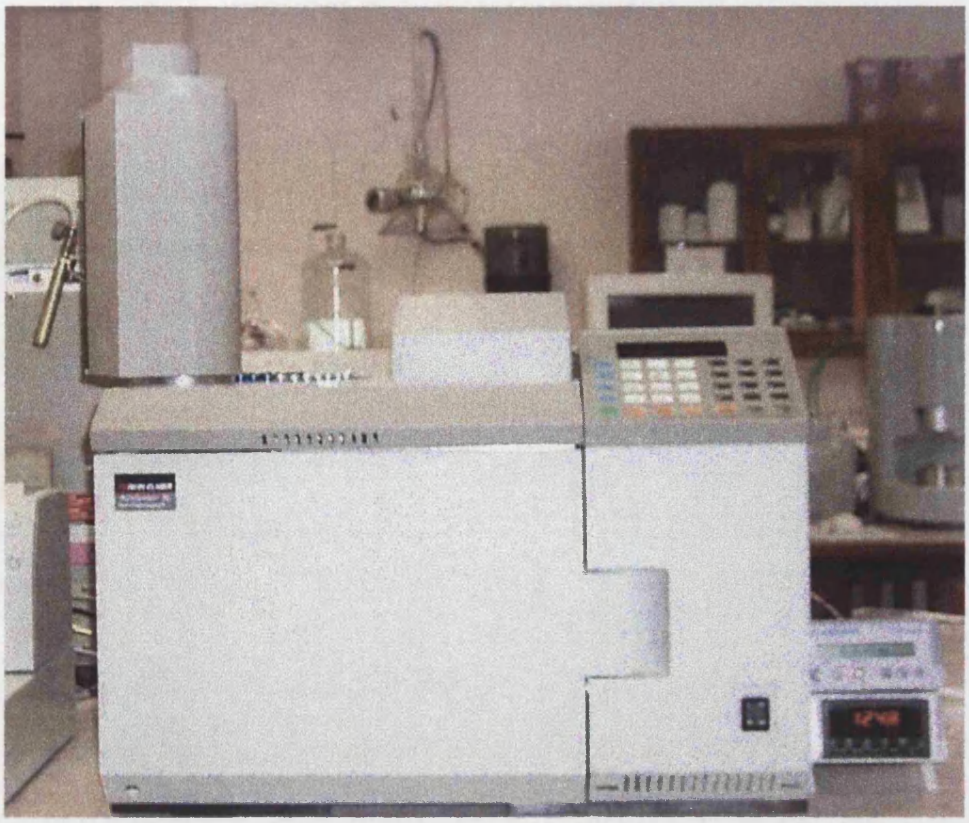

Figure 2.2 The modified gas chromatograph, with pressure/flowmeter and temperature gauge to the right.

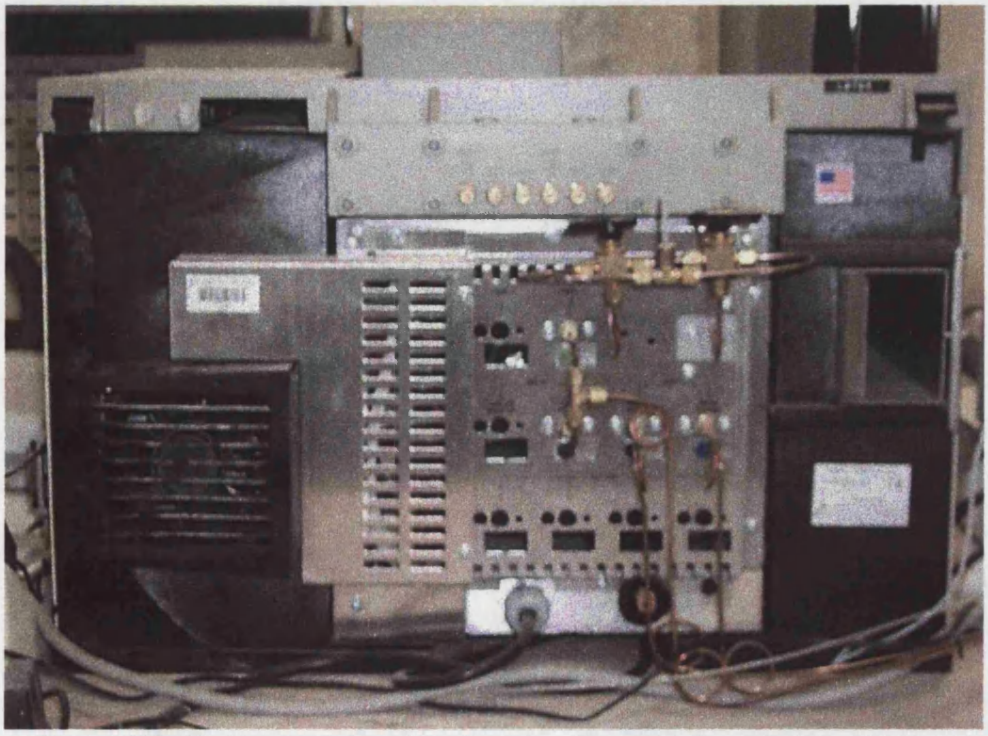

Figure 2.3 The back of the IGC apparatus showing the looped valve system.

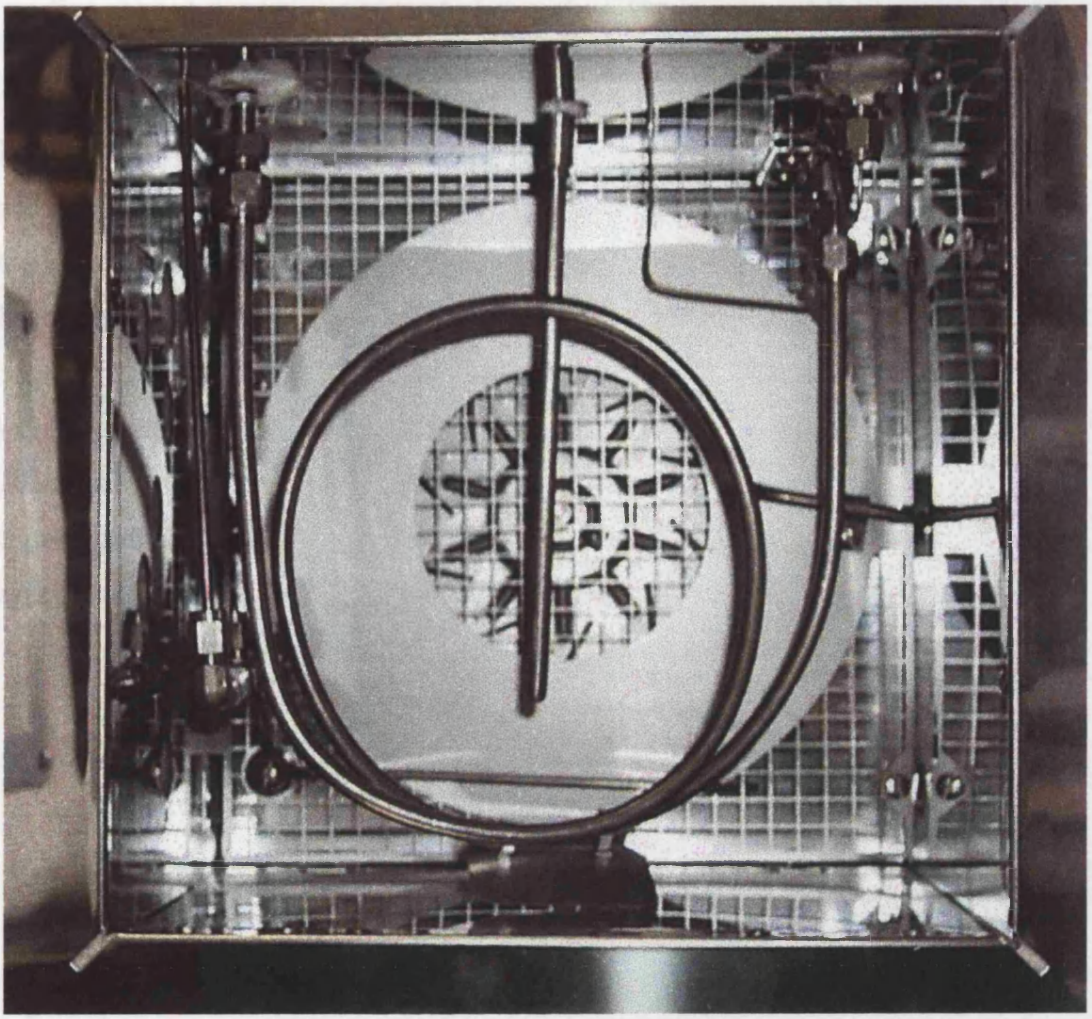

Figure 2.4 The interior of the oven, showing the coiled stainless steel column and vertical temperature probe.

During data collection, the valves were closed, and the carrier gas allowed to flow through the column. At the beginning and end of each run the valves were opened, and pressure and flow readings measured using an independent flow meter.

Gas flow was calibrated from 0 to 80 cm^3 min^{-1} at 5 cm^3 min^{-1} intervals. The carrier gas used was "white spot" nitrogen from BDH, certified at 99 % purity. Gas was passed through a Perkin-Elmer three-stage drying and purification system, before entering the chromatograph.

A Chrompack RDT thermometer was calibrated by comparison against an NPL calibrated Tinsley Type 5840 platinum resistance thermometer, between 313 K and 353 K, in an isothermal water bath. The true temperature, T was obtained from linear regressions of the data (Figure 2.5).

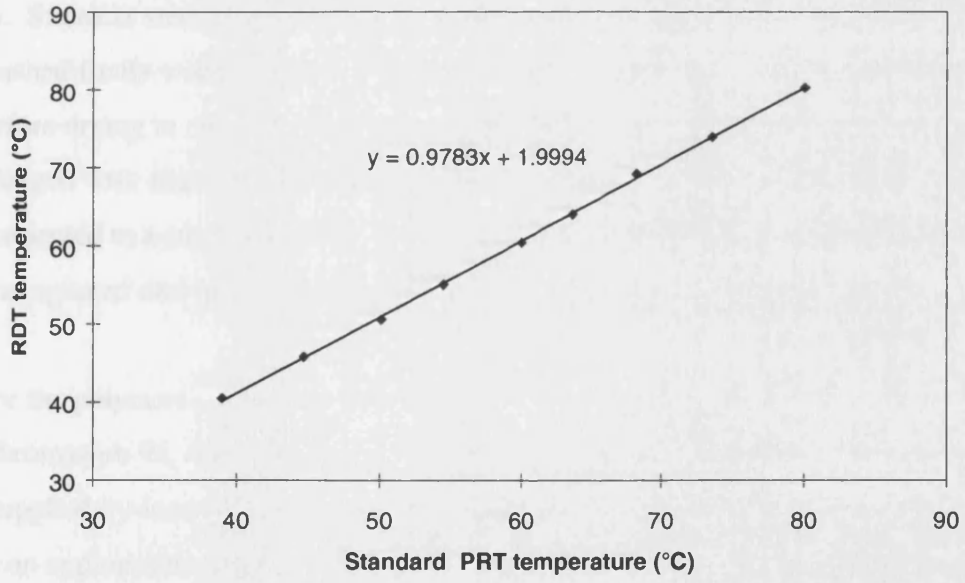

Figure 2.5 Calibration graph for the Chrompack RDT thermometer against a standard platinum resistance thermometer.

The RDT thermometer sensor was placed inside the oven. The GC oven temperature was calibrated, between 303 K and 353 K at 5 K intervals.

The accuracy of temperature measurement was within ± 0.2 °C, and gas flow measurement was within ± 0.3 cm^3 min^{-1}. Two measurements of these parameters were recorded, one set from internal sensors, and the second from external sensors. Corrected temperature and pressure data were used for all calculations. Data from the two were compared during application studies.

Barometric pressure was measured at the beginning and end of each run using a BDH precision aneroid barometer. The mean of the two was used for all calculations. The instrument was located in a temperature-controlled laboratory, maintained at 23 °C ± 1 °C. Instrument modification fulfilled objective 1 of the study.

2.1.2 *Column preparation*

Three techniques were used to prepare columns for the studies in chapters 3 to 7. A copper column, ¼" ED (external diameter), was used for the polystyrene study (chapter 3). Stainless steel columns, ¼" ED, were used in all other studies. The tubing was washed firstly with de-ionised water, then acetone and finally n-hexane (AnalR grade) before drying in an oven at 80 °C. Once dried, the column was coiled and one end was plugged with silanized glass wool before connecting to a vacuum. The open end was connected to a small funnel and the stationary phase introduced gradually. The column was agitated during packing to ensure even distribution of the stationary phase.

For the polymers (with the exception of polyethylene and polyamide) and masterbatches, Chromasorb W, AW DMCS treated, 100-120 mesh, was used as an inert support (supplied by Jones Chromatography). A weighed quantity of the polymer was dissolved in an appropriate solvent and coated onto the Chromasorb W by conventional stirring and rotary evaporation. The coated support was dried in vacuum at 60 °C to a constant weight. The mass of packing was determined by weight loss of the remaining material. The exact loading of the stationary phase was determined by repeat calcination at 1000 °C in a CEM AirWave 7000 microwave furnace and confirmed by Soxhlet extraction.

For the minerals, the compaction technique was used[132]. The material was compacted into 10 mm diameter pellets using an IR pellet press at 20 tonnes pressure. Several pellets were pressed and then crumbled and sieved to retain aggregates of 425 – 850 μm. For polyamide and polypropylene, the polymer granulates were placed in a stainless steel vessel and cooled with liquid nitrogen. The granulates were then ground to an approximate diameter of 0.5 mm. These were sieved to retain aggregates of 425 – 850 μm.

The column was connected to the GC and conditioned at an appropriate temperature for 24 hours. The conditioning temperature depended on the stationary phase. For the minerals, 150 °C was used to remove any low temperature volatiles, such as water. For the polymers, conditioning depended on the thermal stability and glass transition temperature, but was typically 80 to 120 °C. After initial conditioning the column was held at the measurement temperature for a minimum of twelve hours before readings were taken. The second conditioning step was repeated for each temperature change. The precise conditions used are described in chapters 3 to 7.

The surface area of the stationary phase was measured with a Micromeritics Flowsorb II 2300 by the BET, single-point nitrogen adsorption method. Three readings were taken and the mean used in calculations.

2.1.3 *Experimental data*

All probes were chromatographic grade supplied by BDH (UK). 0.1μl aliquots of the vapour phase were injected by Hamilton syringe through the autosampler system. Injector temperature was maintained at 150° C, with the FID at 250 °C.

Retention times were recorded and processed by the PE-Nelson Turbochrom data management software. Methane was used as a non-interacting probe to determine the void volume of the column. Oven temperature, pressure drop across the column and atmospheric pressure were measured as detailed previously (section 2.1.3).

3 VALIDATION WITH POLYSTYRENE

3.0 Introduction

Two studies were undertaken using a polystyrene stationary phase to validate the GC system for polymer analyses. To evaluate its use for determining phase transitions, a single probe was injected across a temperature range. The thermal transitions were compared with literature values. A range of linear alkanes was then injected and the retention times used to calculate the dispersive component of surface free energy. The results were compared with published data.

3.1 Materials

Polystyrene beads, MW 280 000 were obtained from Aldrich Chemicals. Chromasorb W, AW DMCS treated, 100-120 mesh, was used as an inert support.

3.2 Experimental

1.5 g polystyrene was dissolved in chloroform (AnalR grade) and coated onto 15 g Chromasorb W by conventional stirring and rotary evaporation. The column was packed as detailed in section 2.1.3. The exact loading of the stationary phase was determined by repeat calcination and confirmed by Soxhlet extraction. The column was pre-conditioned above the T_g (glass transition temperature) at 150 °C for 24 hours, before further conditioning. Data were collected as detailed in section 2.1.3.

Two studies were undertaken to assess the equipment for future use in determining polymer phase transitions and obtaining surface thermodynamic data. In the first, a single alkane probe, n-dodecane, was injected over a range of temperatures from 60 to 130 °C.

Dodecane was chosen because the retention times were sufficiently long to ensure good accuracy, without any significant skew to the chromatographic peaks. In the second, a series of n-alkanes from C_5 to C_{13} was injected isothermally at two temperatures, above and below the T_g of the stationary phase. Again retention data were obtained, and chromatograms printed to compare deviation of the peaks from Gaussian distribution.

3.3 **Results and discussion**

The percentage coating of polystyrene on the stationary support was determined as 10.81 ± 0.23 % by loss on ignition and 9.85 ± 1.75 % by Soxhlet extraction. The calcination result was used in calculations, due to the much higher standard deviation of the classical method. Adjustment was made for the inert support. Figure 3.1 gives a plot of log of net retention volume versus the reciprocal of absolute temperature for polystyrene.

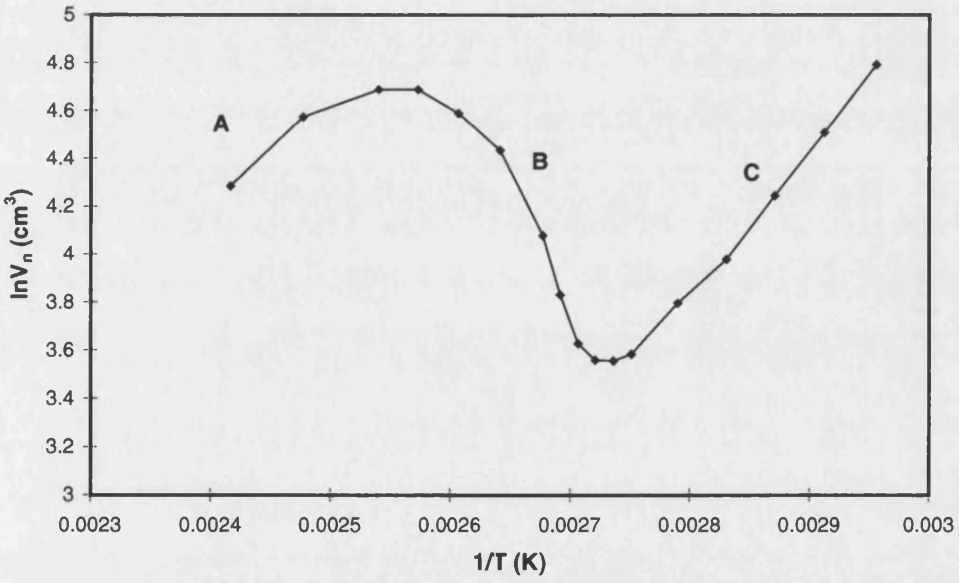

Figure 3.1 Plot of lnV_n versus reciprocal of absolute temperature.

Where no phase transitions occur, the plot would be a straight line. However, in the case of non-crystalline polymers, where glass transition occurs, a characteristic, z-shaped curve is observed (as detailed in section 1.6.3 and illustrated in Figure 1.29). Below the T_g (region C) the equilibrium is dominated by surface adsorption and condensation of the probe onto the polymer surface, since the probe is unable to diffuse into the bulk polymer[37].

The slope of this segment is given by $(\Delta H_v - \Delta H_a)/R$ where ΔH_v is the latent heat of vaporisation of the probe and ΔH_a is the enthalpy of adsorption of the probe on the polymer surface.

The first deviation from linearity corresponds to the T_g (97 °C ± 1 °C). (Literature value given as 98 °C). This represents the first detectable contribution from bulk sorption to the total retention volume. It is attributed to the interaction of the probe with the bulk polymer as it gains limited mobility of the smaller chain segments. As the temperature increases, the non-equilibrium region B is observed. The probe diffuses slowly into the bulk polymer, and the retention volume is dependent on flow rate. Bulk contribution to the retention volume increases up to T_{max} when the rise in bulk sorption is balanced by the decrease in retention time due to probe volatility. After this point, at approximately 115 °C, a second equilibrium region (A) occurs, as the polymer molecules gain full mobility, and the probes interact with all of the molecules. The retention volumes are governed by bulk sorption into the amorphous polymer phase and decrease with increasing temperature.

Below T_g, at zero surface coverage the differential heat of adsorption q_a^0 (equal to $-\Delta H_a^0$) can be calculated from equation (3.1),

$$\frac{d(\ln K_s)}{d(1/T)} = \frac{q_a^0}{R} \qquad (3.1)$$

From the initial linear portion of the curve in Figure 3.1, the slope is defined as $-\Delta H_a^0/R$. The enthalpy of adsorption calculated for n-dodecane is -54.0 ± 0.5 kJ mol^{-1}.

This is the same order of magnitude as the value of -43.9 kJ mol^{-1} obtained for n-heptane on polystyrene at 30 °C as determined by Kontominas et al.[212]. The difference may be due to the slightly lower interaction of high-energy surface sites to dodecane compared with heptane, or the surface itself being less homogenous. Anhang and Gray quote values of –41.9, -46.4 and -51.6 kJ mol^{-1} for octane to decane respectively on polyester film[59]. The enthalpy of adsorption was found to decrease with increasing carbon chain length as this correlates directly with the enthalpy of vapourisation (if no specific interactions occur). Thus the latter explanation is more likely. A low adsorption enthalpy also indicates that the polystyrene surface is energetically homogenous towards saturated alkane adsorption[58]. Thus there is a low concentration of high energy sites on the polystyrene surface.

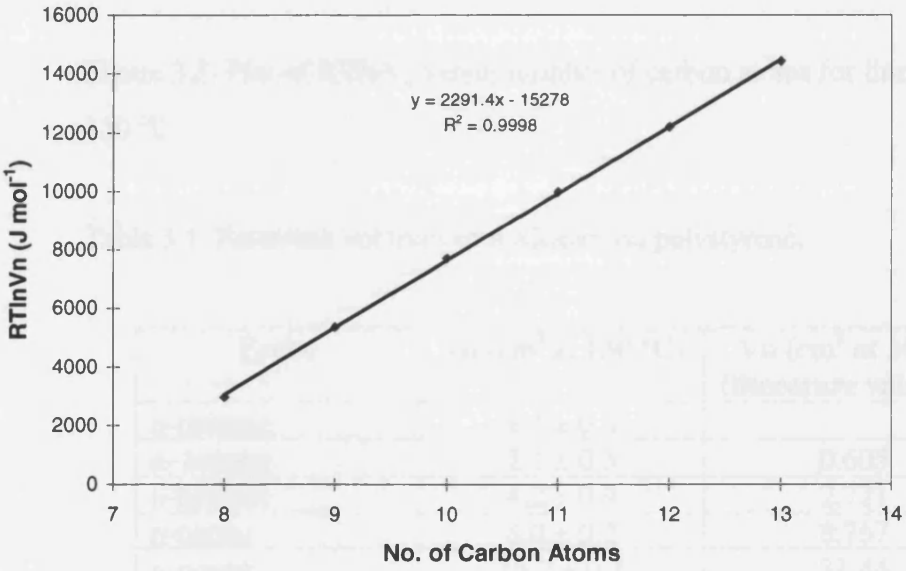

Figure 3.2 Plot of $RT\ln V_n$ versus number of carbon atoms for linear alkanes at 75 °C.

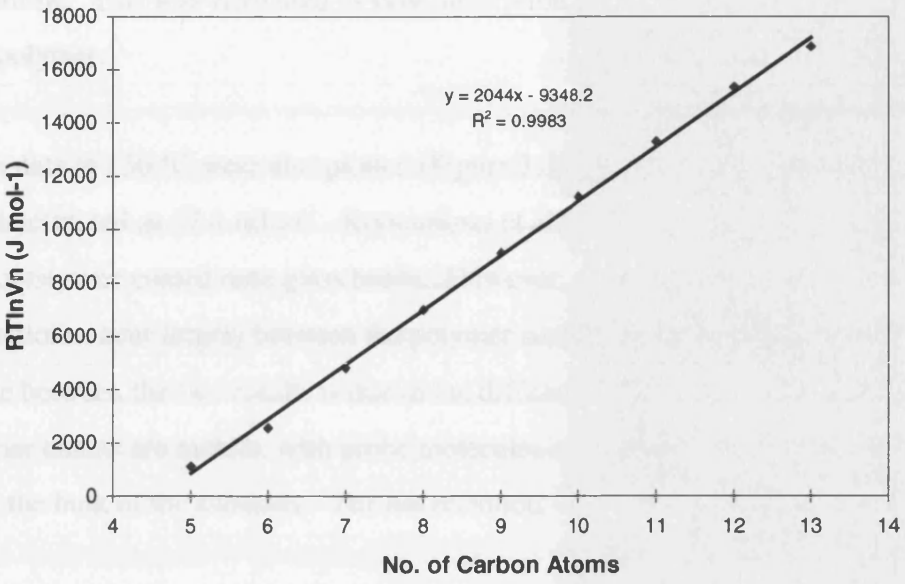

Figure 3.3 Plot of RT*ln*V_n versus number of carbon atoms for linear alkanes at 130 °C.

Table 3.1 Retention volumes of n-alkanes on polystyrene.

Probe	Vn (cm^3 at 130 °C)	Vn (cm^3 at 30 °C) (literature values[212])
n-pentane	1.4 ± 0.4	
n- hexane	2.1 ± 0.3	0.605
n-heptane	4.2 ± 0.4	2.721
n-octane	8.0 ± 0.2	8.767
n-nonane	15.2 ± 0.7	31.44
n-decane	28.5 ± 0.8	
n-undecane	52.9 ± 1.2	
n-dodecane	97.0 ± 4.0	
n-tridecane	152.7 ± 5.5	

Below T_g, a plot of RT*ln*V_n versus number of carbon atoms for a series of linear alkanes gives a slope of ΔG^0_a. Figure 3.2 illustrates such a plot at 75 °C, with a positive linear correlation of $r^2 = 0.9998$. From the slope, the surface free energy was found. This corresponded to 31 mJ m^{-2}.

It was noted that the retention peaks for the higher alkanes (C_{12} and above) showed a marked tailing. This was attributed to slow adsorption of the less mobile molecules into the bulk polymer.

Retention data at 130 °C were also plotted (Figure 3.3) and the bulk free energy of mixing, determined as 27.4 mJ m^{-2}. Kontominas et al.[212] give a value of 60 mJ m^{-2} at 30 ° C for polystyrene coated onto glass beads. However, at 30 °C, polystyrene is below the T_g, interactions occur largely between the polymer surface and probe molecules. The difference between the two results is due to the difference in substrate phases. At 130 °C, the polymer chains are mobile, with probe molecules consequently being able to penetrate the bulk of the substrate. The net retention volumes are given in Table 3.1.

3.4 **Conclusions**

The study of polystyrene using IGC confirmed its validity in determining phase transition temperatures, satisfying objective 2. Values calculated were comparable with those from literature, within 1 °C. Results were within experimental error, calculated as ± 0.8 °C. Isothermal retention data for linear alkanes were used to determine enthalpies and free energy of the polymer. Results obtained were in agreement with literature values. The chromatographic peaks for the alkanes showed little skew, indicating that the polystyrene surface was relatively homogenous with few specific sites with high affinities for the alkanes used. The enthalpy of adsorption value, calculated as -54 kJ mol^{-1} for dodecane, was similar to the heats of vaporisation for n-alkanes, indicating the absence of strong interactions. Differences in surface free energy and bulk free energy obtained below and above T_g respectively were attributed to surface and bulk penetration of the probes.

In chapter 4, a further polymer (polypropylene) was studied. The scope was also extended to include multiphase systems (a calcium carbonate/polypropylene composite).

4 HIGH PURITY CALCIUM CARBONATE IN POLYPROPYLENE

4.0 Introduction

A precipitated calcium carbonate (PCC) was prepared and used to validate the GC system for mineral analysis. Data were compared with literature values. The PCC was then treated with sodium polyacrylate, a dispersing agent used in calcium carbonate processing. The differences between the non-treated and treated PCCs were compared.

Both PCCs were then coated with stearic acid, and compounded in polypropylene homopolymer. Injection moulded test specimens were produced, and some physical properties were measured. The original, untreated PCC and PP were also included as comparisons. Differences were equated to surface energetics, measured by IGC.

4.1 Materials

A pure calcium carbonate was prepared by chemical precipitation[213]. 0.5 mol dm^{-3} solutions of BDH AnalR sodium carbonate and calcium chloride were prepared separately in de-ionised water. Equimolar equivalents of the two were combined slowly with stirring, whilst maintaining the mixture between 25 and 30 °C. The precipitate was filtered through a 541 Whatman filter, and the supernatant through a 50 Whatman filter. The two were combined and dried in a vacuum oven at 60 °C to a constant weight.

The PCC (PCC1) thus prepared was analysed by X-ray diffraction (XRD) with a Siemens D5000 XRD with a Braun position sensitive detector, and by scanning electron microscopy (SEM), with a Philips-Electroscan 2020 SEM. From the XRD data the crystal structure was determined as calcite with trace amounts (< 0.1 %) of vaterite (see section 1.2.2). No aragonite was observed. Calcite has a characteristic rhombohedral shape, easily distinguished when viewed by SEM. The crystal structure was therefore confirmed by SEM (Figure 4.1).

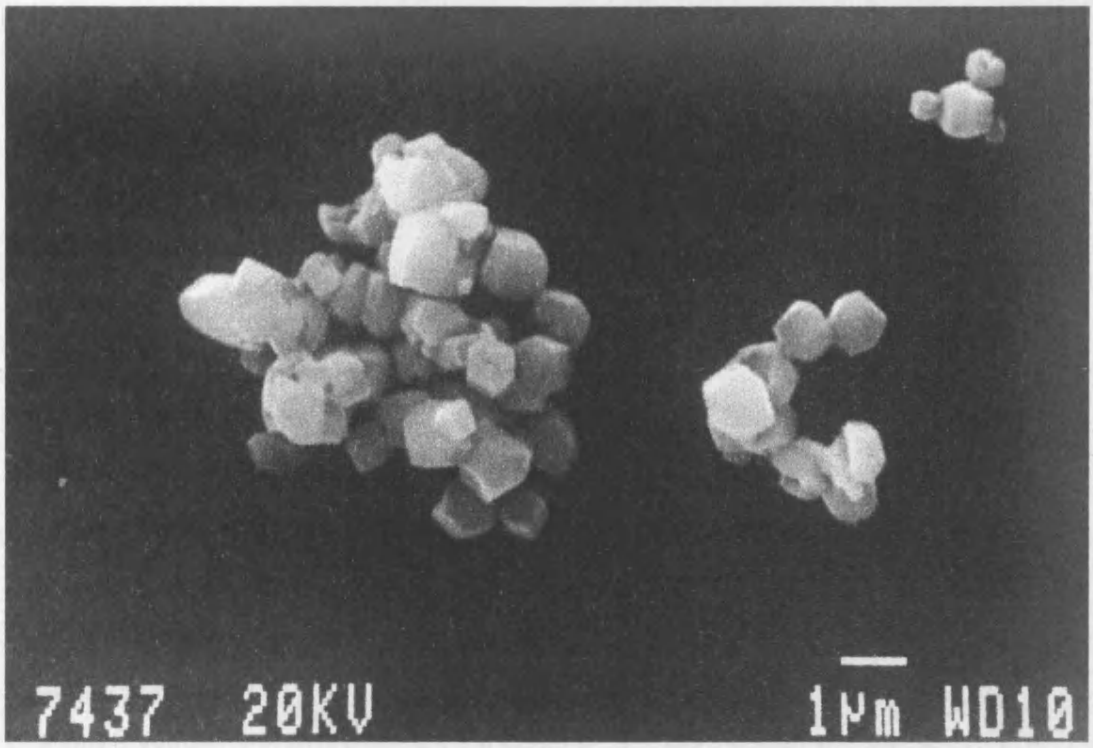

Figure 4.1 SEM image showing the crystal structure of PCC1.

The surface areas of the natural and compressed material were determined by the single point BET nitrogen absorption method[214]. A sample of the PCC was then diluted to a 60 wt.% solids aqueous suspension with a Heidolf mixer.

0.4 % sodium polyacrylate (N40 Dispex from Allied Colloids) was added and the sample mixed for a further fifteen minutes. The treated PCC (PCC2) was removed and pressure filtered under nitrogen through a 0.2 µm Millipore filter. The filter cake was dried to a constant weight at 60 °C in a vacuum oven.

PCC1 and PCC2 were each coated with 2 wt.% stearic acid (Pristerene 1870) in a Steele and Cowlishaw high shear mixer at 80 °C. The addition level corresponded to the theoretical surface monolayer[215]. Each was mixed for ten minutes to ensure surface homogeneity[216] and conditioned at 23 °C, 50 % relative humidity, for one week.

The coated PCCs were compounded into polypropylene homopolymer (GWE 27 from ICI, see Table 4.1) at 40 wt.%. Compounds were prepared on an APV MP2030 twin screw extruder at a constant 50 % torque. The die temperature was 210 °C, with a screw speed of 250 RPM. After drying overnight at 60 °C in a Conair Churchill desiccant dryer, each compound was injection moulded in an Arburg 320M Allrounder injection moulder.

An unfilled polymer was included as a comparison. Two moulding geometries were produced: 80 x 80 x 2 mm plaques; and 80 x 10 x 4 mm bars. Mould temperature was 60 °C, with a die temperature of 230 °C.

Once moulded, test specimens were conditioned for four days at 23 °C, 50 % relative humidity before testing. Plaque colour was measured with a Minolta Chrometer to give L, a and b values. Plaque gloss was measured at 20, 60 and 85 ° with a Gardner BYK haze-gloss meter[20]. Falling weight impact strength of the plaques was measured with a Rosand IFIW5 impact tester[19]. Notched and un-notched Izod strength of the bars was measured with a Ceast pendulum tester[217]. Bar flexural modulus was measured with a Monsanto T10 tensometer by the three-point bend technique[218].

The thermal transitions for the PP were measured by differential scanning calorimetry (DSC) with a Perkin-Elmer V1.8TA. Scanning rate was 10 °C min^{-1}, with a temperature range of – 50 to 250 °C, under a nitrogen atmosphere.

Table 4.1 Physical Properties of GWE 27 PP (from ICI technical datasheet[219]).

Property	**Test Method**	**Value**
Melt flow index (g 10 min^{-1})	230 °C, 216 kg	4.2
Density (kg m^{-3})		905
Melting range (°C)		165 – 175
Tensile yield stress (MPa)	ISO H572	34.5
Flexural modulus (GPa)	ISO 178	1.50

4.2 **Chromatography**

The GC fractions were prepared by compaction (as detailed in section 2.1.2). The mass of packing was determined by weight loss of the remaining material. The columns were pre-conditioned at 120 °C.

For PCC1, a series of n-alkane probes (from C_5 to C_9) were injected at 70 °C. Three elutions were carried out for each probe. The FID was set to its most sensitive range. Retention times were extrapolated by the integral data processor and the chromatograms were stored in the data file system.

Each chromatogram was printed to compare deviation of the peaks from Gaussian distribution. To ensure the infinite dilution region was reached, retention data for n-pentane was collected with varying flow rates.

The method was repeated at 5 °C intervals, up to 110 °C, with the column (PCC1) being conditioned for 12 hours between each temperature change. Conditions were chosen to compare data from previous studies. The column was then held at 110 °C for 250 hours before the sequential study was repeated, this time with 10 °C reductions in temperature. This was done to quantify any surface modifications by heat during the initial study. After conditioning at 70 °C, a series of polar probes were eluted and retention data obtained at 10 °C intervals up to 100 °C.

A small quantity of the original, compacted PCC was placed in the GC oven at the start of the experiment. On completion, this was removed and re-examined by XRD and SEM to determine whether the heating cycles altered the crystal structure. No changes were observed.

The experimental procedures were repeated for the surface-modified PCCs.

The PP pellets (approximately 3 mm in diameter) were ground in a Janeke and Kunkel mill under liquid nitrogen. The material was sieved to produce 425 – 850 μm fractions, and packed into the GC column for analysis.

Table 4.2 Details of GC columns.

	PCC1	PCC2	PCC1(SA)	PCC2(SA)	PP
Length of column (mm)	1500	1000	1000	1000	1200
Mass in column (g)	24.0135	14.4726	12.9734	13.8931	6.6131
Surface area ($m^2 g^{-1}$)	2.68	2.25	2.59	2.18	1.12
Stearic acid coating (wt.%)	none	none	1.95	1.93	none

4.3 **Results and Discussion**

4.3.1 *Confirmation of the infinite dilution region*

The retention times for increasing injection volumes of n-pentane were found to be constant (Figure 4.2).

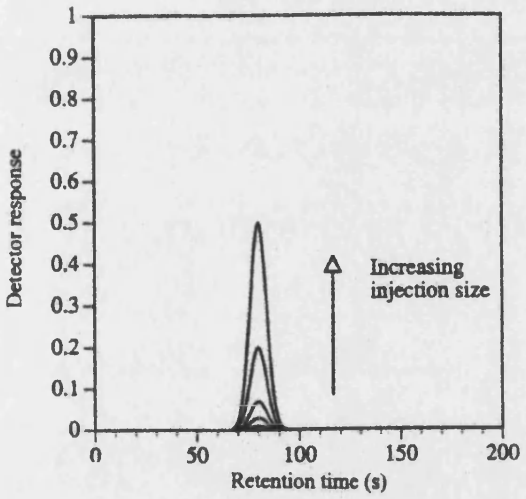

Figure 4.2 Plot of GC detector response versus retention time for n-pentane, to determine the effect of injection volume.

The retention times were independent of volume injected (2.447 ± 0.005 min). Thus the study was confirmed to be within the infinite dilution region.

4.3.2 *Adsorption enthalpy and surface free energy*

J, the correction factor for pressure drop across the column, was calculated from (1.14), as outlined earlier in section 1.4.1. f_0, the corrected gas flow rate was also calculated, as was T_0, the absolute temperature, calibrated against a standard thermometer, as detailed in section 2.1.1. From these and the net retention time t_n, the net retention volume, V_n, was calculated.

The standard free enthalpy of adsorption, ΔG_a^0, was calculated from net retention volumes for each probe at each temperature from equation (1.28),

$$\Delta G_a^0 = -RT\left[\ln(Vn) + \ln\left(\frac{p_{s,g}}{\pi W_s S_a}\right)\right] \qquad (1.28).$$

where $p_{s,g}$ is the standard surface pressure, given as 1.013×10^5 Pa, and π, the two dimensional surface pressure of the gas, is given as 3.38×10^{-4} Nm^{-1}. W_s is the mass of the stationary phase and S_a is its surface area. These components were combined as k, given by

$$k = \ln\left(\frac{p_{s,g}}{\pi W_s S_a}\right)$$

ΔG_a^0 was thus calculated from (1.29)

$$\Delta G_a^0 = -RT \ln V_n + k \qquad (1.29)$$

The standard enthalpy of adsorption (also the isosteric heat of adsorption, qs^t) was then found by applying equation (1.30),

$$\Delta G_a^0 = \Delta H_a^0 - T\Delta S_a^0 \qquad (1.30).$$

Thus a plot of ΔG_a^0 against T, has an intercept of ΔH_a^0 (Figures 4.3 to 4.7).

Fundamental data for PCC1 and PCC2 are given in Tables 4.3 to 4.6, to illustrate the calculations. ΔH_a^0 data are given in Tables 4.7 and 4.8.

Table 4.3 Experimental data for PCC1.

Temp. (°C)	k	T_0 (K)	J	f_0 ($cm^3\ min^{-1}$)
70	15.353	343.589	0.868	11.269
80	"	353.504	0.871	"
90	"	363.521	0.864	"
100	"	373.641	0.863	"
110	"	383.710	0.859	"

Table 4.4 Net retention times, net retention volumes and standard free enthalpies of adsorption calculated for PCC1.

Temp. (°C)	Probe	t_n (min)	V_n (cm^3)	ΔG_a^0 ($kJ\ mol^{-1}$)
70	C_5H_{12}	2.40	23.5	13.4
"	C_6H_{14}	6.54	63.9	16.3
"	C_7H_{16}	17.80	174.2	19.1
"	C_8H_{18}	48.40	473.6	22.0
80	C_5H_{12}	1.63	16.0	12.7
"	C_6H_{14}	4.22	41.4	15.5
"	C_7H_{16}	10.87	106.7	18.2
"	C_8H_{18}	27.73	272.1	21.0
90	C_5H_{12}	1.29	12.5	12.3
"	C_6H_{14}	3.16	30.8	15.0
"	C_7H_{16}	7.74	75.4	17.7
"	C_8H_{18}	19.24	187.4	20.5
100	C_5H_{12}	0.97	9.4	11.7
"	C_6H_{14}	2.16	21.0	14.2
"	C_7H_{16}	5.00	48.6	16.8
"	C_8H_{18}	11.46	111.5	19.4
110	C_5H_{12}	0.73	6.9	11.1
"	C_6H_{14}	1.79	17.3	14.0
"	C_7H_{16}	3.48	33.6	16.1
"	C_8H_{18}	7.66	74.1	18.6

Table 4.5 Experimental data for PCC2.

Temp.(°C)	k	T_0 (K)	J	f_0 (cm^3 min^{-1})
70	16.054	343.488	0.977	21.713
80	"	353.504	0.976	"
90	"	363.521	0.976	"
100	"	373.641	0.974	"

Table 4.6 Net retention times, net retention volumes and standard free enthalpies of adsorption calculated for PCC2.

Temp. (°C)	Probe	t_n (min)	V_n (cm^3)	ΔG_a^0 (kJ mol^{-1})
70	C_5H_{12}	0.17	3.5	10.0
"	C_6H_{14}	0.45	9.5	12.8
"	C_7H_{16}	1.01	21.4	15.1
"	C_8H_{18}	2.69	57.0	17.9
80	C_5H_{12}	0.12	2.5	9.3
"	C_6H_{14}	0.31	6.4	12.1
"	C_7H_{16}	0.80	16.9	14.9
"	C_8H_{18}	1.75	37.2	17.2
90	C_5H_{12}	0.09	1.9	8.7
"	C_6H_{14}	0.12	4.9	11.5
"	C_7H_{16}	0.52	10.9	14.0
"	C_8H_{18}	1.10	23.3	16.3
100	C_5H_{12}	0.07	1.4	8.0
"	C_6H_{14}	0.16	3.3	10.7
"	C_7H_{16}	0.31	6.5	12.8
"	C_8H_{18}	0.68	14.4	15.2

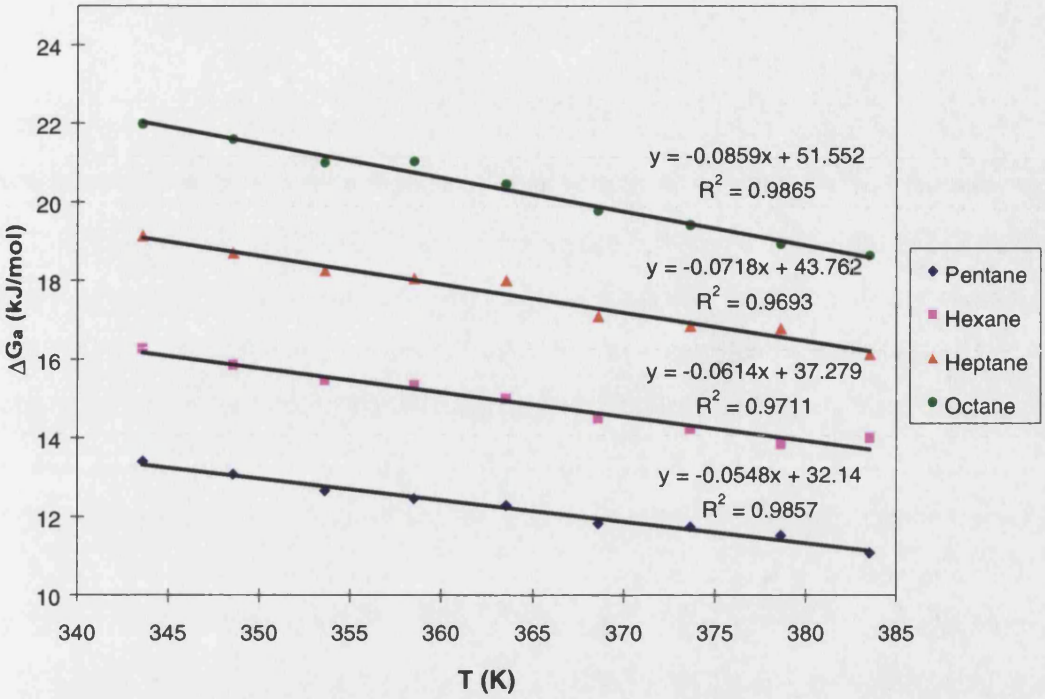

Figure 4.3 Plot of ΔG_a^0 versus T for PCC1 to determine isosteric enthalpies of adsorption.

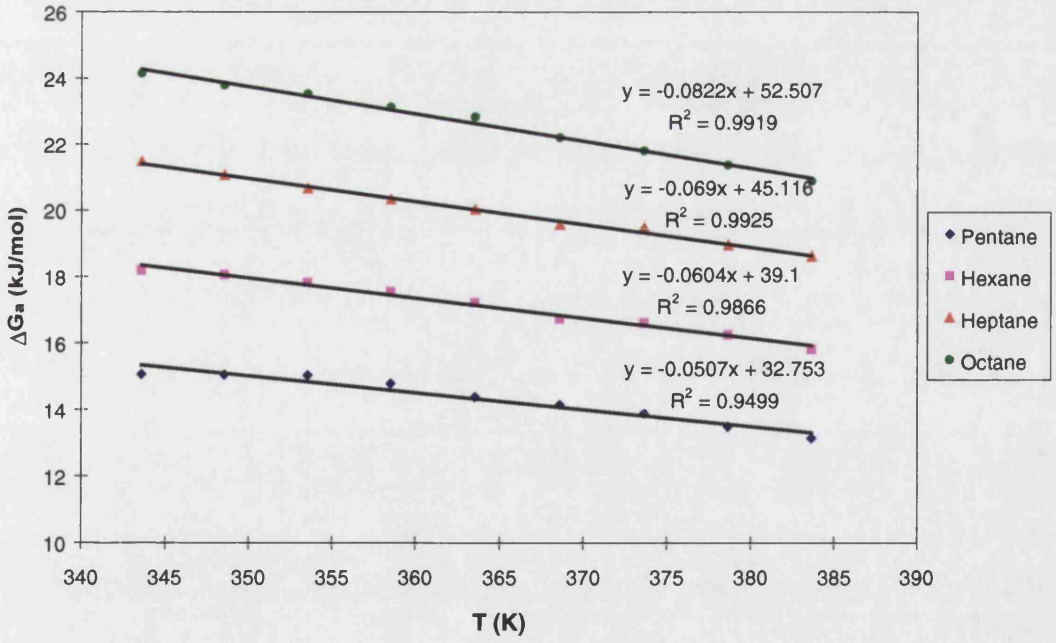

Figure 4.4 Plot of ΔG_a^0 versus T for PCC1, after 150 hours conditioning, to determine isosteric enthalpies of adsorption.

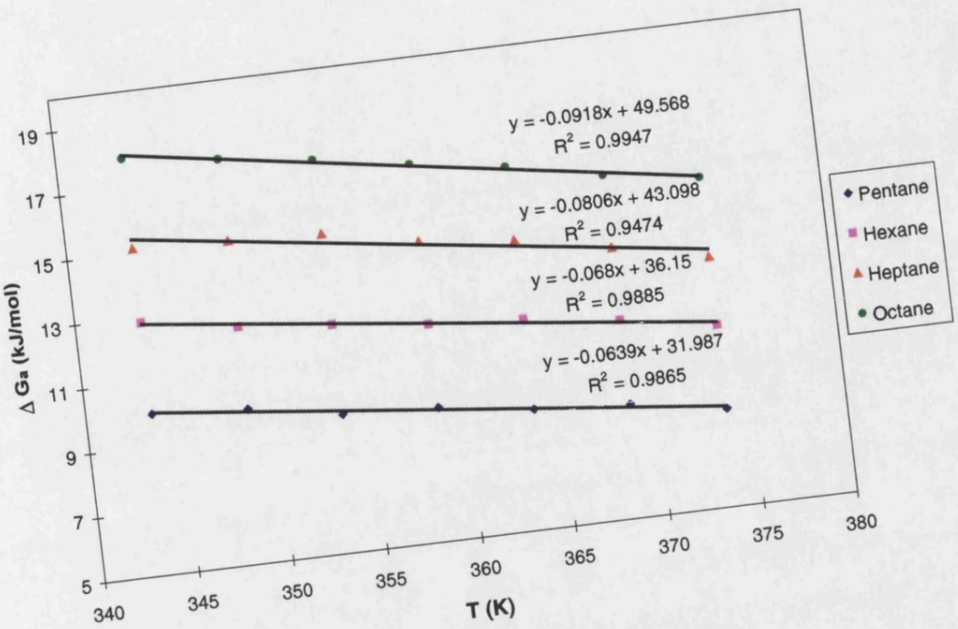

Figure 4.5 Plot of ΔG_a versus T for PCC2 to determine isosteric enthalpies of adsorption.

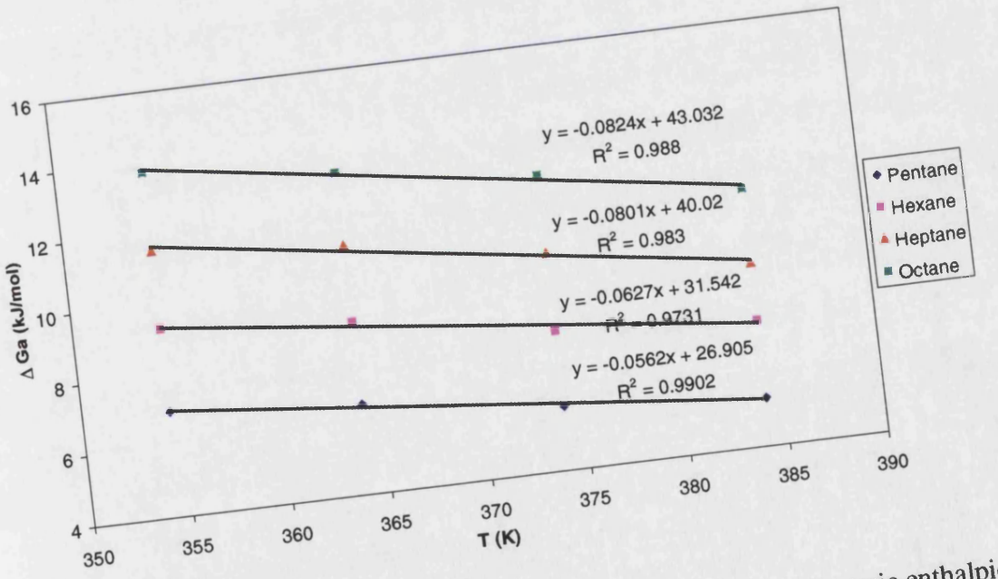

Figure 4.6 Plot of ΔG_a versus T for PCC1(SA) to determine isosteric enthalpies of adsorption.

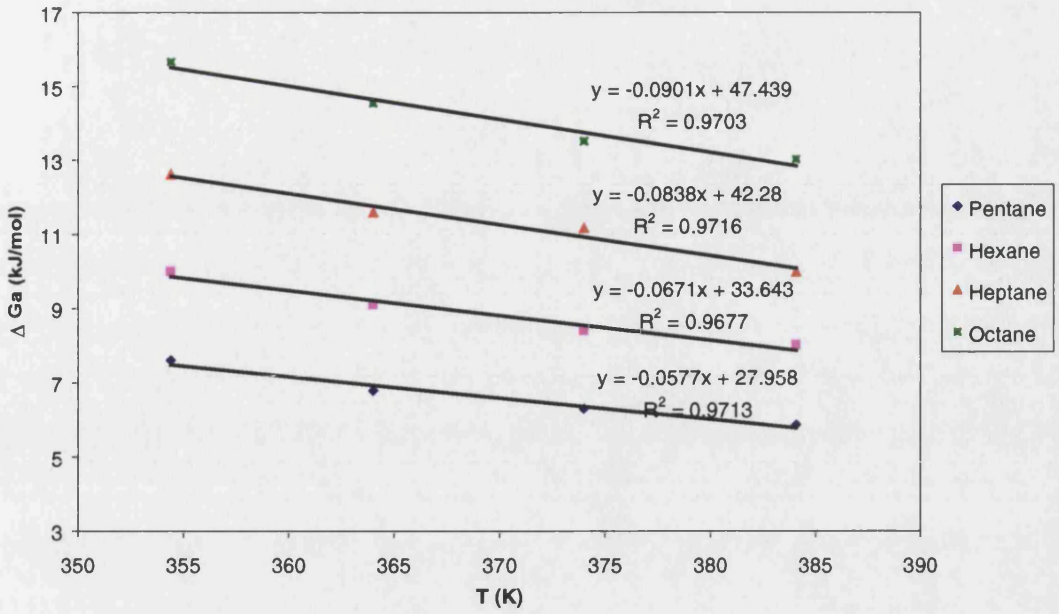

Figure 4.7 Plot of ΔG_a versus T for PCC2(SA) to determine isosteric enthalpies of adsorption.

Table 4.7 Comparison of enthalpy of adsorption data for uncoated calcium carbonates.

	Isosteric Enthalpy of Adsorption (kJ mol.$^{-1}$)						
Probe	**Initial Results PCC1**	**250 hours Condit. PCC1**	**PCC2**	**Keller & Luner**[220] (a)	**Schmitt et al.**[133] (b)	**Ahsan et al.**[221] (c)	**Okonkwo et al.**[134] (d)
Pentane	32.1± 1.2	32.8± 0.6	32.0± 0.8		9		
Hexane	37.3± 0.8	39.1± 0.7	36.2± 1.0	41	11	36	38
Heptane	43.8± 0.8	45.1± 1.3	43.1± 1.4	48	15	44	46
Octane	51.6± 0.4	52.5± 0.9	49.6± 0.6	53	17	53	54

(a) Results for commercial, aragonitic PCC[220].

(b) Results for laboratory prepared, calcitic PCC[133].

(c) Results for re-precipitated colloidal PCC, by CO_2 method[221].

(d) Results for commercial, calcitic PCC[134].

Table 4.8 Comparison of enthalpy of adsorption data for coated calcium carbonates.

	Isosteric Enthalpy of Adsorption (kJ mol.$^{-1}$)			
Probe	**PCC1(SA)**	**PCC2(SA)**	**Schmitt et al.** [133] **(a)**	**Ahsan et al.**[221] **(b)**
Pentane	26.9 ± 0.9	28.0 ± 0.8		
Hexane	31.5 ± 0.9	33.6 ± 0.9	28	35.3
Heptane	40.0 ± 1.2	42.3 ± 1.2	37	41.1
Octane	43.0 ± 1.3	47.4 ± 1.4	46	47.7

(a) Calcitic PCC treated with a monolayer of stearic acid. Excess removed by toluene extraction.

(b) Colloidal PCC treated with ammonium stearate.

ΔG^{0CH_2} as defined in equation (1.31), was determined from the slope of a plot of $RTlnV_n$ versus the number of carbon atoms at a specific temperature (Figure 4.8). The surface free energy, γ_s^d, defined as the change in the Gibbs free energy as a function of the change in area of the surface, was calculated from the alkane elution data (section 1.4.4, equation (1.31)).

$$\gamma_s^d = \frac{1-\left(\Delta G_a{}^{0CH_2}\right)^2}{\gamma_{CH_2}\left(2N.a_{CH_2}\right)} \qquad (1.31)$$

where N is Avogadro's number, a_{CH2} is the cross sectional area of the methylene group and γ_{CH2} is the surface tension of hypothetical surface of polyethylene containing only methylene groups[222].

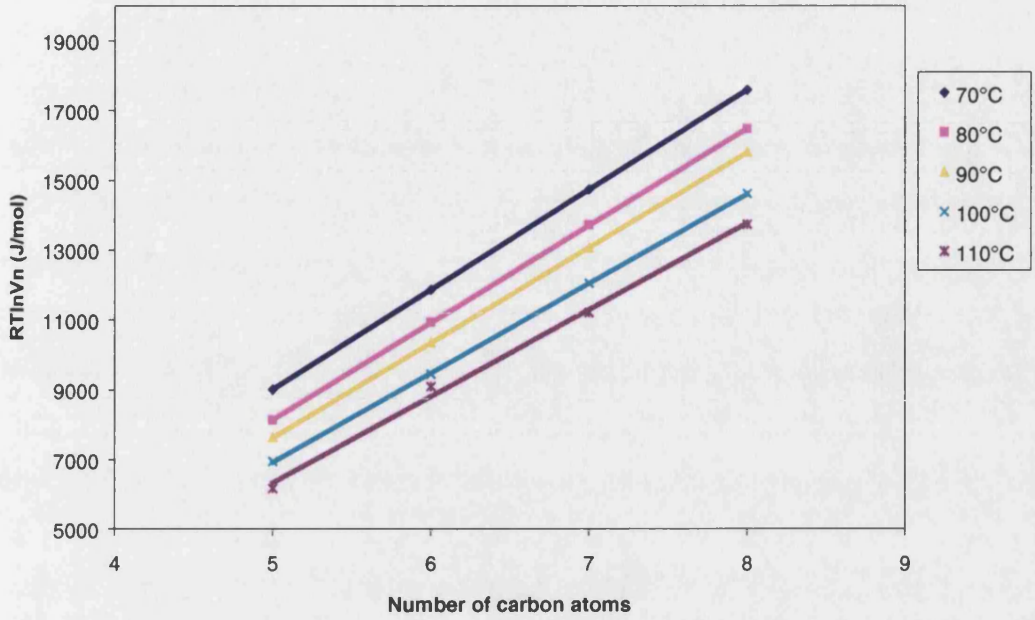

Figure 4.8 Plot of RT*ln*V_n versus number of carbon atoms (from alkane probes) for PCC1 to determine the dispersive component of surface free energy.

This was repeated for the PCC2, PCC1(SA) and PCC2(SA). Results for PP are illustrated in Figure 4.9.

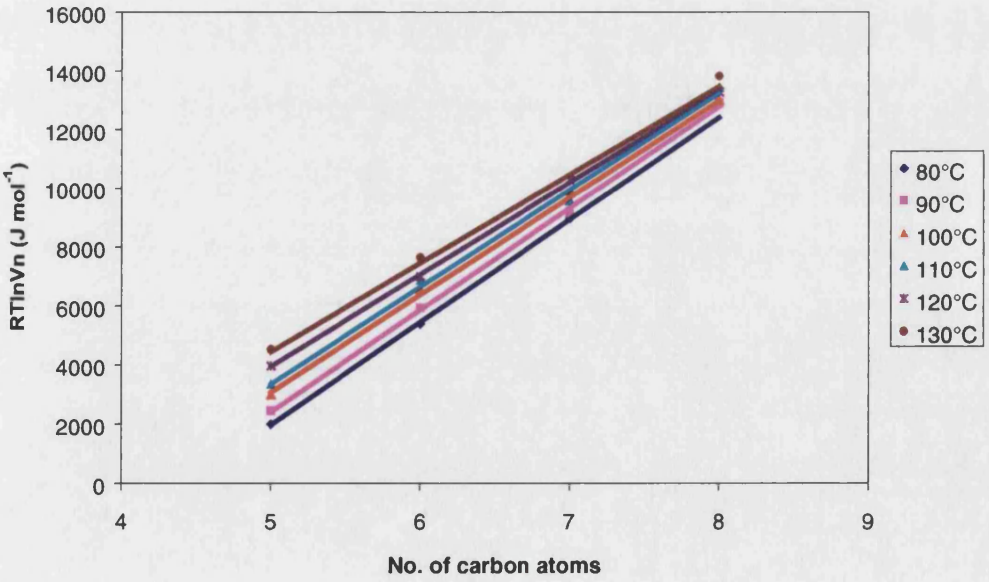

Figure 4.9 Plot of RT*ln*V_n versus number of carbon atoms (from alkane probes) for PP to determine the dispersive component of surface free energy.

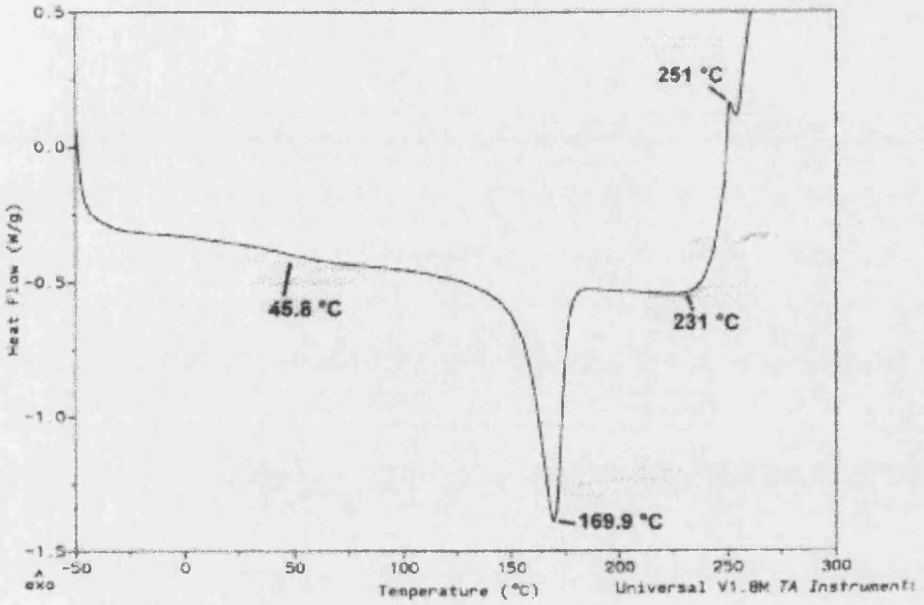

Figure 4.10 DSC thermogram of heat flow versus temperature for PP.

Table 4.9 Comparison of the dispersive component of surface free energy results for uncoated PCCs compared with those from published data.

	Dispersive Component of Surface Free Energy (mJ m^{-2})				
Temp. (°C)	**PCC1**	**PCC2**	**Balard and Papirer**[206] (a)	**Keller & Luner**[220]	**Schmitt et al.**[133]
Reference					
70	48 ± 1	40 ± 1			44
80	46 ± 1	42 ± 2			46
90	46 ± 2	38 ± 1			45
100	41 ± 2	35 ± 3	52, 53		45
110	39 ± 2				
140				50-65	

(a) Results for commercial PCCs. Some processing chemicals may be present. No details were given.

Table 4.10 Comparison of the dispersive component of surface free energy results for coated PCCs (and PP) compared with those from published data.

	Dispersive Component of Surface Free Energy (mJ m^{-2})				
Temp. (°C)	**PP**	**PCC1(SA)**	**PCC2(SA)**	**Balard & Papirer[206] (a)**	**Schmitt et al.[133]**
70					29
80	36 ± 2	31 ± 1	43 ± 2		21
90	36 ± 2	29 ± 2	40 ± 1		22
100	34 ± 1	29 ± 1	37 ± 2	31	18
110	36 ± 1	24 ± 1	35 ± 2		
120	31 ± 2				
130	30 ± 2				

(a) Results given for a ground marble, treated with a monolayer of stearic acid.

Isosteric enthalpies of adsorption for the uncoated PCCs (Table 4.7) compared well with those of Ahsan et al.[221], Okonkwo et al.[134] and Keller and Luner[220]. Schmitt et al.[133] cited much lower values for C5 to C8 under similar experimental conditions. Ahsan et al. considered these differences to be due to water adsorption from the carrier gas, or surface modification of the cationic sites by the hydrocarbon probes. The presence of impurities in the carrier gas could give rise to surface variability, if the impurities, such as water, were adsorbed onto the stationary phase. The latter explanation seems unlikely, as the probes were non-polar. The differences between similar studies highlighted the need for high-purity carrier gas. The equipment used in this work included a gas drying and purification system to avoid surface modification by the carrier gas.

In each case the isosteric enthalpy of adsorption was found to increase with increasing carbon number of the probe. Cationic sites present on calcium carbonate undergo specific polarisation interactions with the probes. As the hydrocarbons increase in molecular weight they are more readily polarised, and thus exhibit greater interaction energies.

Repeating the experiment on PCC1 after 250 hours conditioning resulted in an increase in isosteric enthalpies of adsorption of 0.7 – 1.8 kJ mol^{-1} for PCC1.

The differences were small, and similar to the deviations of the test method. However, as the same trend was observed with each probe, the probes were considered to display a greater affinity for the PCC surface with time. The results from this second study were closer to the results of both Ahsan et al.[221] and Keller and Luner[220]. The latter reported a similar trend, although the differences were greater. Their detailed studies of preconditioning and sequential isothermal IGC suggested that the presence of physisorbed water gave rise to increased retention volumes. The water could only be removed by prolonged heat treatment above 300 °C. The presence of adsorbed water on calcium carbonate surfaces is a widely recognised phenomenon and the desorption of the water monolayer would result in the changes observed[223].

Results of SEM analysis for PCC1, stored in the GC oven, revealed no structural changes with time. BET surface area measurement showed a slight increase in surface area, from 2.68 ± 0.05 m^2g^{-1} to 2.83 ± 0.05 m^2g^{-1}. This was considered to be due to slight porosity increases known to occur with heating.

The surface modified PCC2, gave enthalpies of adsorption 0.1 – 2.0 kJ $mol.^{-1}$ lower than PCC1. The differences were small, but significant, each showing the same trend. Similar results were found by Ahsan et al.[221] when comparing a colloidal PCC with one modified with Calgon S (sodium hexametaphosphate). Thus a small change in net adsorption properties occurred.

The coated PCCs both had lower isosteric enthalpies of adsorption than the uncoated equivalents (Table 4.8). For PCC1(SA), stearic acid addition lowered the result by 3.8 - 8.6 kJ $mol.^{-1}$. The value was also reduced for PCC2(SA), although to a much lesser extent (0.8 to 4.0 kJ $mol.^{-1}$). On addition of sodium polyacrylate to a calcium carbonate suspension, calcium polyacrylate is precipitated[224]. This is then redistributed over the surface to form a layer of calcium polyacrylate. The lowering of the surface free energy is probably, therefore, due to a reduction in the available Ca^{2+} high energy Lewis acid sites. Stearic acid also binds to these sites.

Thus the sodium polyacrylate effectively masked these sites preventing stearic acid chemisorption. Complete coverage of stearic acid, as calcium stearate, must therefore result in a lower enthalpy of adsorption than coverage with calcium polyacrylate.

Limited data are available for comparison, but Ahsan et al.[221] found a reduction in isosteric enthalpy of adsorption with stearic acid addition of 0.7 – 5.3 kJ $mol.^{-1}$. Differences reported by Schmitt et al.[133] were much greater (17 – 29 kJ $mol.^{-1}$). Their results for stearic acid coated calcium carbonates were similar to those from this study, and those of Ahsan et al. If adsorbed water were present on the uncoated calcium carbonate studied by Schmitt et al., then surface treatment in toluene solution, followed by evaporation may have removed, or masked this layer. The GC preparative methods for the uncoated and coated samples were also different, with the uncoated material being agglomerated in water and the coated material being agglomerated in acetone before drying and sieving. It would seem likely, therefore, that the enthalpy of adsorption results cited by Schmitt et al. for the uncoated calcium carbonate were lower than those reported in consequent studies because of the presence of surface water.

The surface free energy of 41 mJ m^{-2} for PCC1 at 100 °C was lower than that observed by Schmitt et al.[133] or Balard and Papirer[206]. Higher results were obtained from commercially available PCCs, which may be considered less uniform than those made under rigorous laboratory conditions. Any impurities may give rise to variations in surface energetics. As detailed in Section 1.2.2, PCCs are most commonly prepared by the recarbonation of heat-treated limestone. Limestone will contain a proportion of silica, silicates and heavy metal impurities. These are not completely removed during manufacturing and are present in commercial PCCs.

A comparison of PCC1 and PCC2 (Table 4.9) revealed a significant difference between the two products. The value gives an indication of the high energy sites. Sodium polyacrylate interacted with these high energy sites, preventing interaction with the alkane probes. At higher temperatures (100 °C) the differences were less significant, primarily due to a lowering of the dispersive component of surface free energy for PCC1. Stearic acid addition on PCC1 resulted in a net lowering of the surface free energy (Table 4.10). The results were lower at higher temperatures.

This trend was also observed by Schmitt et al.[133] and was attributed to the penetration of the alkanes between the grafted acid chains, with longer chains penetrating more readily at higher temperatures. The differences between PCC2 and PCC2(SA) were significant (9 – 12 mJ m^{-2}). No data are available for comparison. These differences were considered to be due to preferential adsorption by sodium polyacrylate on the calcium carbonate surface, masking these sites for stearic acid addition. Sodium polyacrylate is therefore acting as a high energy site, resulting in a higher dispersive component of surface free energy.

These results for PCCs compared well with the majority of literature values. The study was therefore extended to consider other, specific contributions to adsorption enthalpies.

Polypropylene (PP) was also studied by IGC between 80 and 130 °C. Surface energy results for PP of 30 to 36 mJm^{-2} agreed well with literature values quoted between 30 to 35 mJm^{-2} [225]. If PP is considered as essentially non-polar, with surface sites dominated by methylene groups, then one would expect the surface free energy to be similar to a closely-packed CH_2 structure, given as 32 – 35 mJ m^{-2} [226], and indeed these results are of the same order. Results at 130 °C showed a considerable deviation from linearity, and should, perhaps be discounted due the very short retention times of the lower alkane probes. Deviations may also be due, in part, to a softening of the polymer, as the experimental temperature approached the melt temperature, determined as 169.9 °C (Figure 4.10).

4.3.3 *Specific Interactions*

Adsorption data for various acidic, basic and neutral probes were used to determine the specific energy of adsorption ($\Delta G^0_{specific}$), where the total free energy is the sum of the specific components (see (1.33), Section 1.4.5).

The specific components may be resolved utilising Fowkes equation

$$\Delta G_a^0 = 2N (\gamma_s^d)^{½}. a(\gamma_L^d)^{½} + k \qquad (4.1)$$

where γ_s^d and γ_L^d are the dispersive components of the surface tension for the solid and liquid components respectively.

By plotting ΔG_a^0 as a function of $a(\gamma_L^d)^{½}$ a straight line graph was produced with the slope corresponding to $2N (\gamma_s^d)^{½}$ (Figures 4.11 to 4.14). The slope corresponds to the response of an alkane probe, having a dispersive component only. If probes with a non-dispersive contribution are used, the deviation from the slope of ΔG_a^0 corresponds to $\Delta G^0_{specific.}$ Results for adsorption of specific probes on PCC1 and PCC2 are given in Table 4.6. Due to the very low retention time differences (compared with alkanes) for specific probes on the stearic acid-treated PCCs, only alkene probes were injected. γ_L^d, the surface tension of the pure liquid, is obtained from published data. a, the area of the molecule when it is adsorbed on a surface, is estimated from[227]

$$a = 1.09 \times 10^{14} (M/\rho N)^{2/3} \qquad (4.2)$$

where M is the molecular weight of the probe, ρ is the density of the liquid at STP and N is Avogadro's number.

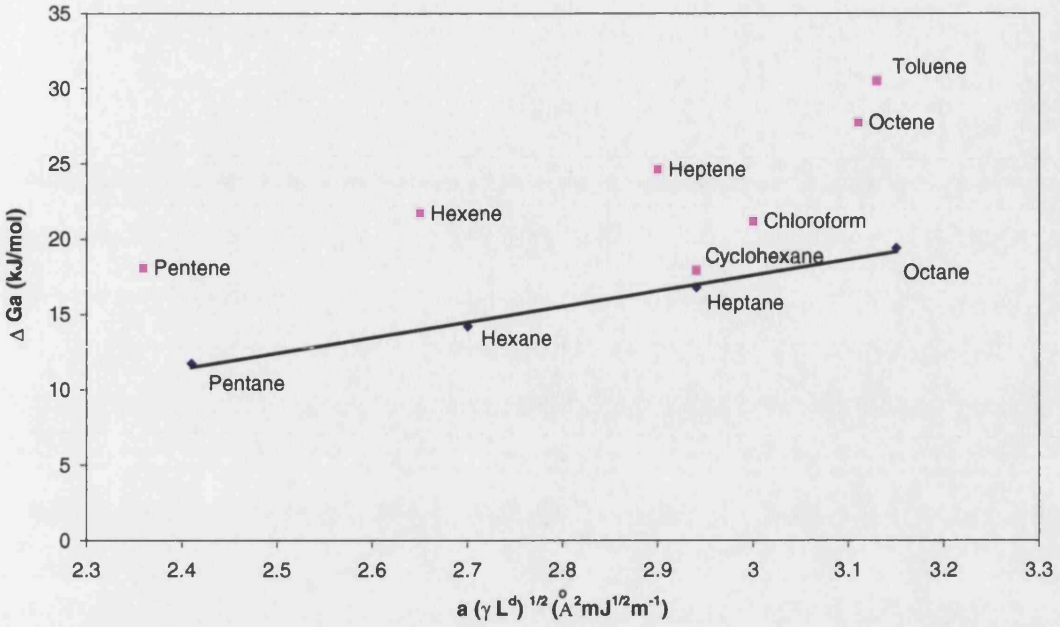

Figure 4.11 Plot of ΔG_a^0 versus $a(\gamma_L^d)^{1/2}$ to determine specific interactions for PCC1 at 100 °C.

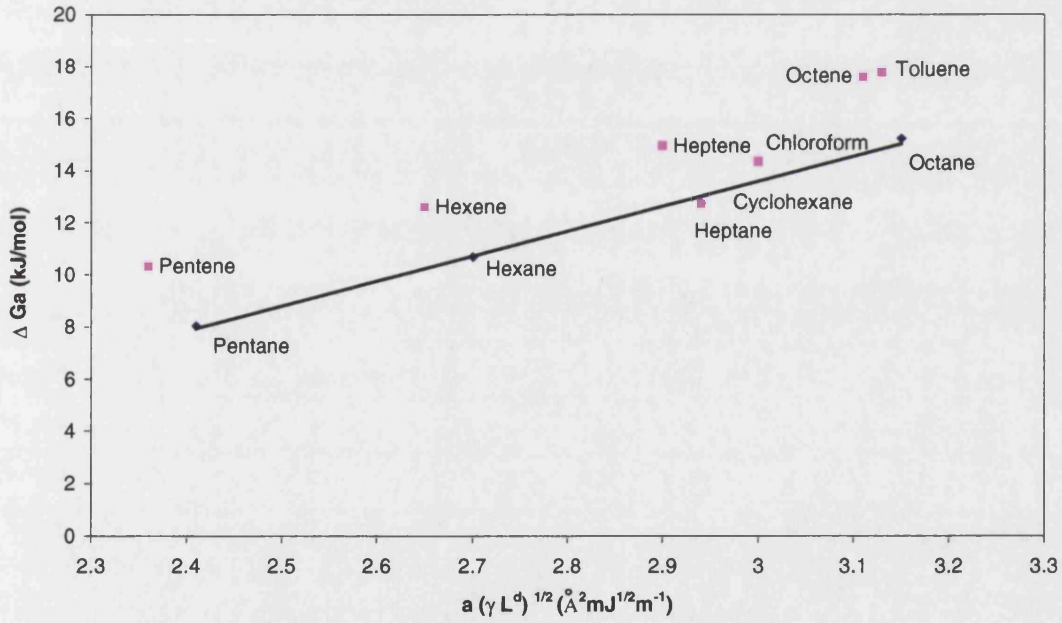

Figure 4.12 Plot of ΔG_a^0 versus $a(\gamma_L^d)^{1/2}$ to determine specific interactions for PCC2 at 100 °C.

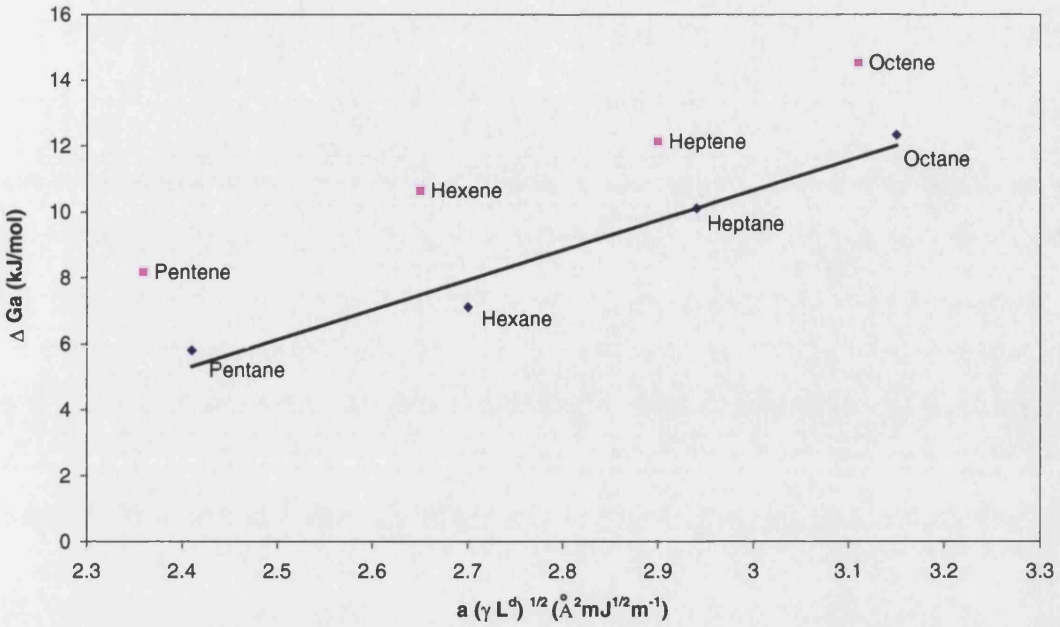

Figure 4.13 Plot of ΔG_a^0 versus $a(\gamma_L^d)^{1/2}$ to determine specific interactions for PCC1(SA) at 100 °C.

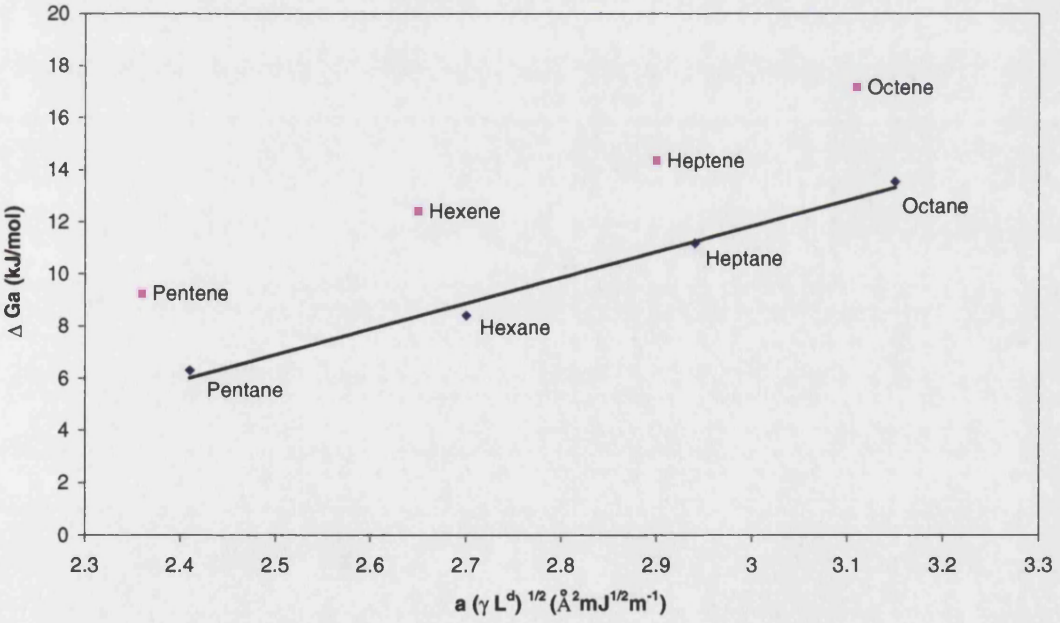

Figure 4.14 Plot of ΔG_a^0 versus $a(\gamma_L^d)^{1/2}$ to determine specific interactions for PCC2(SA) at 100 °C.

Table 4.11 Specific enthalpies of adsorption, derived from Figures 4.11 to 4.14.

	$-\Delta Ha_{specific}$ (kJ mol.$^{-1}$)			
Probe	**PCC1**	**PCC2**	**PCC1(SA)**	**PCC2(SA)**
Pentene	6.3 ± 0.6	2.3 ± 0.5	2.4 ± 0.5	2.9 ± 0.2
Hexene	7.5 ± 1.0	1.9 ± 0.6	2.5 ± 0.6	3.0 ± 0.6
Heptene	7.8 ± 1.2	2.2 ± 0.9	2.0 ± 0.6	3.2 ± 0.4
Octene	8.3 ± 0.8	2.4 ± 0.4	2.2 ± 0.8	3.6 ± 0.6
Chloroform	4.0 ± 0.7	1.6 ± 0.6		
Toluene	11.1 ± 2.1	2.5 ± 0.4		
Cyclohexane	1.1 ± 0.3	- 0.04 ± 0.6		

The isosteric enthalpy of adsorption for each alkene may be found by plotting ΔG_a versus T, as in Figures 4.3 to 4.7. The polar contribution may then be expressed as the difference between the values for the alkane and corresponding alkene (Figures 4.15 to 4.18, summarised in Table 4.12).

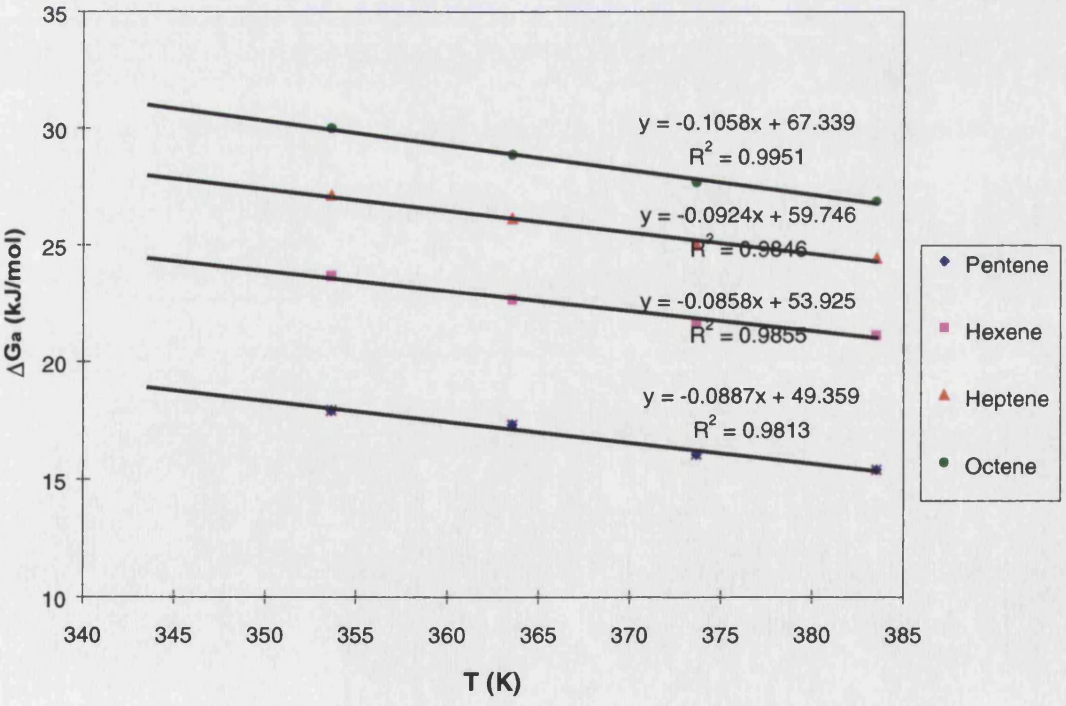

Figure 4.15 Plot of ΔG_a versus T for PCC1 to determine alkene isosteric enthalpies of adsorption.

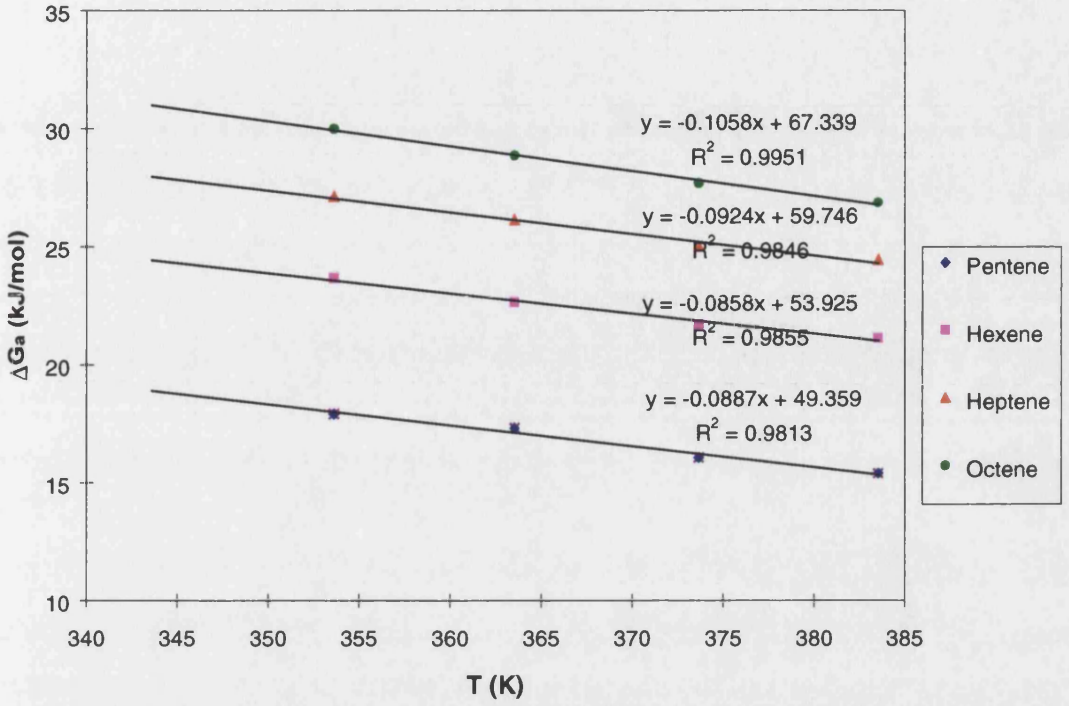

Figure 4.16 Plot of ΔG_a versus T for PCC2 to determine alkene isosteric enthalpies of adsorption.

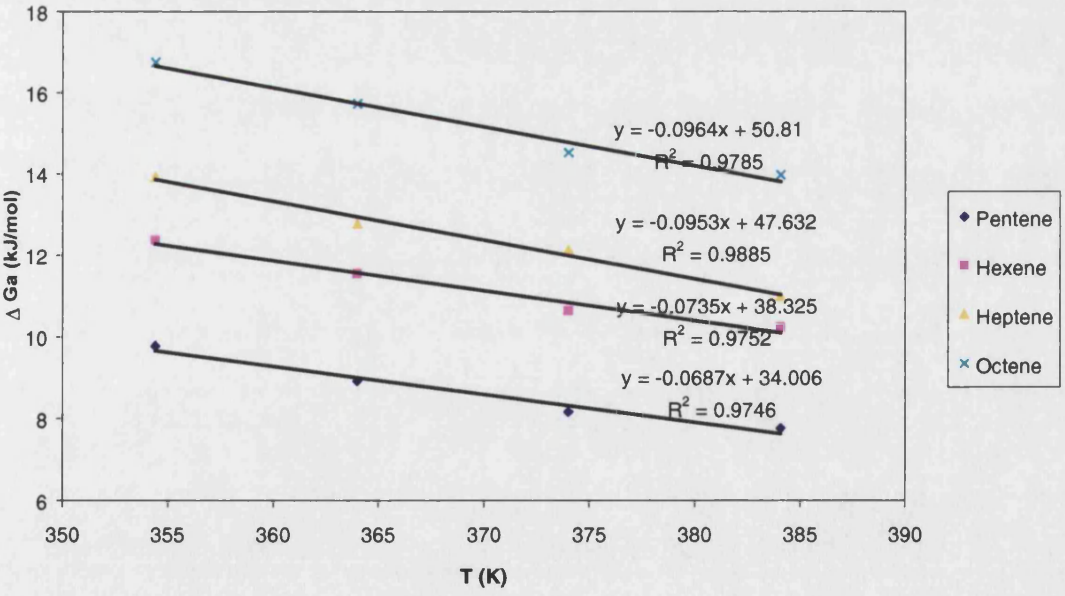

Figure 4.17 Plot of ΔG_a versus T for PCC1(SA) to alkene determine isosteric enthalpies of adsorption.

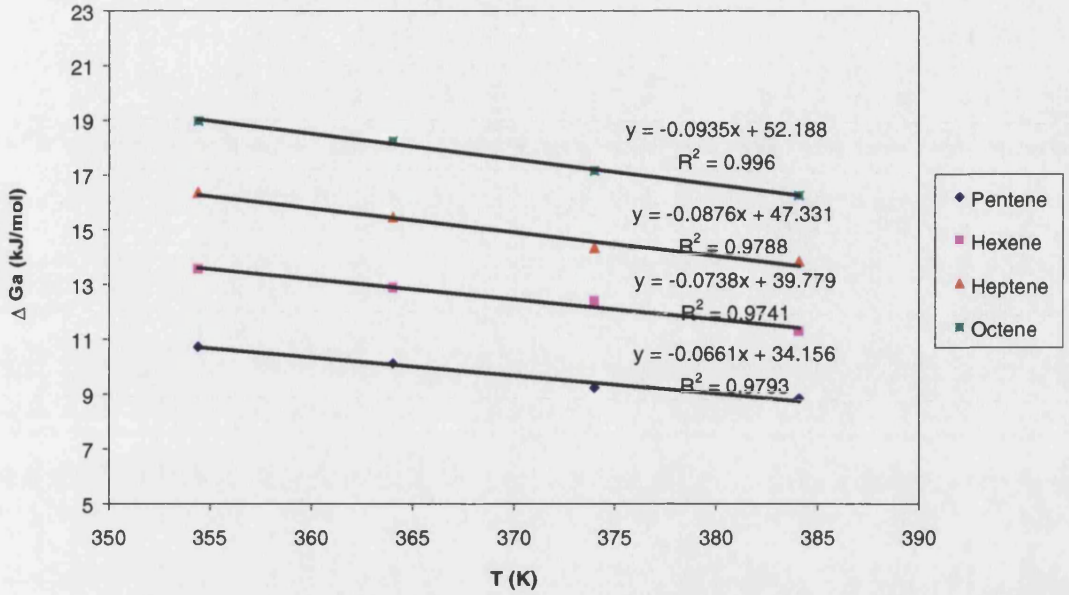

Figure 4.18 Plot of ΔG_a versus T for PCC2(SA) to alkene determine isosteric enthalpies of adsorption.

Table 4.12 Differences in isosteric enthalpies of adsorption between alkane and corresponding alkene.

	ΔH_a^0 alkane - ΔH_a^0 alkene (kJ mol^{-1})			
	PCC1	**PCC2**	**PCC1(SA)**	**PCC2(SA)**
C5	- 17.2	- 16.7	- 7.1	- 6.2
C6	- 16.7	- 16.8	- 6.8	- 6.1
C7	- 16.0	- 15.6	- 7.6	- 5.1
C8	- 15.8	- 15.1	- 7.8	- 4.8

Using alkene probes, the specific enthalpies of adsorption were reduced slightly for PCC2 compared with PCC1 (Table 4.11). As the π -bonds interact most readily with active surface sites, sodium polyacrylate effectively masked these sites, preventing interactions. This confirms the conclusions for the dispersive component of surface free energy results (Section 4.3.2). The results were comparable with those for PCC1(SA), but slightly higher for PCC2(SA), with greater interactions being measured for the higher alkenes.

The acid-base results for PCC1 and PCC2 revealed the extent to which surface modification of polar sites occurred. Retention data for ethanol, a strong acid, was not collected, as the probe was not detected within the time constraints of the experiment. This was unsurprising considering the strongly basic nature of calcium carbonate. Chloroform is moderately acidic, and its retention on PCC was reduced with polyacrylate treatment. Toluene, another acidic probe, interacted more strongly with PCC1, but only moderately with PCC2. Addition of sodium polyacrylate thus resulted in a net reduction in both basic and acidic sites. The cyclohexane probe behaved essentially as a linear alkane, but with a much bulkier molecular structure. A high specific enthalpy of adsorption would suggest differences due to steric effects. A comparison of PCC1 and PCC2 did not reveal notable differences, and thus steric variation between them was not significant.

The differences in isosteric enthalpies of adsorption between PCC1 and PCC2 (Table 4.12) were not significant. On addition of stearic acid, both PCCs showed a marked reduction in enthalpy for all carbon chain lengths. Differences between PCC1 and PCC1(SA) were greater than the polyacrylate modified PCCs.

The aim of the study was to correlate thermodynamic differences found by IGC with surface and mechanical differences within a composite matrix. Applications testing of injection moulded specimens were therefore carried out, as detailed in section 4.1.

4.4 Physical testing of polypropylene injection mouldings

Table 4.13 Physical testing results of PP mouldings.

		PP	PP + 40 wt.% PCC1	PP + 40 wt.% PCC1(SA)	PP + 40 wt.% PCC2(SA)
Colour	**L**	not applicable	87 (3)	85 (2)	84 (3)
	a	"	0.5 (0.01)	-0.5 (0.02)	-0.5 (0.03)
	b	"	3.0 (0.2)	2.5 (0.1)	2.3 (0.1)
Gloss	**20 °**	81 (1)	40 (3)	59 (2)	54 (4)
	60 °	106 (4)	58 (3)	74 (2)	71 (2)
	85 °	101 (1)	86 (2)	97 (1)	95 (2)
Falling weight impact strength	**Peak force ($N\ mm^{-1}$)**	167 (37)	500 (15)	1220 (60)	970 (40)
	Peak Energy ($J\ mm^{-1}$)	1.7 (0.2)	3.5 (1.2)	8.3 (1.3)	5.2 (2.1)
	Fail Energy ($J\ mm^{-1}$)	1.3 (0.2)	3.7 (1.1)	9.1 (1.5)	4.6 (1.3)
Izod strength	**Notched ($kJ\ m^{-2}$)**	1.4 (0.2)	2.6 (0.2)	4.6 (0.1)	3.4 (0.4)
	Un-notched ($kJ\ m^{-2}$)	60 (1)	30 (3)	45 (3)	32 (2)
Flexural properties	**Modulus (MPa)**	1480 (110)	2840 (125)	2710 (102)	2920 (117)
	Yield strength (MPa)	32 (1)	38 (2)	44 (1)	46 (1)

N.B. Standard deviations are given in parenthesis.

The polypropylene-calcium carbonate composites had a lower surface gloss at all three measuring angles (Table 4.13) compared with the unfilled system. Filler particles at the surface of the mouldings cause scattering of the light, reducing the reflected light measured. This effect can be directly correlated to particle size, provided the filler is well dispersed, with coarser particles giving greater scattering, and thus lower gloss. Poorly dispersed particles will form aggregates, which effectively act as coarse particles. No differences were seen between plaques containing PCC1(SA) and PCC2(SA).

This was unsurprising, as both materials were prepared from the same uncoated calcium carbonate. The results also served to confirm that both fillers were well dispersed in the polypropylene matrix.

Mechanical properties were altered significantly with PCC addition. Falling weight impact strength, Izod impact strength and flexural modulus all increased.

Polypropylene homopolymer is brittle, and has a relatively low impact strength. Calcium carbonate addition increases this property by a "crack pinning" effect[228],[229]. The filler particles serve to retard microcrack propagation by physically blocking these tear zones. For PCC1, falling weight fail energy was doubled, compared with the unfilled PP. For test specimens containing stearic-acid treated PCC1(SA) and PCC2(SA) the increase was greater, with PCC2(SA) giving a marginal improvement over PCC1, and PCC1(SA) giving double that of moulding containing PCC1. The Izod impact strength results follow the same trend, with the mouldings containing the surface modified PCCs having higher impact strength than those containing PCC1, and PCC1(SA) mouldings having greater strength than PCC2(SA).

Izod impact strength results for mouldings with PCC1(SA) were also higher than those containing PCC2(SA), with results of 45 and 32 kJ m^{-2} respectively for notched specimens. Differences in mechanical properties could be equated to surface energy differences measured by IGC. In order to achieve good impact properties, differences between the polymer matrix and mineral surface must be minimal[230]. Thus the dispersive component of surface free energy for the surface-modified PCC should be comparable with the polypropylene. Polypropylene, having a measured surface energy of 30 – 36 mJ m^{-2} was similar to that obtained for PCCI(SA), but lower than PCC2(SA).

Flexural modulus increases with filler addition because of the greater rigidity of the filler compared with the polymer matrix. The degree of increase is related to particle shape, packing fraction and physical interactions between the two phases.
It is widely believed that as the interactions between the calcium carbonates and the matrix were negligible, and the particle size was the same, no differences between mouldings containing PPC, PCC1(SA) and PCC2(SA) were expected.

The flexural moduli for test specimens with PCC2(SA) were slightly higher than those with PCC1(SA), although both were within experimental error.

Physical property results are summarised in Table 4.14 and compared with surface free energy results from Tables 4.9 and 4.10.

Table 4.14 Summary of physical testing results of PP mouldings.

	Physical properties of mouldings			
System	**Surface finish**	**Impact strength**	**Modulus**	**Surface free energy of components ($mJ\ m^{-2}$)**
PP	excellent	low	low	30 – 36
PP + 40 wt.% PCC1	good	medium	medium	39 – 48
PP + 40 wt.% PCC1(SA)	good	high	medium	24 – 31
PP + 40 wt.% PCC2(SA)	good	medium	medium	35 - 43

In a polymer matrix, good wetting of the filler surface is necessary for thorough dispersion. This is essential in reducing particulate agglomeration and ensuring uniform spatial distribution. Any undispersed filler or agglomerate will act as defects. A flaw or defect in the test specimen initiates impact failure. Low adhesion is also necessary for de-bonding at the matrix-mineral interface, imparting toughness in filled test specimens. The interfacial adhesion between the two components must therefore be low, to minimise any interactions. Pukanszky studied interfacial interactions in polypropylene composites[231]. He correlated yield stress of the composites with interaction strength differences (measured by contact angle). Using stress analysis, a stearic acid treated calcium carbonate had a lower yield stress, and a lower interaction difference than an untreated calcium carbonate in a polypropylene matrix.

Ahsan and Taylor[135] measured the physical properties of polypropylene-calcium carbonate composites. The calcium carbonates were treated with increasing levels of stearic acid from 0 to 1.5 wt.%. The surface free energies of the fillers were measured by IGC. They found a direct relationship between impact strength and stearic acid coating level, up to a theoretical monolayer coverage. From the results summarised in Table 4.14, the impact strengths of the composites were directly affected by differences in the surface free energy of the two components. Based on previous findings, detailed above, a low interfacial adhesion between the calcium carbonate and polypropylene is necessary for effective dissipation of impact energy. Stearic acid treatment resulted in this net effect. The lower surface free energy measured on PCC1(SA) compared with PCC2(SA) resulted in a slightly greater difference between surface free energies of the filler and PP, as measured. As IGC probes interact with sites of highest energy, the results are dependent on surface homogeneity. Provided complete surface coverage by stearic acid was achieved, PCC1(SA) is more homogenous than PCC2(SA). PCC2(SA) has two distinct surface sites due to the presence of polyacrylate groups and stearate groups. The net effect appears to be a greater interaction difference than might be predicted from surface free energy differences alone. The sites of greater surface free energy, contributed by the polyacrylate groups, may act as stress concentration regions in a similar manner to the uncoated calcium carbonate or an aggregate, and consequently increase the interfacial adhesion energy in these regions.

4.5 **Further discussion**

Reproducibility between injections was good and the linearity of plots (with R^2 values of 0.96 to 1) showed the precision of data collection. Although the changes in net retention volume with prolonged conditioning were relatively small, a standard conditioning time is recommended for all future work. In addition, new columns should be prepared if the experiment is to continue over an extended period. If these precautions are taken, the data obtained are reproducible and reliable.

IGC at infinite dilution was considered a suitable and robust technique for the characterisation of both specific and non-specific interactions of the surfaces of mineral fillers. Criticism has been levelled at the significance of altering the mineral itself during preparative stages, with heat treatment potentially oxidising or redistributing the surface layer[51]. The surfaces will not oxidise provided the columns are maintained under a flow of inert carrier gas throughout the experiment. The method of aggregation and sieving, to ensure suitable material for column packing, has not been found to affect the surface chemistry or accessible surface area of the material. Indeed a method of sandwiching inert fillers between layers of glass beads has been used on unaltered calcium carbonate and found to produce comparable surface activity values[232].

Enthalpy of adhesion data obtained for uncoated and surface-modified PCCs revealed an increase in enthalpy with surface modification. The polar contributions of these interactions were, however, reduced. The addition of sodium polyacrylate to the uncoated PCC also reduced the surface polarity. Surface free energy data showed subtle, but significant differences in the high energy sites on these materials. These data were then related to interaction energy differences at the polymer-filler interface. The mechanical properties of composites are related to the adhesion energy between the components. This study showed that a stearate-modified PCC with lower surface free energy (PCCI(SA)), resulted in a composite with greater toughness than those with higher surface free energies (PCC1 and PCC2(SA)).

4.6 **Conclusions**

1. The data obtained from the Autosystem-XL were in good agreement with literature values for PCCs, thus fulfilling objective 3.

2. Enthalpy of adhesion increased with stearic acid surface modification, with a reduction in polar interaction energies.

3. The addition of sodium polyacrylate to the uncoated PCC reduced the polar interaction energies for both acidic and basic probes.

4. IGC was proven useful in predicting the efficiency of surface modification, and offering the potential of optimising processing routes. Thus objective 4 of the thesis was attained.

The study was then extended to more complex mineral systems, to ensure IGC was more widely applicable. Kaolinites were chosen as having suitably complex surface chemistries. They are also of industrial significance in the field of mineral composites. Two methods for determining specific interactions were also considered, and the merits of each were compared.

5 A COMPARISON OF KAOLINITE AND CALCINED CLAY

5.0 Introduction

Within the UK, primary deposit clays are found in both Cornwall and Devon, where they are commercially significant. Extraction and processing involves the use of refining and improving chemicals, such as floatation and bleaching agents. Clays are also calcined, or heat-treated, to alter their chemical and physical properties. Both hydrous and calcined clays are used in composite materials (section 1.2.2).

Some work has been published on the study of clay minerals by IGC[233]. No data have been published on the use of IGC for measuring the thermodynamic changes on the dehydroxylation of such kaolinites. As a preliminary investigation into the suitability of IGC for studying kaolinite and its modification, a locally extracted clay, chemically untreated, was obtained from archive materials (coded as a hydrous clay, HYC). This was studied, along with a commercially available, locally-sourced calcined clay, PoleStar 200R (coded as a calcined clay, CAC). The effect of calcination on the surface chemistry of HYC was measured. Two methods of determining polar interactions are commonly used (section 1.4.5)[39],[40]. The study was also used to assess the suitability of each procedure for expressing specific parameters.

5.1 Materials

The kaolin sample (HYC) was a high-purity china clay of local extraction, washed and refined without the use of chemicals. The calcined clay (CAC) was modified from the original feedclay by soak calcining in a fixed bed kiln to 1100 °C. Details of both materials are given in Table 5.1.

Table 5.1 Physical Properties of HYC and CAC.

		HYC	CAC
XRD analysis (%)	Kaolinite	98	Amorphous
	Quartz	2	-
BET Surface area ($m^2 g^{-1}$)		8.8	7.0
Particle size (wt.%)	> 10 μm	0	5
	> 5 μm	2	15
	< 2 μm	82	49
Composition (wt.%)	SiO_2	46.2	55.8
	Al_2O_3	39.2	41.0
	Fe_2O_3	0.23	0.59
	TiO_2	0.09	0.06
	CaO	0.06	0.01
	MgO	0.07	0.19
	K_2O	0.21	2.21
	Na_2O	0.09	0.01
	Loss on ignition	13.8	0.30

After drying overnight at 110 °C in a vacuum oven, standard particle size fractions (425 – 850 μm) were prepared for column packing as detailed in section 2.1.2. Three columns were produced, two containing HYC and the third containing CAC. Details are given in Table 5.2.

5.2 Experimental

GC conditions were defined as in the high purity calcium carbonate study, section 4.2. The first HYC column was conditioned overnight at 150 °C, followed by four hours conditioning at 100 °C. Attainment of the infinite dilution region was confirmed by eluting pentane at a range of flow rates and injection volumes. Data were collected and variations in the retention volumes with repeated injections were noted.

Measurements were taken for a series of alkanes at temperatures of 80 ° to 140 °C at 10 °C intervals. In addition, polar probes, listed in Table 5.3, were injected at 140 °C. To determine the variability of data with column preparation, a second column containing the same stationary phase was evaluated at 140 °C. The CAC column was then studied from 80 ° to 140 °C with linear alkane probes. Specific interactions were measured at 100 °C, to compare results with published data.

Table 5.2 Details of GC columns.

	HYC1	**HYC2**	**CAC**
Length of column (m)	0.90	0.915	0.90
Mass in column (g)	11.3043	14.1923	10.5557
Surface area ($m^2\ g^{-1}$)	8.8	8.8	7.0

If a polar probe is used, the deviation from the slope on the $RTlnV_n$ axis results in the determination of $\Delta G^0_{specific}$. In this case, the characteristics for the probes were taken from measured data by Shultz and Lavielle[111], and are given in Table 5.3. A second, empirical method for estimating specific interactions was also applied, as suggested by Saint-Flour and Papirer[39]. In this, ΔG^0_a is plotted against saturated vapour pressure (readily obtained from literature). Alkanes are taken as the reference line, and the deviation cited as the specific interaction parameter. The two methods were compared.

Table 5.3 Data for Non-polar and Polar Probes (after Schultz and Lavielle[111]).

Probe	Surface area, a ($Å^2$)	Dispersive component, v_l^d (mJm^{-2})
Hexane	51.5	18.4
Heptane	57.0	20.3
Octane	62.8	21.3
Nonane	68.9	22.7
THF	45	22.5
Ether	47	15
$CHCl_3$	44	25.0
CCl_4	46	26.8
Acetone	42.5	16.5
Ethyl acetate	48	19.6

5.3 **Results and Discussion**

5.3.1 *Confirmation of the infinite dilution region*

Table 5.4 Variation of retention times with injection volume.

	Vapour volume of pentane (μl)				
	0.5	**0.4**	**0.3**	**0.2**	**0.1**
Retention time (min)	1.007 (0.019)	1.052 (0.026)	1.027 (0.014)	1.063 (0.008)	1.019 (0.021)

Standard deviations of repeat injections are given in parenthesis.

Table 5.5 Variation of net retention volumes for pentane with carrier gas flow rate.

	Flow rate of N_2 (cm^3 min^{-1})				
	10	**20**	**30**	**40**	**50**
V_n (cm^3)	11.27 (0.37)	8.89 (0.33)	8.86 (0.37)	8.65 (0.32)	8.68 (0.32)

Standard deviations are given in parenthesis.

From Table 5.4, five injections of pentane over a range of volumes gave a mean retention time of 1.034 min ± 0.023 min. These results were within experimental uncertainty. Standard deviations of the repeat injections varied from 0.008 to 0.026 min (0.7 % to 2.4 %). The errors for sample volume were considered to be within the deviation of the test procedure, and that the infinite dilution test region was attained. This was confirmed by calculating net retention volume of pentane with varying flow rates (10 to 50 cm^{-3} min^{-1}, Table 5.5). With the exception of the lowest flow rate, results were within the deviation of the test method.

5.3.2. *Adsorption enthalpy and surface free energy*

From Figures 5.1 and 5.2 (plots of ΔG_a^0 versus T), the enthalpies of adsorption for HYC and CAC were determined. These are listed in Table 5.6.

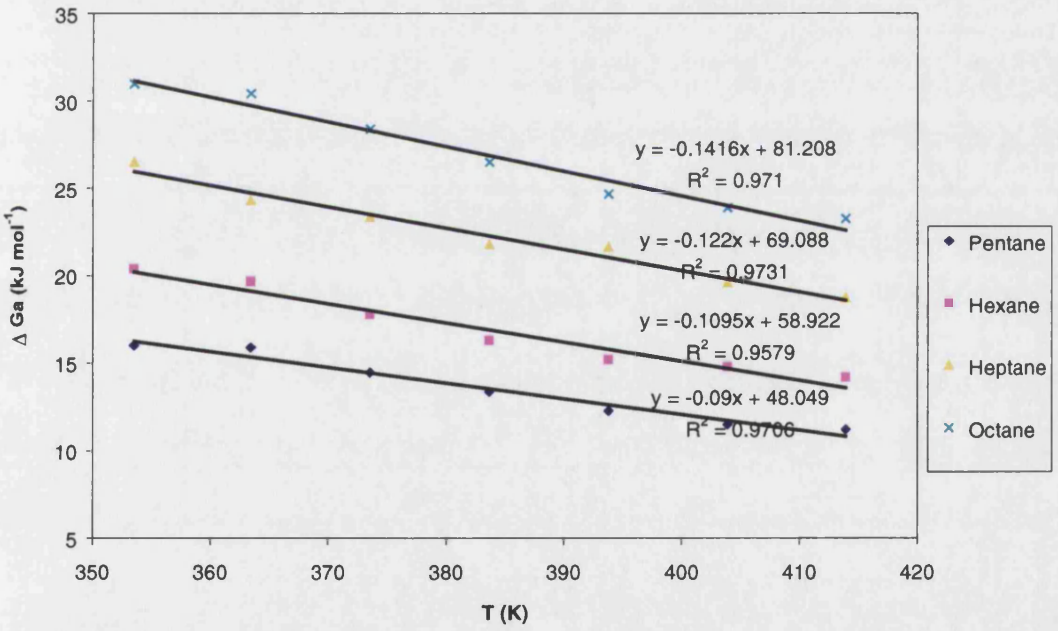

Figure 5.1 Plot of ΔG_a^0 versus absolute temperature for HYC to determine enthalpies of adsorption.

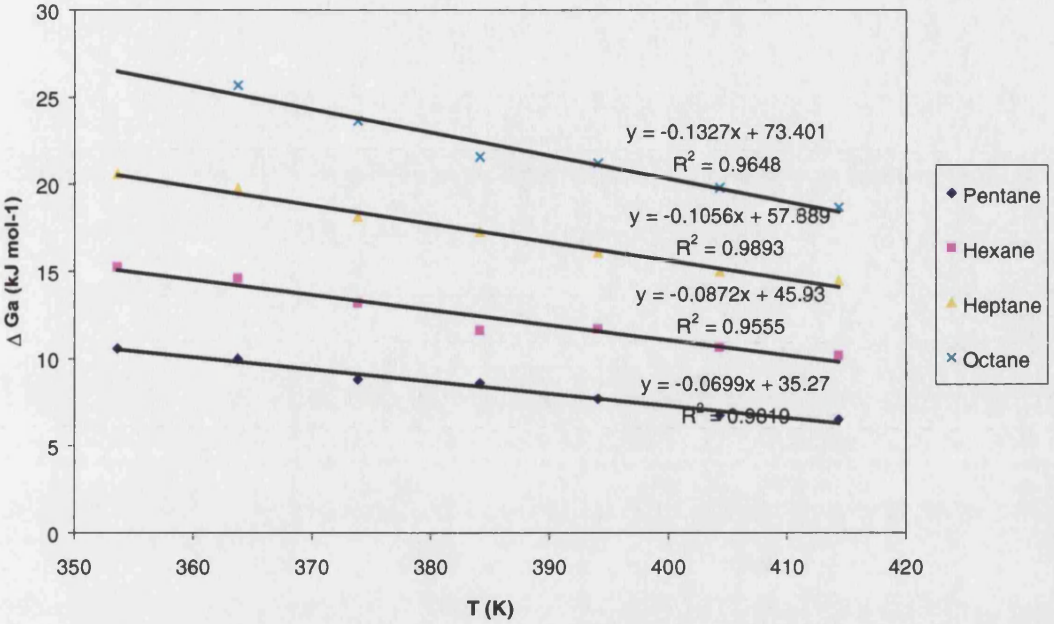

Figure 5.2 Plot of ΔG_a^0 versus absolute temperature for CAC to determine enthalpies of adsorption.

Table 5.6 Comparison of the adsorption enthalpies of kaolinites and illites.

	Enthalpy of Adsorption (kJ mol.$^{-1}$)			
Probe	**HYC**	**CAC**	**Kaolinite Saada et al.[146]**	**Illite (same ref.)**
Pentane	48 ± 3	35 ± 2	50	42
Hexane	59 ± 4	46 ± 4	62	51
Heptane	69 ± 4	58 ± 3	69	65
Octane	81 ± 5	73 ± 4	79	

A comparison of HYC with published data for kaolinites and illites revealed comparable enthalpy of adsorption results. (Illites are mica-like clay minerals, with the general formula $(OH)_4K_y(Si_{8-y}.Al_y)(Al_4.Fe_4.Mg_4.Mg_6)O_{20}$[234]). Saada et al.[146] studied three different kaolinites, ΔH_a for hexane varying from 49 to 62 kJ mol.$^{-1}$. The last, a heritage formation ground kaolinite was within experimental error of ΔH_a for HYC for alkanes C5 to C8.

Results for CAC were slightly lower than the published data for illites. The differences between clay types studied by Saada et al. were considerable, indicating the high variability of the complex clay surfaces. The enthalpies of adsorption for CAC compared with HYC were between 9 to 13 kJ mol^{-1} lower for the alkanes studied, with the differences becoming less pronounced with increasing carbon chain length. Although the calcined clay was not prepared from the HYC, the feed clay for CAC was sourced locally, and was of similar composition. The reduction in adsorption enthalpy may be explained in terms of physical changes that occur during calcination.

Kaolinite, $Al_2Si_2O_5(OH)_4$, is an alumino-silicate, as described in Section 1.2.2. On heating to 750 °C, dehydroxylation takes place with the formation of metakaolinite[235]. The silica sheets are relatively unchanged, although they may relax to a more symmetrical pattern. The aluminium changes from octahedral to tetrahedral co-ordination with the net loss of hydroxyl groups. Further heating to around 900 – 1000 °C causes two reactions to occur. The first is the formation of a defect silicon spinel structure from the metakaolinite, with the formula $Si_3Al_4Va_2O_{12}$, where Va indicates vacancies (defects) in the octahedral sites. Segregation within the structure occurs, with aluminium-rich areas in a defect spinel arrangement balanced by silicon-rich areas where the spinel structure is disordered, or degenerates to form amorphous silica. The oxygens at the base of the silica tetrahedra become close-packed. The oxygens in the middle of the tetrahedral rings also form a close-packed oxygen layer, stacked for the formation of a spinel structure. Only one oxygen per unit cell remains, as a relic of the hydroxyl layer of kaolinite. This oxygen, together with the 0.5 Si unit per cell, must migrate or displace other oxygen atoms to allow the spinel to form. The silica is contained within the crystal structure. Some random hydroxyl groups are still, however, present at the surface[236].

The second reaction occurring above 980 °C is the onset of the formation of mullite as minute needles within the particles (of variable formulae $2Al_2O_3.SiO_2$ and $3Al_2O_3.2SiO_2$). The displaced silica, from the spinel formation, causes the orientation of the mullite needles.

These changes on calcination result in a close-packed structure, with the more ordered defect spinel and mullite structures formed. This leads to a reduction in adsorption enthalpy as the surface is less accessible and has lower polarity species at the surface.

From the slope of a plot of $RTlnV_n$ versus number of carbon atoms, the surface free energies of HYC (for both columns) and CAC were calculated (Figures 5.3 to 5.5). Results are shown in Table 5.7.

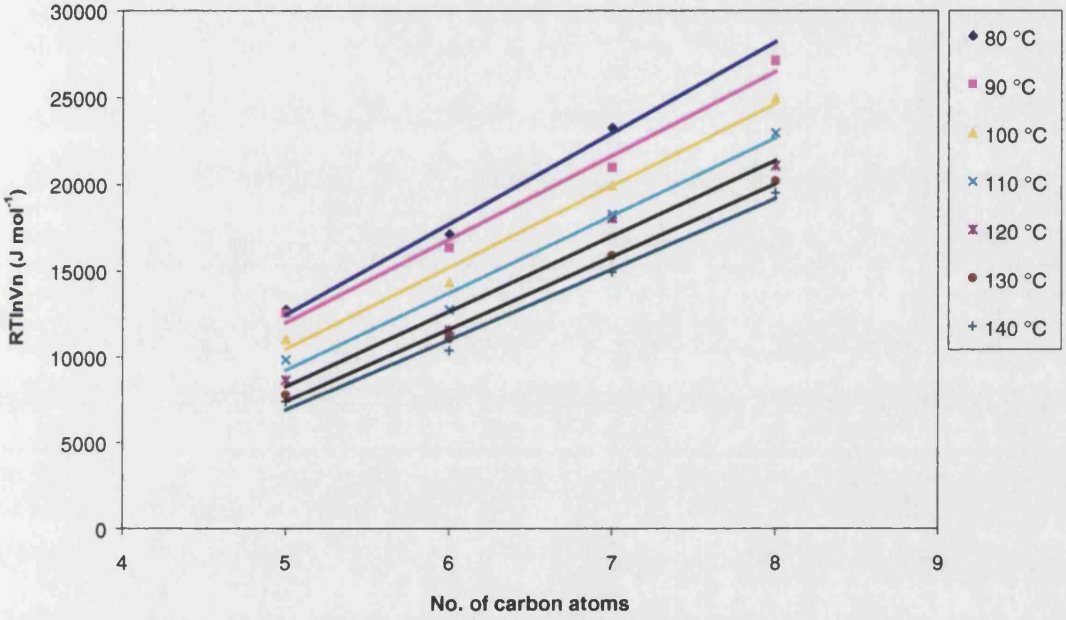

Figure 5.3 Plot of $RTlnV_n$ versus number of carbon atoms (from alkane probes) for HYC (1) to determine the dispersive component of surface free energy.

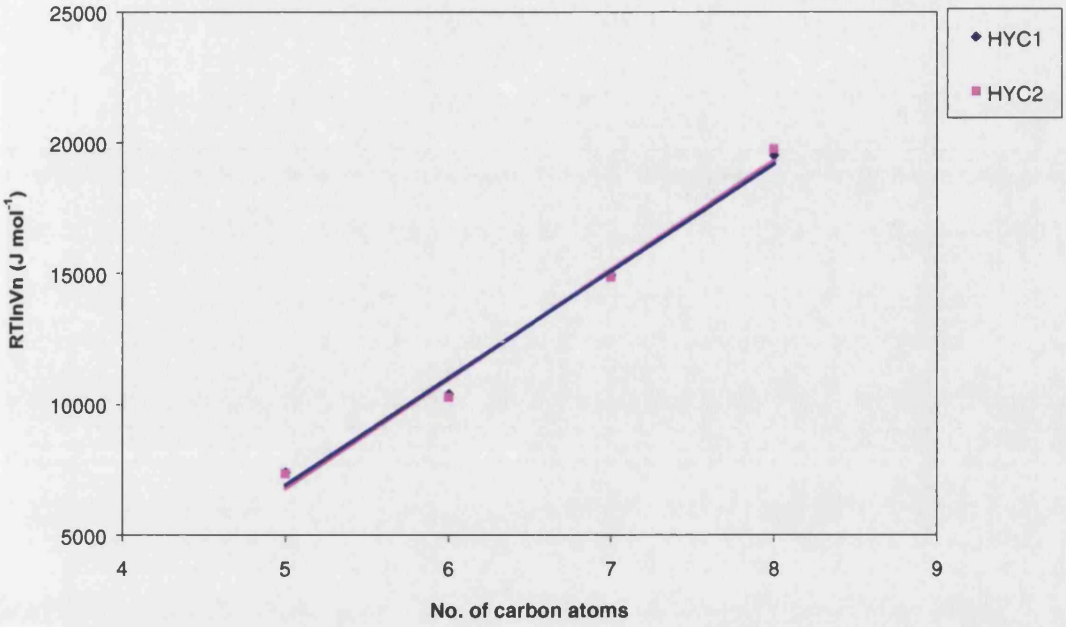

Figure 5.4 Plot of RT*ln*V_n versus number of carbon atoms (from alkane probes) for HYC (1) and HYC (2) at 140 °C to determine the dispersive component of surface free energy.

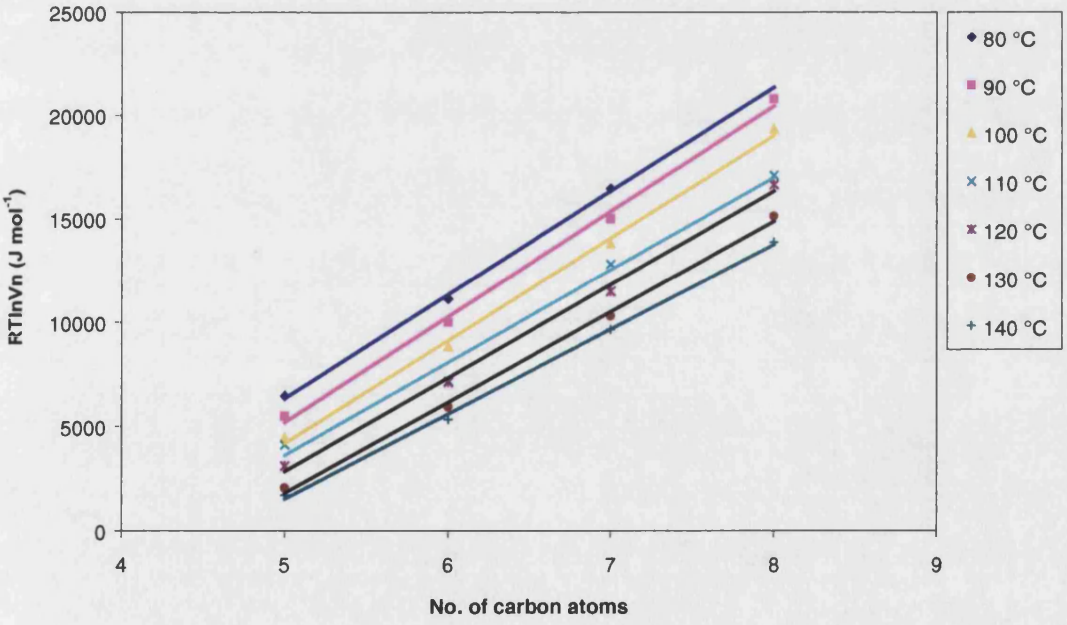

Figure 5.5 Plot of RT*ln*V_n versus number of carbon atoms (from alkane probes) for CAC to determine the dispersive component of surface free energy.

Table 5.7 Comparative data of the surface free energy for kaolinites.

	Dispersive Component of Surface Free Energy (mJ m^{-2})			
Temp. (°C)	**HYC**	**CAC**	**Kaolinite 3 (Saada et al.[146])**	**Illite 3 (Saada et al.)**
80	165 ± 5	139 ± 4	154	138
90	156 ± 6	137 ± 3		
100	149 ± 5	132 ± 3	167	147
120	151 ± 4	130 ± 2	156	145
140	147 ± 5 (149 ± 4 HYC2)	103 ± 3	160	142

Surface free energy results (from Table 5.7) gave excellent agreement between HYC (1) and HYC (2) measured at 140 °C. The results were comparable to the Kaolinite 3 results of Saada et al.[146], but lower than the other two kaolinites quoted (given as 217 and 183 mJ m^{-2}). Kaolinite 3 was a finely ground clay, whereas Kaolinites 1 and 2 were unrefined clays of different formations. They suggested that the lower retention volumes found for K3 resulted from surface alteration causing a partial elimination of surface structural defects. Additionally, clays with high surface areas are more porous and may retain small probes more strongly. Kaolinites studied by Saada et al. had surface areas ranging from 14 to 40 m^2g^{-1} (compared with 8.8 m^2g^{-1} for HYC). The structural porosity may increase the accessibility of high surface energy sites, thus leading to higher surface free energy results. Indeed the authors comment that the results should more rightly be considered as "apparent" rather than true results because the probes are not simply being adsorbed onto a flat surface. If the probe were inserted into the lateral clay layers, it would be submitted to van der Waals forces from both layers, giving higher retention times. They postulated that lower results for agraded (processed clays) were due to a more uniform surface with lower crystallinities. The lower results for CAC, compared with HYC, support this theory.

As detailed in section 1.2.2, once calcined, the surface structure of kaolinite is altered dramatically. The high-energy hydroxyl sites are removed, reducing the total surface free energy.

For example, at 100 °C, the surface free energy of CAC is 11 % lower than that of HYC. Interestingly, γ_s^d is reduced with increasing temperature for CAC, but no correlation was found with HYC. Saada et al.[146] found no significant variation in surface free energy with temperature.

5.3.3 *Specific interactions*

Two methods were used to determine the specific interaction parameters. The first was the standard method, where ΔG_a is plotted versus a $(\gamma_l^d)^{1/2}$ to determine specific interaction energies. With this method, data from Table 5.3 was used in calculations. Results for HYC are illustrated in Figure 5.6. A plot of ΔG_a versus log P_o was also used to determine specific interactions (Figures 5.7 and 5.8). Data from both methods are summarised in Table 5.8.

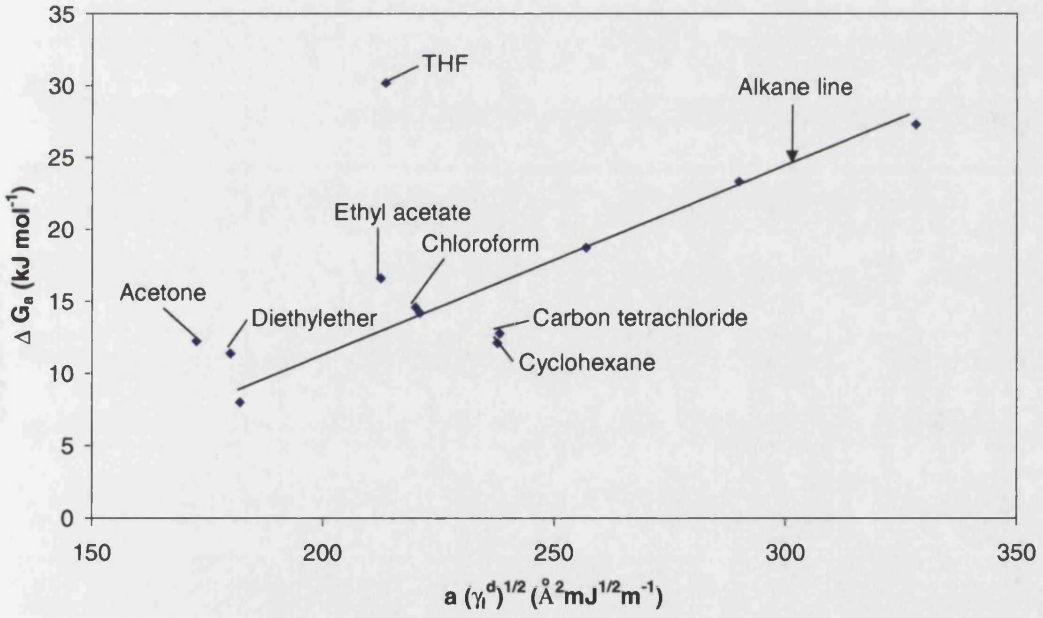

Figure 5.6 Plot of ΔG_a versus a $(\gamma_l^d)^{1/2}$ for HYC to determine specific interaction energies for polar probes.

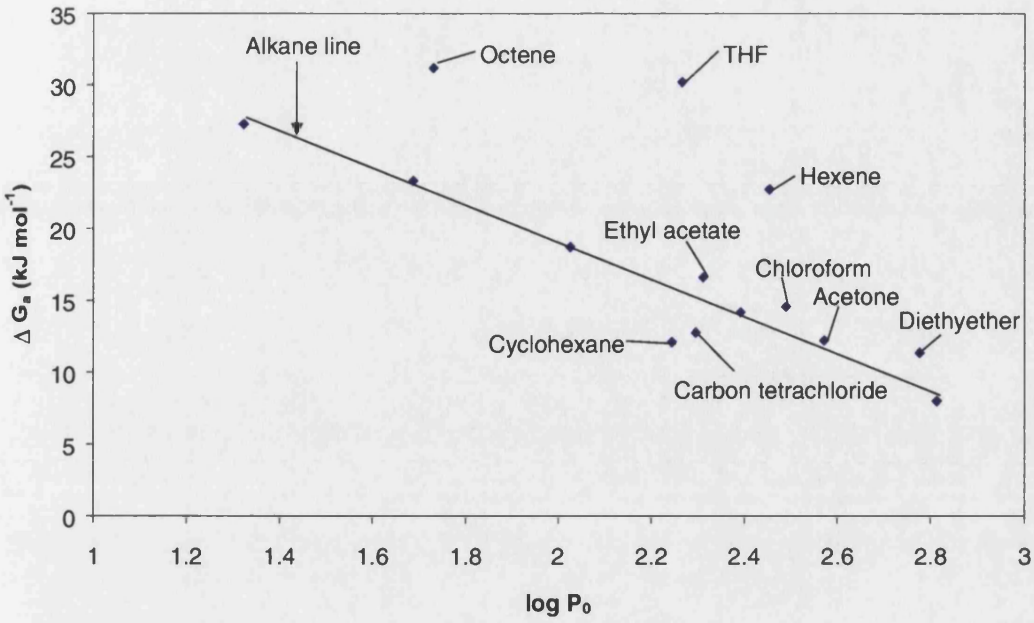

Figure 5.7 Plot of ΔG_a versus log P_o for HYC to determine specific interaction energies for polar probes.

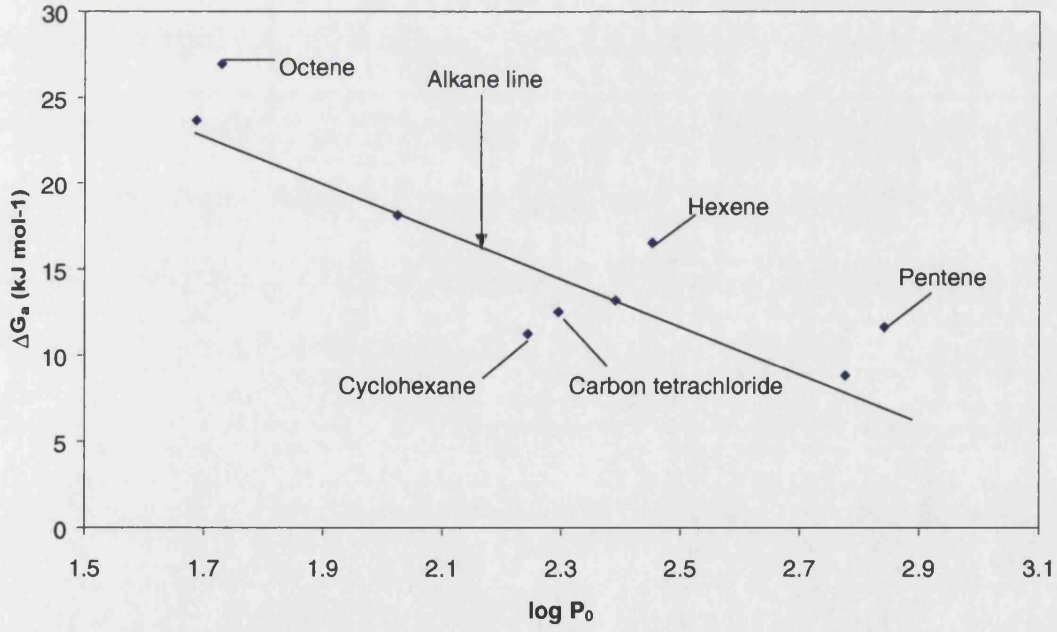

Figure 5.8 Plot of ΔG_a versus log P_o for CAC to determine specific interaction energies for polar probes.

Table 5.8 Specific interaction energies results for polar probes on HYC and CAC.

	Variation in free energy of adsorption from the alkane line ($-\Delta G_{sp}$) (kJ mol.$^{-1}$)		
Probe	**HYC ($a(\gamma_l^d)^{1/2}$ plot)**	**HYC (log P_o plot)**	**CAC (log P_o plot)**
THF	21.5 ± 1.0	18.2 ± 0.9	NPD*
Diethyl ether	13.7 ± 0.8	---	NPD
Chloroform	5.1 ± 0.4	5.0 ± 0.4	NPD
Carbon tetrachloride	-4.8 ± 0.4	-4.9 ± 0.4	- 2.1 ± 0.3
Cyclohexane	---	-7.9 ± 0.5	-4.2 ± 0.6
Acetone	8.5 ± 0.3	4.3 ± 0.3	NPD
Ethyl acetate	7.1 ± 0.4	5.1 ± 0.4	NPD
Hexene		8.6 ± 0.4	4.0 ± 0.4
Octene		8.8 ± 0.4	4.2 ± 0.4

* NPD = no peak detected with in reasonable experimental time.

Agreement between the two methods for HYC was good, with the exception of the amphoteric probes acetone and ethyl acetate. For these, the results of the vapour pressure plots were 2-4 kJ mol.$^{-1}$ lower.

Generally, interactions with polar probes on CAC were lower than for HYC or could not be detected within reasonable experimental time. Those polar probes not detected were either retained over an excessive period, or underwent some chemisorption at the surface, and could not be removed. Specific interaction results for the alkenes hexene and octene for CAC were approximately half of those compared with HYC. Retention volumes for strongly basic probes were not used, as the retention times were excessive, and showed marked tailing. These results are characteristic of the physical and chemical changes occurring on calcination of a hydrous kaolin.

5.4 **Further discussion**

Comparisons of surface free energy results for HYC and kaolinites in the studies of Saada et al.[146] showed some variations, with two of the three French kaolinites having higher values. This was attributed to the higher purity of the HYC and absence of chemicals used during purification and grinding. The French kaolinites were also finer and more porous, as indicted by their higher surface area. This could have resulted in greater probe accessibility. At infinite dilution the probes interact most strongly with the high surface energy sites. Thus if the surface is structurally heterogenous, the surface free energy results will predominantly reflect these sites, rather than the bulk surface. The values obtained for HYC, therefore, compared with those of Saada et al., are an indication of heterogeneity and surface activity, rather than a true representation of surface free energy.

Although HYC was not used as the feed material for CAC, they were both sourced locally. The results on calcination could thus be considered as representing the effect of heat treatment upon such a hydrous clay. Calcination altered the clay's surface chemistry, reducing both adsorption enthalpies, and the dispersive component of the surface free energy. Clay surfaces are known to have strongly acidic properties. These are related to layer defects, and hydroxyl and oxygen atoms in the aluminium structures and silicate layers[237]. Strong Lewis acids are formed by cations of interlayer materials. On calcination both of these sites are altered as the interlayered structure collapses. For CAC, the probe will be subjected to van der Waals forces from a single surface layer, rather then undergoing partial insertion between the layers in the HYC. Although the results indicate a reduction in surface activity on calcination, they are higher than expected if the interactive forces were halved. The probes are therefore being adsorbed onto the remaining high energy sites, which, although fewer, are still having a significant effect on retention times.

Free energy of adsorption results demonstrated the degree of surface alteration with calcination of the HYC. The high values for specific enthalpies of adsorption for alkenes on the hydrous clay were due to very strong specific interactions of the π-electrons of the alkenes with the metallic cations of the clay acting as Lewis acid sites.

The interactions with calcined clay resulted in a halving of the specific adsorption enthalpy. The reduction is due to lessening of the strength of these acidic sites, as the aluminium oxide sites act as weaker Lewis centres than those containing hydroxyl groups. Similar effects have been noted by Bandosz et al. during the intercalation and heat treatment of smectites[141].

The negative values for carbon tetrachloride on HYC were also noted for kaolinites by Saada et al.[146]. They suggested this was due to limited interactions between the polar surface of the clay and also hindering of access to these sites by bulky probe molecules. Negative values were also found with cyclohexane probes. This may be attributed to the same steric hindrance effects, especially when considered relative to the result for hexane. After calcination, the results for carbon tetrachloride and cyclohexane were also negative. The accessibility of the surface sites to these bulky probes has therefore increased. However, the polarity of surface sites on CAC is significantly lower than those on HYC, as indicted by the difference in alkane-alkene results. The relatively small difference in specific free energy of adsorption between HYC and CAC for the bulky probes appears less than would be predicted if both steric and polar contributions were equally important. The greatest effect must therefore arise from a change in specific surface polarity, rather than accessibility of the probes. This also suggests that these probes may not be inserted between the silicate layers on the HYC, and are subjected predominantly to forces from the outerlayers.

The expression of specific interaction parameters by two techniques was evaluated for HYC. The first technique utilised surface tension data that are not readily obtainable at typical experimental temperatures. Estimation of the probe's surface area was also required. The second technique expressed specific interaction parameters in terms of saturated vapour pressure. These data are readily obtained from literature across a broad temperature range.

Although the latter data were not absolute, they correlated well with those from the first technique. The results were used to explain differences in surface activity on calcination of a hydrous clay. IGC was proven suitable for measuring thermodynamic parameters of a complex mineral, such as kaolinite. These data were, however, representative of the highest energy sites, and not the bulk. Interpretation should thus be undertaken with this in mind.

5.5 Conclusions

1. The infinite dilution study of a high-purity, non-chemical clay demonstrated the variation in kaolinite surface chemistry with processing history and source. Good agreement was achieved between one of the quoted literature samples, and the locally-sourced clay studied.

2. On calcination, there was a reduction in both enthalpy of adsorption and the dispersive component of surface free energy. Specific interaction energies were also reduced, with acidic interaction results found to be half those of the hydrous clay.

3. Comparative results between clays and calcined clays have not been published, and are therefore considered to be the first record of such thermodynamic data. The study thus fulfilled objective 5, in the novel application of IGC.

4. Of the two calculation methods used for determining specific interactions, the application of saturated vapour pressure was found to be more suitable. Data were readily available, and the results were comparable with those calculated using surface tension data. Saturated vapour pressure data were thus used for all further studies.

5. The technique was proven suitable for providing information on the surface polarity changes after physical and chemical alteration of the clay, fulfilling objective 6.

Minor differences in surface activity are known to have a significant effect on a composite system. The study thus far has concentrated on the establishment of the technique and comparisons with literature values. To evaluate the use of IGC at infinite dilution for more subtle differences, two calcined clays from the same ore source were evaluated. These are discussed in the following chapter. The clays were then used in the preparation of polyethylene composites to endeavour to correlate the surface chemistry data with physical differences of the composites.

6 CALCINED CLAYS IN POLYETHYLENE FILM

6.0 Introduction

Calcined clays are added to polyethylene (PE) agricultural films to improve the film's infra red barrier properties[238]. Films are used either as ground cover or in polytunnels. Addition of minerals may reduce the lifetime of films either directly, by catalysing degradation or indirectly, by interacting with stabiliser systems[239]. Recent market trends have demanded films with greater longevity[240].

A commercial grade of calcined clay (CAC1), used in the earlier study (PoleStar 200R, chapter 5) was characterised by IGC and compared with a second calcined clay, CAC2 (the latter has been developed for use in agricultural films to increase film life, compared with CAC1). Both were compounded in PE to produce masterbatches. These, together with the unfilled polymer, were studied by IGC.

Blown films were prepared from each masterbatch and subjected to accelerated and natural weathering. Degradation was assessed by FTIR analysis and mechanical testing. Differences were related to the surface thermodynamic properties of the minerals.

6.1 Materials

Physical properties for CAC1 and CAC2 and were measured as detailed in Chapter 3, and are detailed in Table 6.1. Physical properties of the low density PE (Borealis LE 1870) are given in Table 6.2[241].

Table 6.1 Physical and chemical properties of calcined clays CAC1 and CAC2.

		CAC1	CAC2
ISO brightness		88.8	92.0
ECC yellowness		4.9	4.6
BET surface area (m^{-2} g^{-1})		7.0	7.1
Particle size (wt.%)	> 10 μm	5	6
	> 5 μm	15	17
	< 2 μm	49	49
	< 1 μm	12	12
	< 0.5 μm	< 5	6
	< 0.25 μm	< 5	< 5
Composition (wt.%)	SiO_2	55.8	55.9
	Al_2O_3	41.0	41.5
	Fe_2O_3	0.59	0.41
	TiO_2	0.06	0.02
	CaO	0.01	0.02
	MgO	0.19	0.11
	K_2O	2.21	1.90
	Na_2O	0.01	0.01
	Loss on ignition	0.30	0.20

Table 6.2 Physical properties for PE.

Property	**Test Method**	**Value**
Melt flow index (g 10 min^{-1})	190 °C, 2.16 kg, ISO 1133	2.0
Density (kg m^{-3})	ISO 1183	922
Tensile strength (MD/TD) (MPa)	ISO 1184	22/15
Tensile modulus (MD/TD) (MPa)	ASTM D 882-A	180/190
Tear strength (MD/TD) (N)	ISO 6383	4/2
Dart drop impact strength (g)	ISO 7765 1A	90
Haze (%)	ASTM D 1003	9
Gloss	ASTM D 2457	95

The calcined clays were compounded into PE (50 wt.%) with an APV MP2030 twin screw extruder. Die temperature was 180 °C, with a screw speed of 250 RPM. Masterbatches were dried overnight at 60 °C in a Conair Churchill desiccant dryer.

These were diluted with the original polymer in a Betol BK 32 film extruder to produce 30 μm thickness, with 5 wt.% filler in the films.

Samples of the two masterbatches were mounted onto aluminium sample stubs, and gold-coated. The masterbatch surfaces were then viewed by SEM, as detailed in chapter 4. Elemental surface analyses were carried out by XPS. Digital images were produced at low and high magnification to illustrate the surface nature of the granules.

The thermal transitions for the PP were measured by differential scanning calorimetry (DSC) with a Perkin-Elmer V1.8TA. Scanning rate was 10 °C min^{-1}, with a temperature range of – 150 to 250 °C, under a nitrogen atmosphere.

6.2 **Chromatography**

The GC mineral fractions were prepared as detailed in section 2.1.2.

Chromasorb W, AW DMCS treated, 100-120 mesh, was used as an inert support for the PE and masterbatch GC fractions. The stationary phase was dissolved in cyclohexane (AnalR grade) and coated onto Chromasorb W (10 w/w %) by stirring at 90 °C. After rotary evaporation, the coated support was dried in vacuum at 60 °C to a constant weight. The exact loading of the stationary phase was determined by repeat calcination at 1000 °C in a CEM AirWave 7000 microwave furnace. For the masterbatch, a blank was run and the mass loss contribution for the calcined clay was adjusted accordingly. Stainless steel columns were prepared and packed, as detailed previously.

The column was connected to the GC and pre-conditioned at 150 °C for 24 hours, before further conditioning for twelve hours at the required temperature. Data were collected as detailed previously.

For polyethylene, the method was repeated at temperatures from 80 to 170 °C at 5 ° intervals, with the column conditioned for 12 hours between each temperature change. A further data set was collected between 90 and 110 °C at 2 ° intervals.

For the masterbatches data were collected between 70 and 160 °C at 10 ° intervals, with data collected every 2 °C between 100 to 110 °C. For the calcined clays, data were collected between 80 to 140 °C at 10 ° intervals.

6.3 **Results and Discussion**

6.3.1 *Polyethylene*

The net retention volume for each probe was calculated as outlined earlier. To illustrate phase transitions, a plot of log of retention volume versus reciprocal of absolute temperature was used[34] (Figure 6.1).

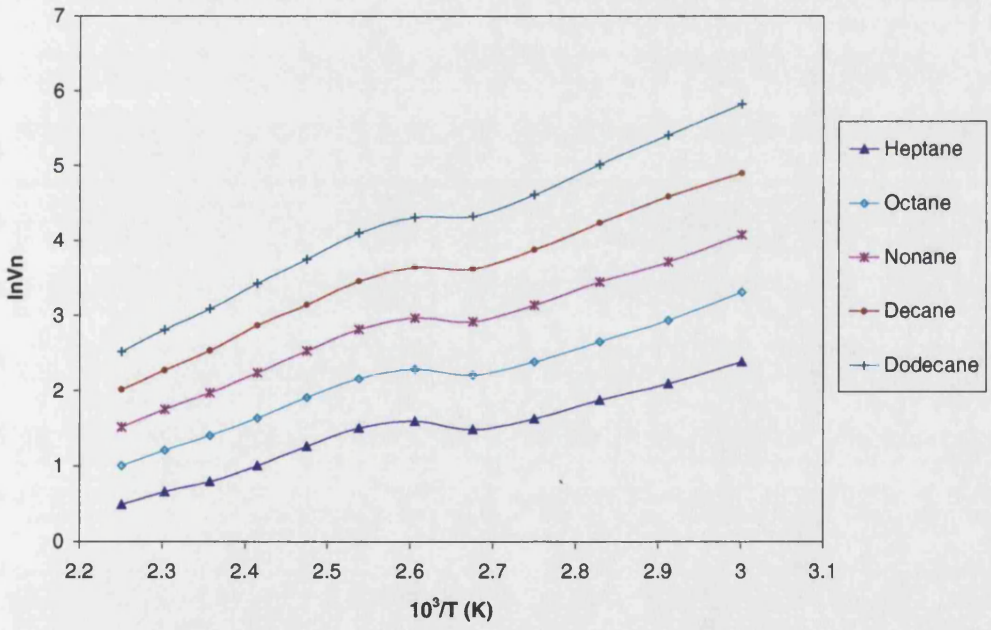

Figure 6.1 Plot of lnV_n versus reciprocal of absolute temperature for heptane to dodecane.

The deviations from linearity correspond to phase transitions. The first deviation from linearity, detectable with all probes, corresponds to the melting point, T_m. Below this, the slope of the segment is given by $(\Delta H_v - \Delta H_a)/R$, where ΔH_v is the latent heat of vaporisation of the probe and ΔH_a is the enthalpy of adsorption of the probe on the polymer surface.

Below T_m, at zero surface coverage the differential heat of adsorption q_a^0 (equal to $-\Delta H_a^0$) can be calculated from equation (6.1),

$$\frac{d(\ln K_s)}{d(1/T)} = \frac{q_a^0}{R} \qquad (6.1)$$

From the initial linear portion of the curve in Figure 6.1, the slope, as shown in Figure 6.2, is defined as $-\Delta H_a^0/R$. Results for each alkane are given in Table 6.3.

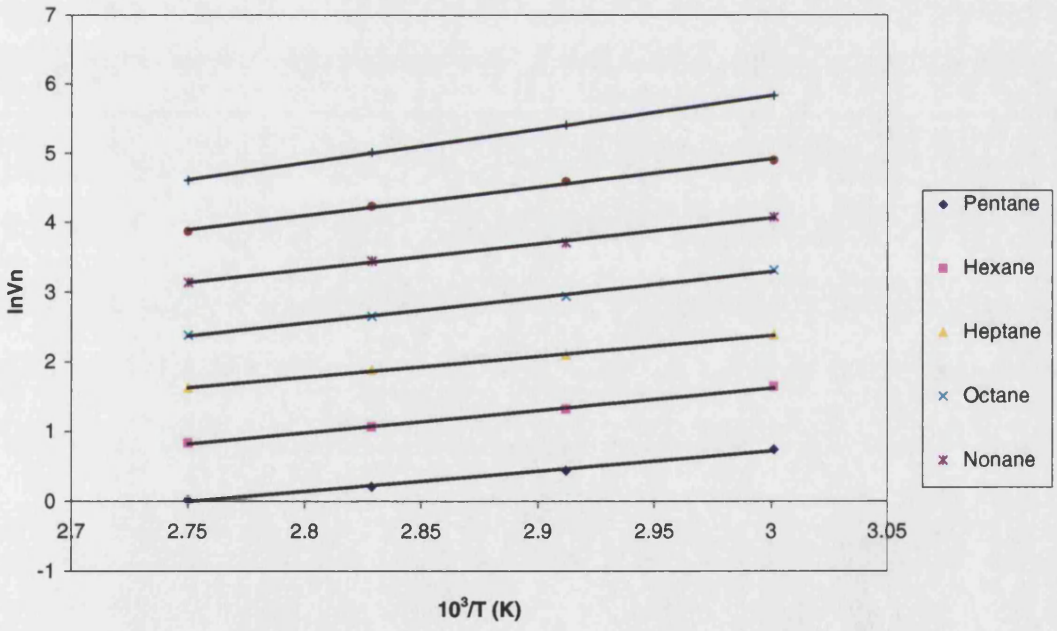

Figure 6.2 Plot of lnV_n versus 1/T to calculate $-\Delta H_a^0$.

Table 6.3 Results for isosteric enthalpies of adsorption for n-alkanes.

	$-\Delta H_a^0$ (kJ mol^{-1})	R^2
Pentane	24 ± 2	0.99
Hexane	27 ± 2	0.98
Heptane	25 ± 2	0.99
Octane	31 ± 1	0.99
Nonane	31 ± 2	0.99
Decane	34 ± 2	0.99
Dodecane	40 ± 2	0.99

To determine T_m, retention volumes for pentane, hexane and heptane were measured at 2 °C intervals (Figure 6.3). The main transition occurred at 108 °C. However, a second transition was seen at 101 °C. Additionally, with these probes, a third possible transition was noted at 151 °C.

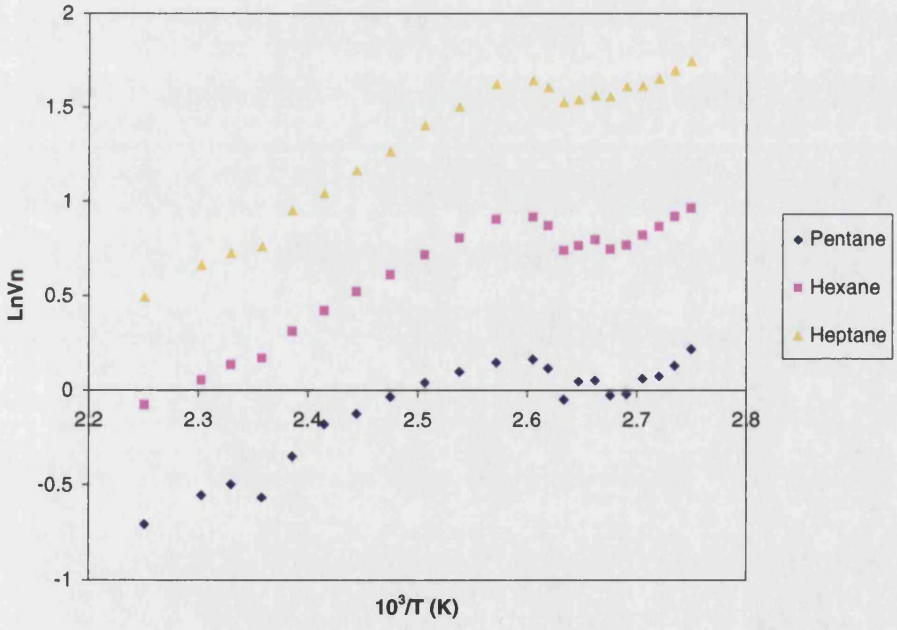

Figure 6.3 Plot of lnV_n versus 1/T for pentane to hexane, illustrating complete phase transitions.

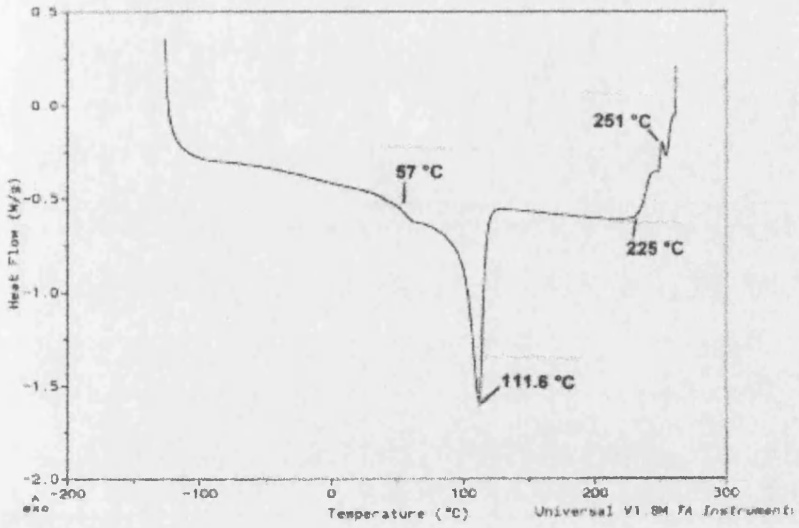

Figure 6.4 DSC plot of heat flow versus temperature for PE.

The main transition occurring at 108 °C corresponds to the melting point. This was determined by DSC as 111.6 °C (Figure 6.4). The differences between these two results may be due to the extensive conditioning used during IGC data collection resulting in a reduction in crystallinity. The minor deviations from linearity, seen in Figure 6.3, are within experimental uncertainty, as retention times were relatively short and the transitions were not reproduced by DSC analysis. Their presence, however, for all three lower alkanes may have some significance in terms of interactions in different crystalline phases, although no further investigations were carried out.

A plot of $RT\ln V_n$ versus number of carbon atoms for a series of linear alkanes gives a slope of ΔG_a. From the slope, the free energy of adsorption can be found, as described previously. Above T_m, retention data can be used to calculate the bulk free energy (Table 6.4).

Table 6.4 Free energy of adsorption results for PE.

Temp. (°C)	ΔG_{ads} (mJ m^{-2})	Temp. (°C)	ΔG_{sol} (mJ m^{-2})
70	33 ± 2	160	28 ± 1
80	33 ± 1	170	28 ± 1
90	32 ± 2		

From published data, surface free energy for polyethylene is quoted as 31 mJ m^{-2} [242]. The results obtained for free energy of adsorption (ΔG_{ads}) below T_m (Table 6.4) were similar to those for the published surface free energy results. Retention volume contributions are due to surface adsorption, bulk absorption and surface condensation of the probes. Enthalpies of solution (ΔG_{sol}) were obtained from retention volumes above T_m. Retention volume contributions arise from sorption in the amorphous polymer phase. ΔG_{sol} results were slightly lower than those found for ΔG_{ads} due to the absence of surface condensation adsorption effects.

From the retention volumes for polar probes at 100 °C, specific interactions were calculated (Table 6.5), using a plot of ΔG_a versus log P_o (Figures 6.5 and 6.6).

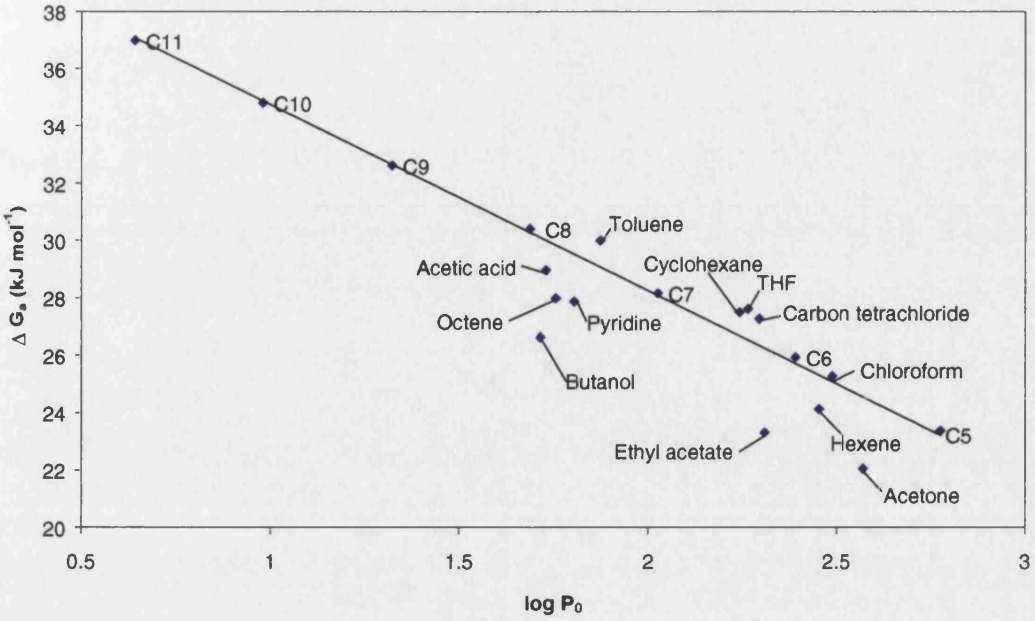

Figure 6.5 Plot of ΔG_a versus log P_o to illustrate specific interactions, including alkanes C5 to C11.

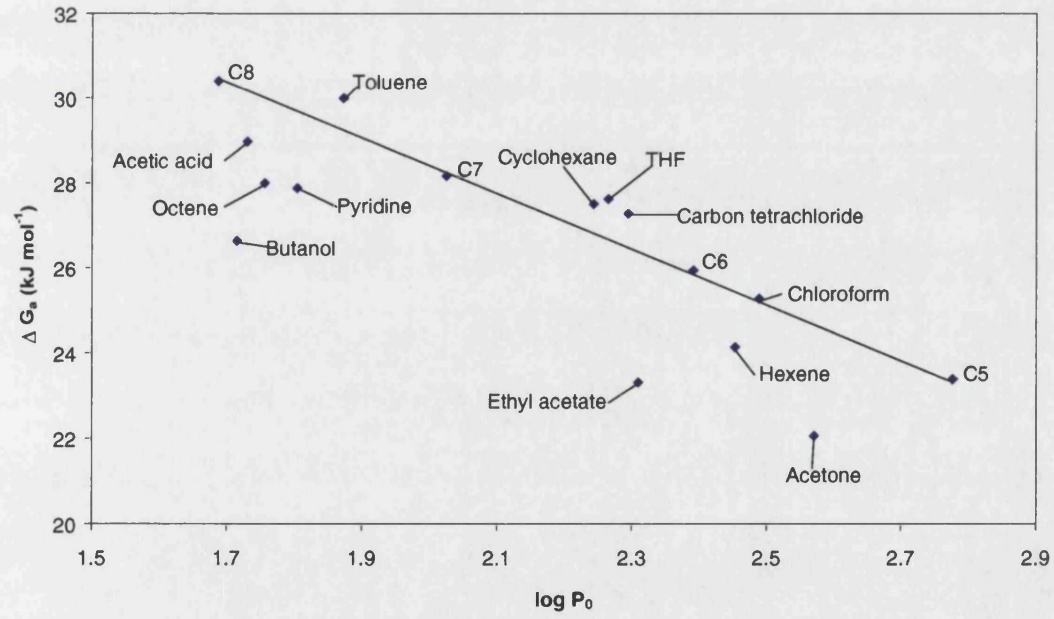

Figure 6.6 Plot of ΔG_a versus log P_o to illustrate specific interactions, C5 to C8 region.

Table 6.5 Specific interaction data at 100 °C.

Probe	Specific interaction $-\Delta G_{specific}$ (kJ mol^{-1})	Acid No.[38]	Donor No.	Characterisation
Acetic acid	-1.3 ± 1.2	52.9		Strong acid
Butan-1-ol	-3.7 ± 2.1			Acid
Chloroform	0.1 ± 1.1	23.1	0	Weak acid
Carbon tetrachloride	0.8 ± 1.3	8.6	0	Weak acid
Cyclohexane	0.6 ± 1.5			Non-polar
Acetone	-2.7 ± 1.6	12.5	17.0	Amphoteric
Ethyl acetate	-3.2 ± 1.3	9.3	17.1	Amphoteric
Hexene	-1.4 ± 0.9			Weak base
Octene	-2.1 ± 1.2			Weak base
Toluene	0.7 ± 1.0			
THF	0.9 ± 0.8	8.0	20.0	Base
Pyridine	-1.9 ± 1.4	14.2	33.1	Strong base

Specific interactions for PE were low, ranging from –3.7 kJ mol^{-1} for butanol to + 0.9 kJ mol^{-1} for THF, with variations in results up to ± 2.1 kJ mol^{-1}. No trends were seen with probe acceptor/donor characteristics. As PE is primarily non-polar, no significant polar interactions would be expected. The results confirmed the predominantly non-polar nature of polyethylene.

6.3.2 *Composites and calcined clays*

For the masterbatches, a plot of $ln V_n$ versus 1/T was used to illustrate phase changes (Figures 6.7 and 6.8), as demonstrated with the polyethylene (Figure 6.1).

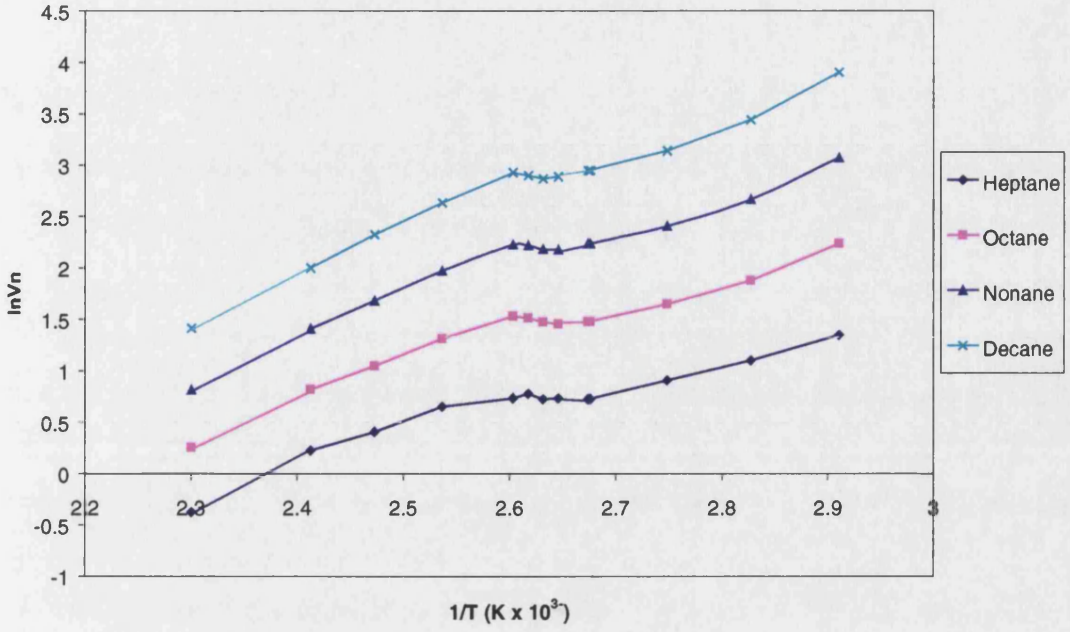

Figure 6.7 Plot of $ln V_n$ versus 1/T for CAC1 masterbatch.

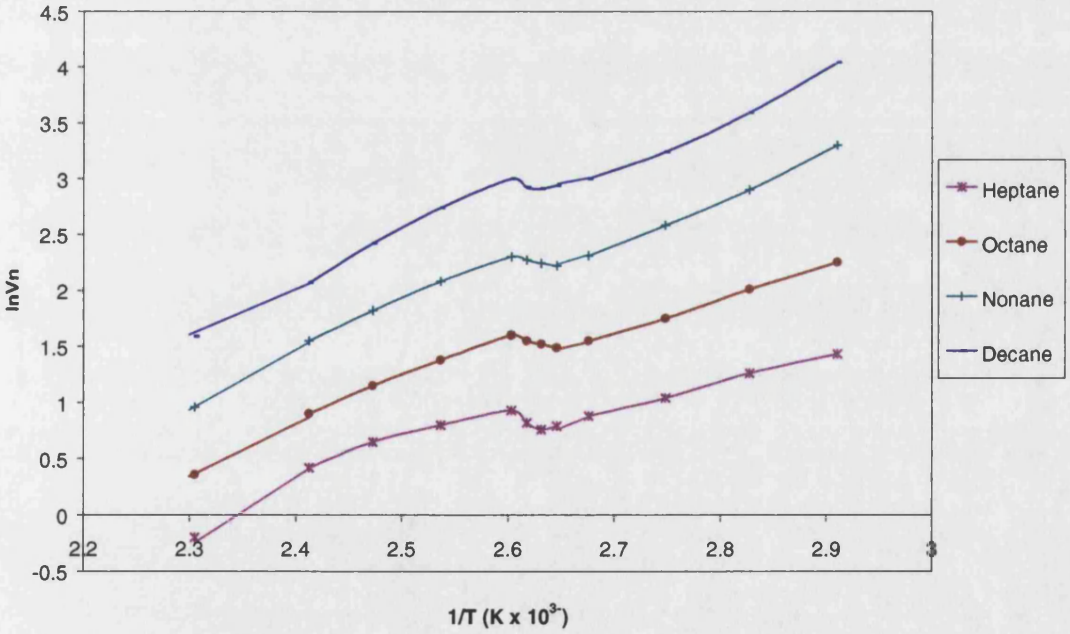

Figure 6.8 Plot of $ln V_n$ versus 1/T for CAC2 masterbatch.

The deviation from linearity for both CAC1 and CAC2 masterbatches was found at 106 °C. This was comparable with the polyethylene phase change of 108 °C. T_m did not therefore change with filler addition.

From the initial linear portion of the curve (Figures 6.7 and 6.8), the slope is defined as $-\Delta H_a^0/R$. Retention volumes for pentane and hexane were very small, with high standard deviations. Thus $-\Delta H_a^0$ was calculated for heptane to decane only (Table 6.6).

For the calcined clays, enthalpies of adsorption were determined from plots of ΔG_a versus T (Figures 6.9 and 6.10), as defined in Chapter 5. Retention volumes for nonane and decane were large and showed marked peak tailing. Thus $-\Delta H_a^0$ was calculated for pentane to octane only (Table 6.6).

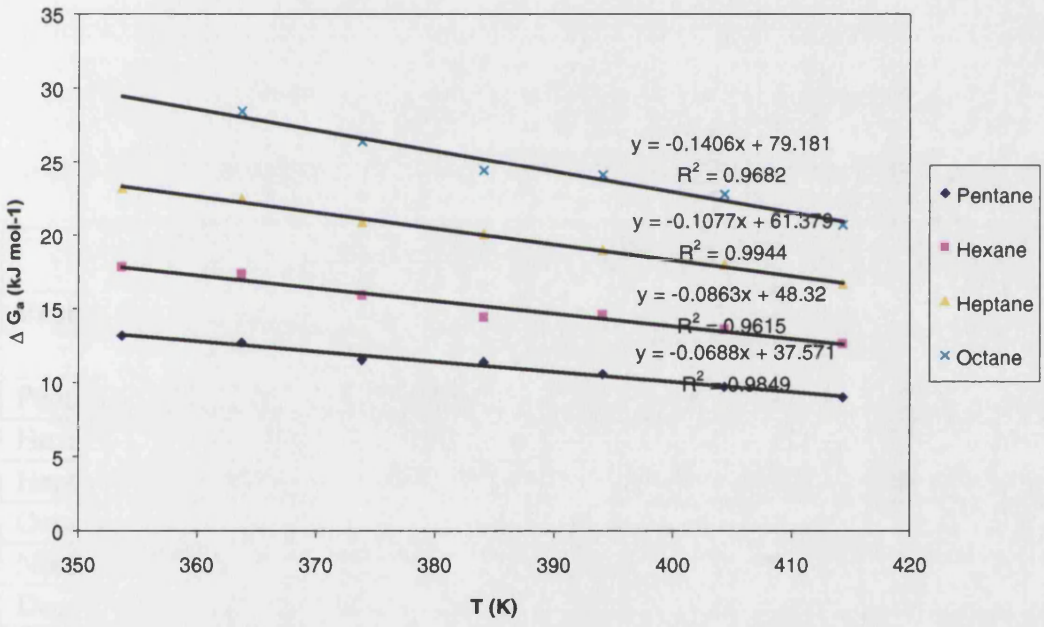

Figure 6.9 Plot of ΔG_a versus T for CAC1.

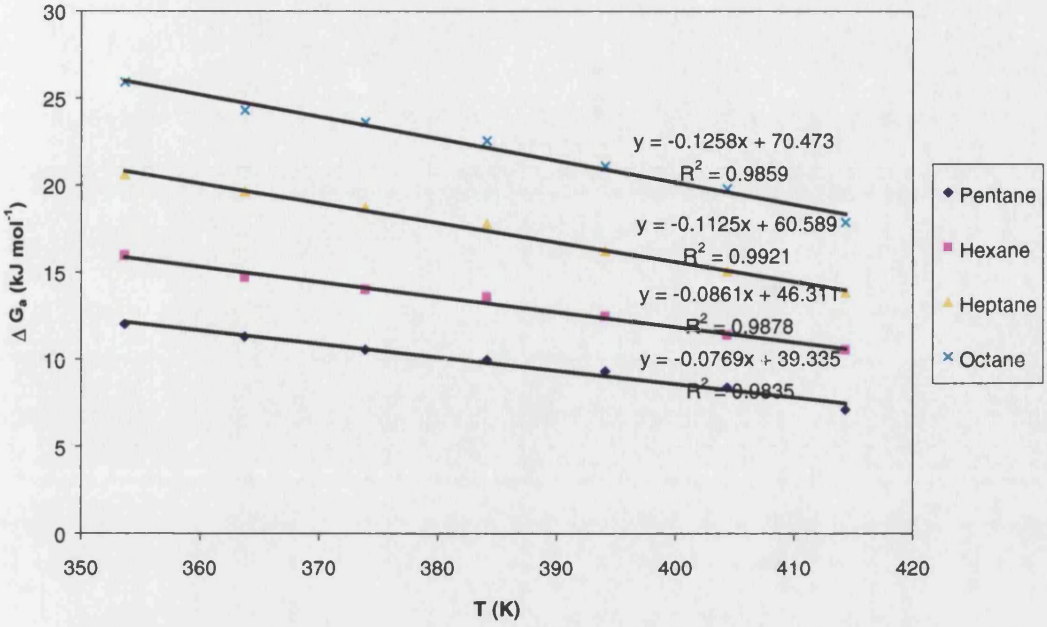

Figure 6.10 Plot of ΔG_a versus T for CAC2.

Table 6.6 Enthalpy of adsorption data for CAC1 and CAC2, and adsorption data for masterbatches (with PE data from Table 6.3).

	Enthalpy of Adsorption (kJ mol^{-1})				
Probe	**CAC1**	**CAC2**	**CAC1 masterbatch**	**CAC2 masterbatch**	**PE**
Pentane	38 ± 2	39 ± 4			24 ± 2
Hexane	48 ± 3	46 ± 2			27 ± 2
Heptane	62 ± 2	61 ± 2	52 ± 3	49 ± 2	25 ± 2
Octane	79 ± 2	70 ± 3	59 ± 2	58 ± 3	31 ± 1
Nonane			60 ± 3	62 ± 2	31 ± 2
Decane			66 ± 2	63 ± 2	34 ± 2

Table 6.7 Dispersive component of surface free energy data for CAC1 and CAC2, with masterbatch and PE results.

	Dispersive component of surface free energy (mJ m^{-2})				
Temperature (°C)	**CAC1**	**CAC2**	**CAC1 masterbatch**	**CAC2 masterbatch**	**PE**
80	139 ± 4	128 ± 4	32 ± 1	30 ± 2	33 ± 1
90	137 ± 5	117 ± 4	32 ± 2	33 ± 1	32 ± 2
100	132 ± 4	115 ± 3	34 ± 2	35 ± 2	
110	126 ± 4	111 ± 5	36 ± 2	32 ± 1	
120	130 ± 3	113 ± 4	34 ± 1	33 ± 2	
130	124 ± 2	111 ± 3	33 ± 1	35 ± 2	
140	113 ± 2	108 ± 4	36 ± 2	34 ± 1	

For the calcined clays, CAC1 and CAC2, the adsorption enthalpies were 10 to 20 kJ mol^{-1} higher than the corresponding masterbatches. The presence of 50 wt.% PE thus had a marked, but lesser contribution to adsorption enthalpy, than the calcined clay component. Differences between CAC1 and CAC2 were not significant either for the calcined clays or the corresponding masterbatches.

The dispersive component of surface free energy results for CAC1 and CAC2 (Table 6.7) were high, but lower than those for the hydrous clays detailed earlier (chapter 5). Free energy was found to decrease with increasing temperature. Results for CAC2 were between 5 to 20 mJ m^{-2} lower than those for CAC1. These differences were considered significant. Differences in results for both masterbatches were within experimental error and equivalent to those for PE. Thus the surface free energy contribution was dominated by the presence of the polyethylene component.

To determine any acceptor-donor differences between CAC1 and CAC2, polar probes were injected at 100 °C. Specific interactions were calculated as detailed above, by plotting ΔG_a versus log P_o (Figures 6.11 and 6.12). Results are summarised in Table 6.8.

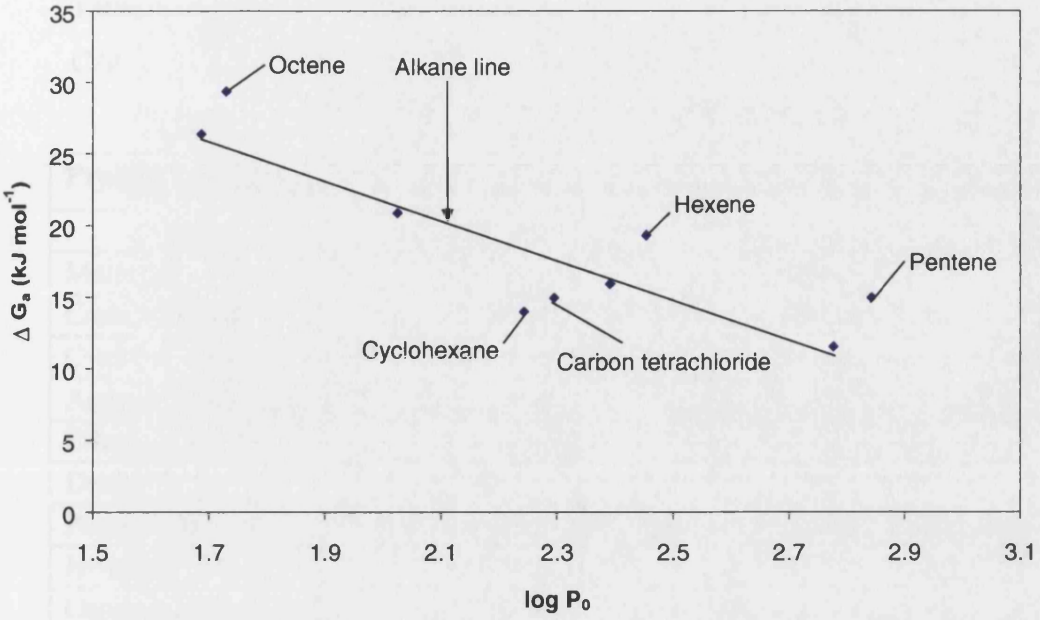

Figure 6.11 Plot of ΔG_a versus log P_o for CAC1.

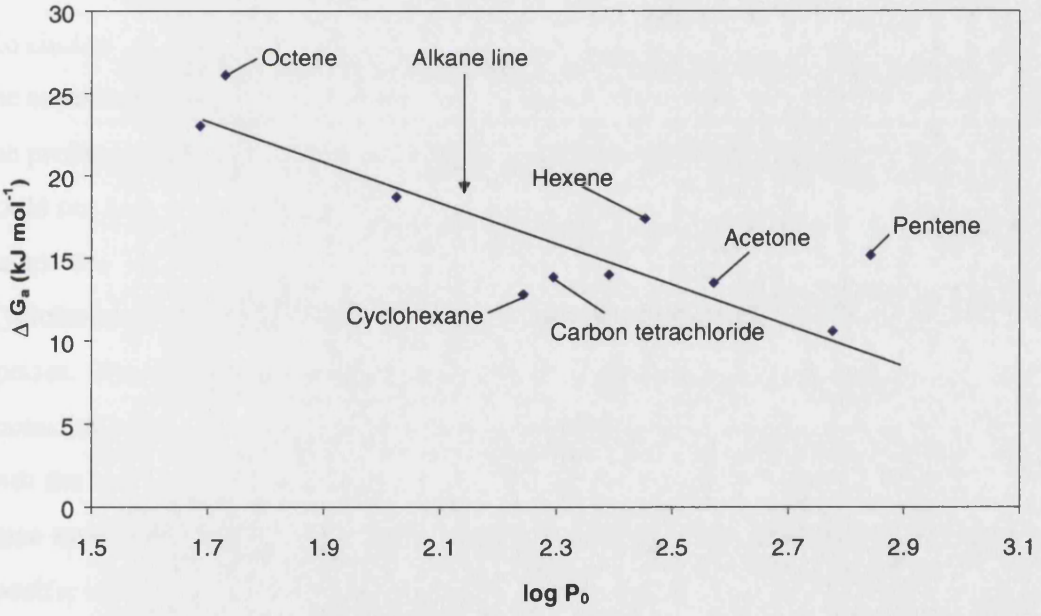

Figure 6.12 Plot of ΔG_a versus log P_o for CAC2.

Table 6.8. Details of specific interactions with polar probes for CAC1 and CAC2.

Probe	Specific interaction $-\Delta G_{specific}$ (kJ mol^{-1})	
	CAC1	CAC2
Methanol	NPD*	NPD
Carbon tetrachloride	-2.7 ± 0.9	-2.1 ± 0.6
Cyclohexane	-4.3 ± 1.1	-3.8 ± 1.0
Acetone	NPD	1.0 ± 0.4
Ethyl acetate	NPD	NPD
Diethyl ether	NPD	NPD
Pentene	4.9 ± 1.2	5.9 ± 1.4
Hexene	4.0 ± 0.9	3.4 ± 0.6
Octene	3.8 ± 0.7	3.0 ± 0.9
Diethylamine	NPD	NPD
THF	NPD	NPD
Pyridine	NPD	NPD

* NPD = no peak detected.

No elution peaks could be detected for strongly basic probes within the sampling time of the experiments. These were thus considered to interact strongly with the surface, with the probes possibly becoming bound irreversibly. The strongly acidic probe, methanol, could not be detected, although carbon tetrachloride interacted weakly, with the datapoints falling below the alkane line. This was also seen with cyclohexane. Cyclohexane was eluted to determine the accessibility of the surface to a bulky probe species. No differences were seen between CAC1 and CAC2, indicating similar accessibility and porosity. For CAC2, a greater deviation from the baseline was seen with the lower alkenes, although this was reduced with increasing chain length. The same trend was seen, to a lesser extent, with CAC1. With the exception of pentene, specific interaction energies were marginally lower with CAC2 than CAC1. It is also noteworthy that the acetone probe was detected after elution from CAC2, but was not detected for CAC1.

6.3.3 *Weathering testing of polyethylene films*

Twelve samples (25 x 150 mm) from each of the three films, CAC1, CAC2 and UF (unfilled) were subjected to accelerated ageing in a QUV Weatherometer, according to standard test methods[243]. A sample of each film was removed every twenty five hours, up to two hundred hours. After this time, the films lost most of their mechanical strength, and started to embrittle significantly.

Degradation of the films was assessed by Fourier Transform Infra-red (FTIR) analysis[244] and tensile testing of unaged and incrementally weathered samples[245]. Tensile strength and elongation at break were measured on a Monsanto T10, with 100N load cell according to standard test procedures[246], with a sample size of 25 x 60 mm (non-standard). FTIR spectra of the films were collected using a Nicolet Magna-IR 550 spectrometer. Carbonyl formation (ketone and carboxylic acid) was quantified by peak area measurement at 1715 cm^{-1}.

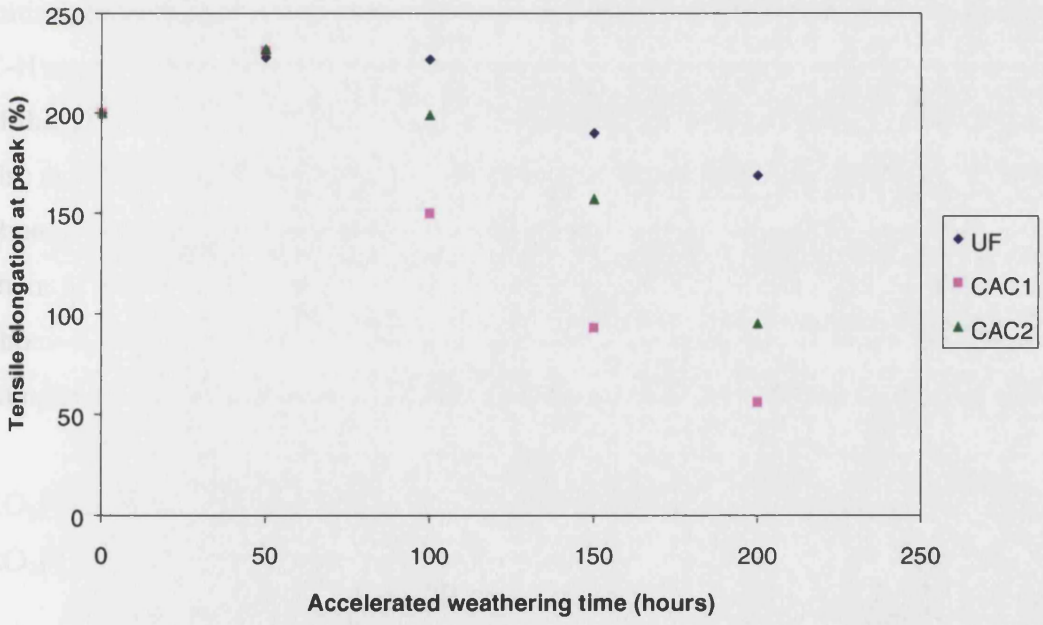

Figure 6.13 Peak elongation versus weathering time for PE films.

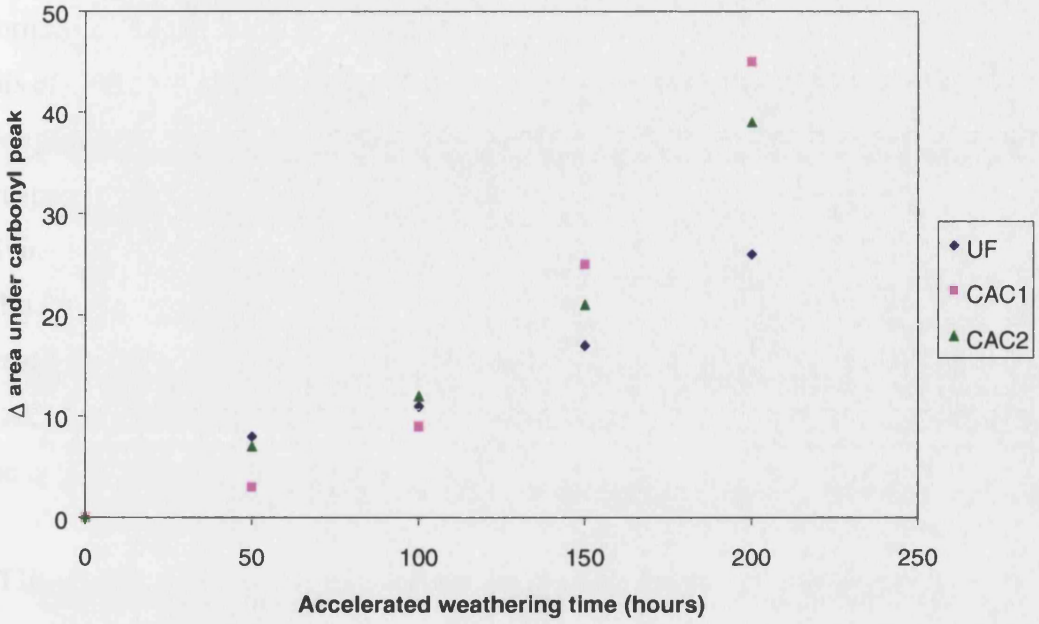

Figure 6.14 Area under the carbonyl peak versus weathering time for PE films.

The UV degradation of polyethylene proceeds via a radical chain reaction involving initiation, propagation, branching and termination[247]. Once a free radical is formed the C-H and C-C bonds adjacent to the radical site undergo cleavage, resulting in a rupture of the polymer chains. This is photo-degradation[248]. The free radicals produced may also react with atmospheric oxygen and lead to further degradation. This is known as photo-oxidation. The presence of trace metals and chemical irregularities in the polymer chain formed during fabrication and processing will act as initiation centres for the photo-oxidation of polyethylene. Metal ions catalyse oxidation by forming unstable complexes with alkyl hydroperoxides, followed by electron transfer to give radicals.

$$RO_2H + M^{n+} \rightarrow RO^{\cdot} + M^{(n+1)+} + OH^-$$

$$RO_2H + M^{(n+1)+} \rightarrow RO_2^{\cdot} + Mn^+ + H^+$$

Thus a strong reducing agent, like ferrous iron, will form $RO^{\cdot}$ radicals. The effect of the metal ion is thus to speed up the rate of initiation by accelerating the rate of peroxide decomposition to free radicals. UV degradation of polyethylene film is characterised by embrittlement due to bond cleavage and depolymerisation.

The elongational component of the film is therefore reduced as degradation occurs. The normalised elongation at peak data for the weathered films (Figure 6.13) demonstrated this effect. After 50 hours accelerated weathering, all films showed an increase in elongation. Increased elongation occurs because of chain relaxation during heating in the weatherometer. After 100 hours, clear differences were seen between the films, with UF giving the least change in elongation, compared with the unaged films, and CAC1-based film showing the greatest reduction in elongation. This trend continued up to 200 hours weathering. After this time, both the filled-films showed significant embrittlement, with CAC1 film giving a value of 30 % of the original value and CAC2 film giving 50 % of the original value.

FTIR analysis was considered to be a more precise method for determining degradation. During the photo-oxidation stage, ketones and carboxylates are formed[240]. These can be detected by the formation of a carbonyl peak. Change in carbonyl peak area, as detailed in Figure 6.14, indicated the rate of degradation. Both CAC1 and CAC2-filled films showed a much greater increase in carbonyl peak with weathering time than UF film. The greatest change in peak area was seen for the CAC1-filled film.

Thus the addition of both CAC1 and CAC2 lead to an embrittlement of the films compared with the unfilled film. The degradation of films containing CAC2, however, was less severe than those containing CAC1.

6.3.4 *XPS and SEM analyses of composites*

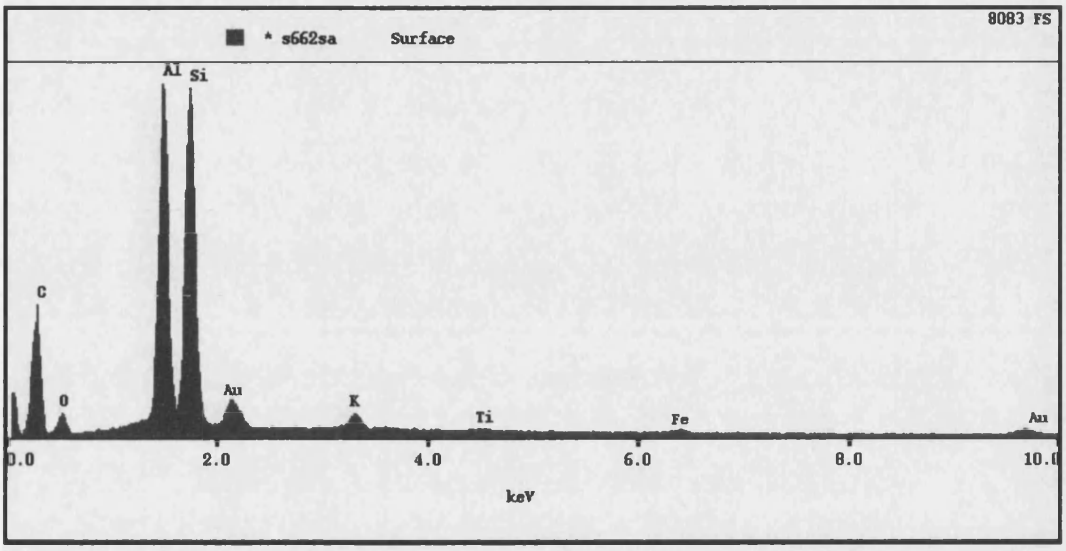

Figure 6.15 XPS analysis of the CAC1 masterbatch.

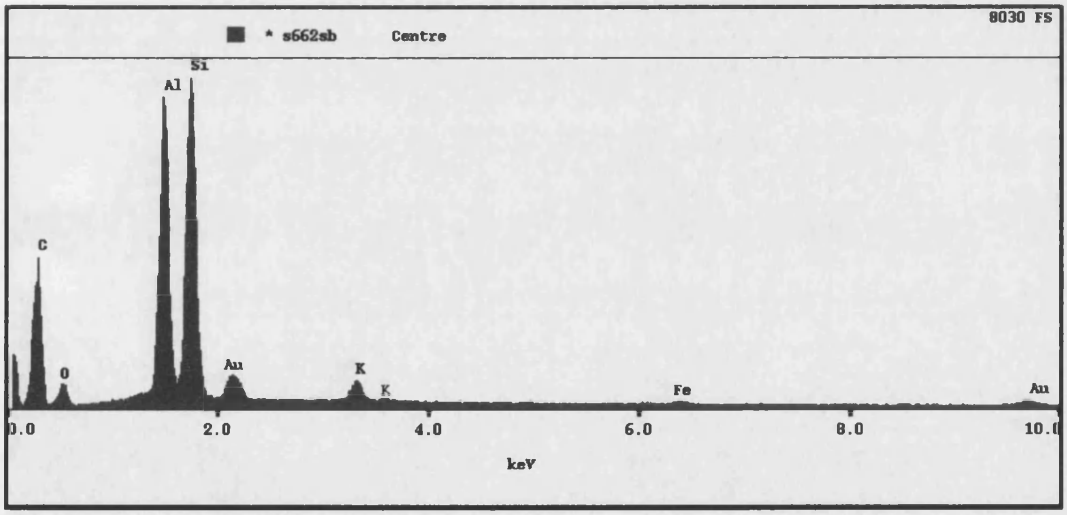

Figure 6.16 XPS analysis of the CAC2 masterbatch.

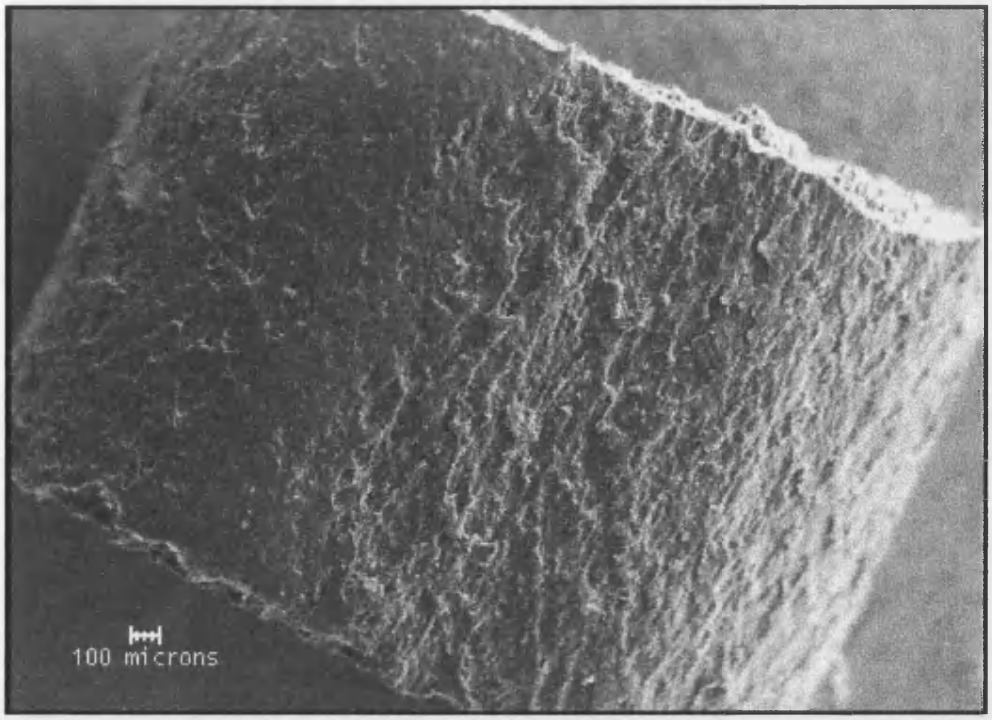

Figure 6.17 SEM image of the CAC1 masterbatch, low magnification.

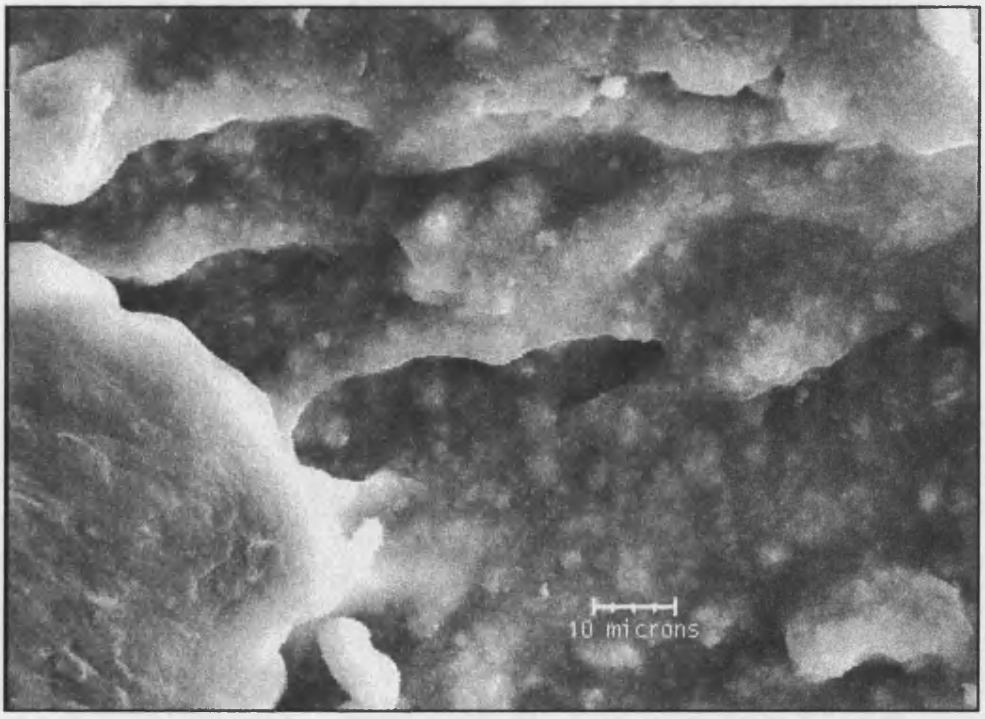

Figure 6.18 SEM image of the CAC1 masterbatch, high magnification.

From the XPS analysis, the composite surface comprised a mixture of silicon and aluminium, as would be expected from a calcined clay. No significant differences were seen between CAC1 and CAC2 masterbatches. A large carbon peak indicated the presence of polyethylene. The SEM images of the masterbatches revealed a rough surface, with the calcined clay particles encapsulated in a thin polymeric film. The surface could thus be described as one predominantly comprising calcined clay embedded within a polymeric matrix.

6.4 **Further discussion**

The elution of linear alkanes at different temperatures was used to determine the phase transitions for PE. The melting point result was found to be slightly lower than that obtained by DSC. This is considered to be due to differences in thermal history of the two samples. Some minor transitions were also noted using the lower alkanes. Although these were not discernible by DSC they may be either due to an artefact of the relatively short retention times, or caused by subtle differences in crystallinity at elevated temperatures.

Adsorption enthalpies of the calcined clays were approximately 20 % higher than those measured for the masterbatches. Adsorption enthalpies for PE were, however, approximately 50 % lower than those determined for the masterbatches. The contribution to adsorption enthalpy was, therefore, disproportionately greater for the calcined clay component than the PE component. No differences were seen between CAC1 and CAC2. The dispersive component of surface free energy was, however, considerably lower for CAC2 than CAC1. This was not reflected in the free energy values for the masterbatches. In this case, results were dominated by the PE contribution, with similar results being obtained at 80 and 90 °C. The strong adsorption forces were, therefore primarily due to the calcined clay. The weaker, short range van der Waals interactions, as indicated by the surface free energies, are affected by the thin covering of polyethylene.

Calculations from retention data for linear alkanes highlight the different interactions taking place at the mineral, polymer and composite surfaces. Sorption mechanisms for the masterbatch and polymer both arise from surface adsorption, surface condensation and bulk sorption in the amorphous regions. No changes in melt temperature were observed between the PE and the masterbatches. The amorphous regions were considered to be comparable, although some alterations may occur depending on their thermal history. The differences in enthalpy of adsorption results must therefore be due to surface effects. Addition of calcined clay to PE permitted greater accessibility of the probe molecules to the total surface area, probably by presenting a more irregular surface onto which the probes adsorbed or condensed.

Specific interaction enthalpies for the calcined clays were higher than for PE, with results for PE showing relatively high standard deviations. Clay surfaces have both acidic and basic sites, giving rise to local interactions (as detailed in chapter 5).

UV film stability was assessed by accelerated weathering, and measured by incremental tensile and FTIR analyses. Both methods revealed differences between the unfilled PE, and films containing CAC1 and CAC2. CAC1 was found to have some surface sites of higher energy than CAC2. These sites must therefore be influential in catalysing UV degradation. These results support the findings of Hancock et al.[249]. They compared the photo-degradability of stabilised polyethylene films containing hydrous clays and calcined clays. Films containing hydrous clays degraded significantly faster than those containing calcined clays, even though the two clays had comparable levels of heavy metals, known to catalyse photo-oxidation. These differences were attributed primarily to the number of surface active Lewis acid sites, rather than the presence of heavy metals. Surface activity, as defined by the dispersive component of surface free energy, was higher for CAC1 than CAC2. Additionally, some differences may also occur due to polar interactions, although these were considered to be less important for the calcined clays.

Studies using FMC have been used to evaluate the effects of stabilisers on LDPE films with silica additives[250]. Interactions were found to be complex, but were influenced firstly by surface area and porosity; secondly by surface activity, including functionality; and thirdly by "hydrophilicity" or surface energy.

Stabilisers were not added to the films produced for this study, and thus their influence was not measured. Polar interactions may, in these instances, play a more dominant role. From IGC results, CAC1 was found to be slightly more accessible to the non-polar, bulky probe cyclohexane. This would indicate a slightly higher porosity.

The IGC results obtained from this study illustrated both the strengths and limitations of the technique. Subtle differences between CAC1 and CAC2 were found. The chemical composition of the minor elements of these clays was also different, and may also have affected these results. The technique could not readily differentiate these two components as the specific interaction data for polar probes were within the variability of the test method. Results from the accelerated weathering study could, however, be explained in terms of thermodynamic disparities between CAC1 and CAC2.

6.5 **Conclusions**

1. Surface energy results for PE, as defined by the free energy of adsorption, were comparable with those from the literature.

2. Enthalpy of adsorption results were highest for the calcined clays and slightly lower for the masterbatches. Results for the polyethylene were less than half of those for the calcined clays. The presence of calcined clay particles very near the surface of the masterbatch (as illustrated by the SEM analyses) therefore had a dominant effect on adsorption.

3. With the PE, the contribution of acidic and basic sites to the total surface free energy was slight. Contributions for CAC1 and CAC2 were higher, with CAC2 having a marginally lower acidic and basic surface activity than CAC1.

4. Changes in the PE films due to accelerated weathering were measured by changes in tensile properties and use of FTIR to quantify the formation of carbonyl species. The PE film was less degraded by exposure to UV radiation than films containing CAC1 or CAC2. The film containing CAC2 was, however, less degraded than that containing CAC1. Differences were attributed to the higher surface free energy of CAC1 compared with CAC2 and PE. Polar contributions were believed to be less significant.

5. Differences in surface free energy were considered to be influential in predicting differences in UV stability with comparable mineral additives. This fulfilled objective 7 in assessing the use of IGC in determining subtle differences in mineral composition and equating these to key characteristics of composite systems.

Polyethylene systems are relatively simple chemically, with no significant polar components. Polyamides (PAs), in contrast, are engineering thermoplastics with complex chemistries. These chemistries are exploited when modifying reinforcing fillers for PA systems. Calcined clays, such as those studied in chapter 6, are used with coupling agents in mineral-reinforced PAs. IGC was considered ideal for quantifying these surface modifications and relating them to physical properties. The following chapter details these studies.

7 SURFACE MODIFIED CALCINED CLAYS IN POLYAMIDE MOULDINGS

7.0 Introduction

Reinforced polyamides (PAs) have been in use since the 1950s. Early materials were based on glass fibre reinforcement[251]. Fibre-reinforced PA mouldings typically have increased toughness, abrasion resistance, tensile strength and modulus compared with unfilled systems. They are, however, anisotropic. For this reason a mixture of glass fibres and mineral fillers, including calcined clays, is more commonly used. These reinforced plastics find many applications, especially in the automotive industry as wheel trims, housings and under bonnet parts.

To ensure good mechanical properties, calcined clays are treated with silane coupling agents. These form "molecular bridges" between the polymer and clay surface through a number of means including chemical and hydrogen bonding and acid-base interactions[252]. Aminosilanes are often used, giving a siloxane bridge at the interface through equilibrium bonding[253]. Understanding of the surface chemistries of both the calcined clays and PA are essential in predicting end performance.

Two commercial grades of calcined clays, PoleStar 200R and PoleStar 400, were treated with an aminosilane coupling agent. These, labelled CAM1 and CAM2, were characterised by IGC to determine the effect of surface modification. CAM1 and CAM2 were compounded in nylon 6 (coded as PA) to produce masterbatches. These, together with the unfilled polymer, were studied by IGC.

Injection moulded test specimens were prepared from the masterbatches. Mechanical properties were measured on conditioned specimens. Results were compared with archive data for unmodified CAM1 (CAC1 from chapter 6). These properties were considered in relation to the surface thermodynamics of the unmodified and modified minerals.

7.1 Materials

Physical properties for CAM1 and CAM2 were measured as detailed in section 1.3, and are given in Table 7.1. Physical properties of the PA (Durethan 30S Nylon 6 from Bayer) are given in Table 7.2[254].

Table 7.1 Physical properties of calcined clays CAM1 and CAM2.

		CAM1	CAM2
ISO Brightness		88.8	91.2
ECC Yellowness		4.9	3.5
BET Surface area (m^{-2} g)		7.0	16.0
Particle size (wt.%)	> 10 μm	5	1
	> 5 μm	15	5
	< 2 μm	49	90
	< 1 μm	12	80
	< 0.5 μm	< 5	40
	< 0.25 μm	< 5	6
Composition (wt.%)	SiO_2	55.8	52.8
	Al_2O_3	41.0	44.2
	Fe_2O_3	0.59	1.0
	TiO_2	0.06	1.49
	CaO	0.01	0.08
	MgO	0.19	0.01
	K_2O	2.21	0.07
	Na_2O	0.01	0.01
	Loss on ignition	0.30	0.40

Table 7.2 Physical properties for PA.

Property	**Test Method**	**Value**
Density (kg m^{-3})	ISO 1183 (1987)	1140
Melting temp. (°C)	-	222
Tensile modulus (MPa)	ISO 527-1	3200
Tensile yield stress (MPa)	"	80
Tensile yield strain (%)	"	4
Deflection temp. under load (°C at 1.8 MPa)	ISO 75, Part 2	55
Deflection temp. under load (°C at 0.45 MPa)	"	180
Vicat softening temp. (°C)	ISO 306	200

The silane used for surface modification was a γ-aminopropyl triethoxysilane, NH_2–$(CH_2)_3$ –Si-(O-C_2H_5) (A1100 from Witco). The calcined clays were coated with a theoretical monolayer of silane, calculated from the footprint of the silane and the specific surface area of the clay. The clays were mixed in a Steele and Cowlishaw high-speed mixer for fifteen minutes. The silane reacted with the calcined clay with ethanol being formed as a bi-product. This was vented to atmosphere. The surface modified clays, CAM1 and CAM2 were conditioned in an air circulating oven for three days at 60 °C to drive off any residual ethanol or water before compounds were produced.

Compounds (at 20 wt.% filler) were prepared on an APV2030 twin screw extruder. The torque was maintained at 40 to 45 %, with a screw speed of 250 rpm. The temperature profile was 200, 240, 245, 250, 255 and 260 °C. After drying for 8 hours at 80 °C, compounds were dried for two hours at incremental temperatures of 60, 80 and 100 °C in a vacuum oven before moulding. Compounds were injection moulded on an Arburg 320M using a mould temperature of 100 °C. The temperature profile was 250 to 260 °C, with an injection speed of 100 cm^3 s^{-1} and an injection pressure to 1250 bar. Three moulding geometries were produced: 80 x 80 x 2 mm plaques; 80 x 10 x 4 mm bars and 120 x 10 x 4 mm dumbbells.

Physical properties of the filled compounds were measured after conditioning for a minimum of 14 days at 23 °C, 50 % relative humidity. Test methods were ISO standards, as detailed in chapter 4.

7.2 **Chromatography**

The GC mineral fractions were prepared as detailed in section 2.1.2. The PA stationary phase was prepared by the same method as the polypropylene (chapter 4) by milling in liquid nitrogen. Stainless steel columns of PA, CAM1 and CAM2 were prepared and packed, as detailed previously. The CAM1 and CAM2 columns were connected to the GC and pre-conditioned at 150 °C for 24 hours, before further conditioning for twelve hours at the required temperature. Data were collected as detailed previously. Data were collected between 80 to 140 °C at 10 ° intervals.

For the polyamide, the column was preconditioned at 120 °C. The method was repeated at temperatures from 60 to 100 °C at 10 ° intervals, with the column conditioned for 12 hours between each temperature change. Above this temperature the retention times were too short for accurate measurement.

7.3 **Results and Discussion**

7.3.1 *Chromatography*

The net retention volume for each probe was calculated as detailed in Section 1.4. Enthalpies of adsorption were determined from plots of ΔG_a versus T (Figures 7.1 to 7.3), as defined in Chapter 5, and are summarised in Table 7.3.

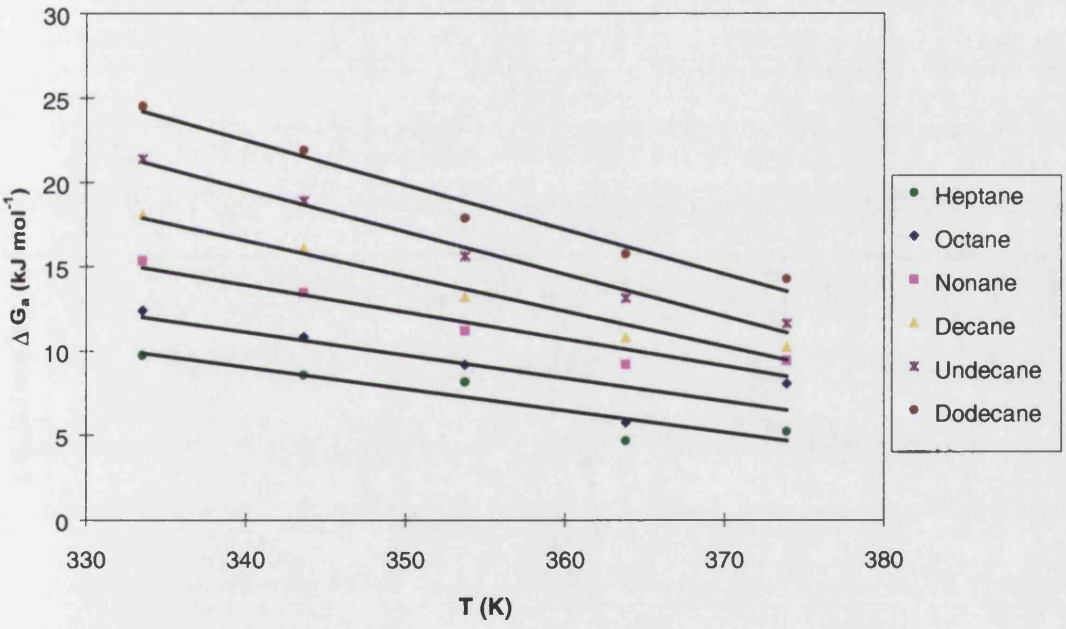

Figure 7.1 Plot of ΔG_a versus T for PA.

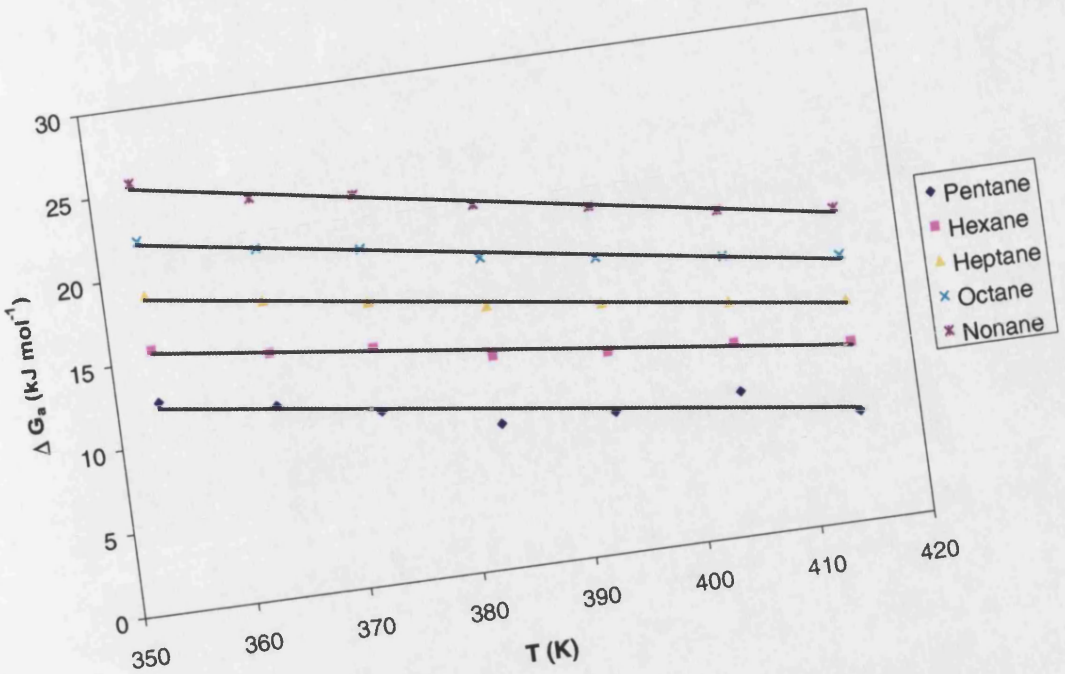

Figure 7.2 Plot of ΔG_a versus T for CAM1.

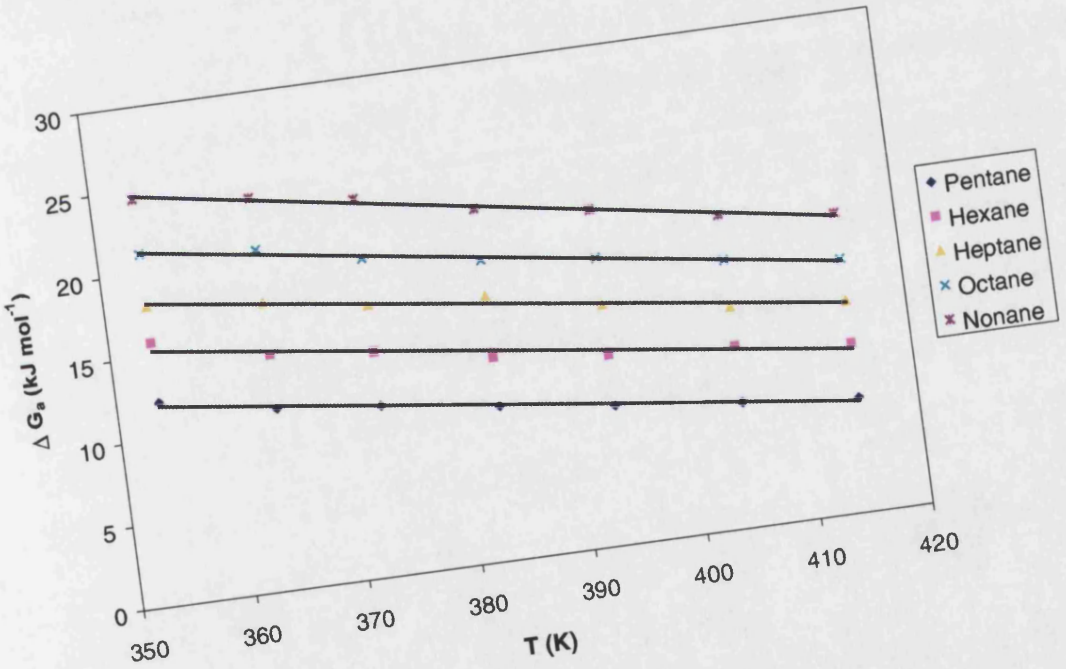

Figure 7.3 Plot of ΔG_a versus T for CAM2.

Table 7.3 Enthalpy of adsorption data for PA, CAM1 and CAM2.

	Enthalpy of Adsorption (kJ mol^{-1})		
Probe	**PA**	**CAM1**	**CAM2**
Pentane		44 ± 1.1	43 ± 0.2
Hexane		45 ± 0.6	47 ± 0.5
Heptane	53 ± 1.2	52 ± 0.3	50 ± 0.5
Octane	57 ± 0.3	59 ± 0.3	57 ± 0.4
Nonane	68 ± 0.8	66 ± 0.3	64 ± 0.2
Decane	88 ± 0.5		
Undecane	105 ± 0.6		
Dodecane	112 ± 0.9		

To determine the dispersive component of surface free energy $RTlnV_n$ was plotted versus number of carbon atoms, as illustrated in Figures 7.4 to 7.6. Results are given in Table 7.4.

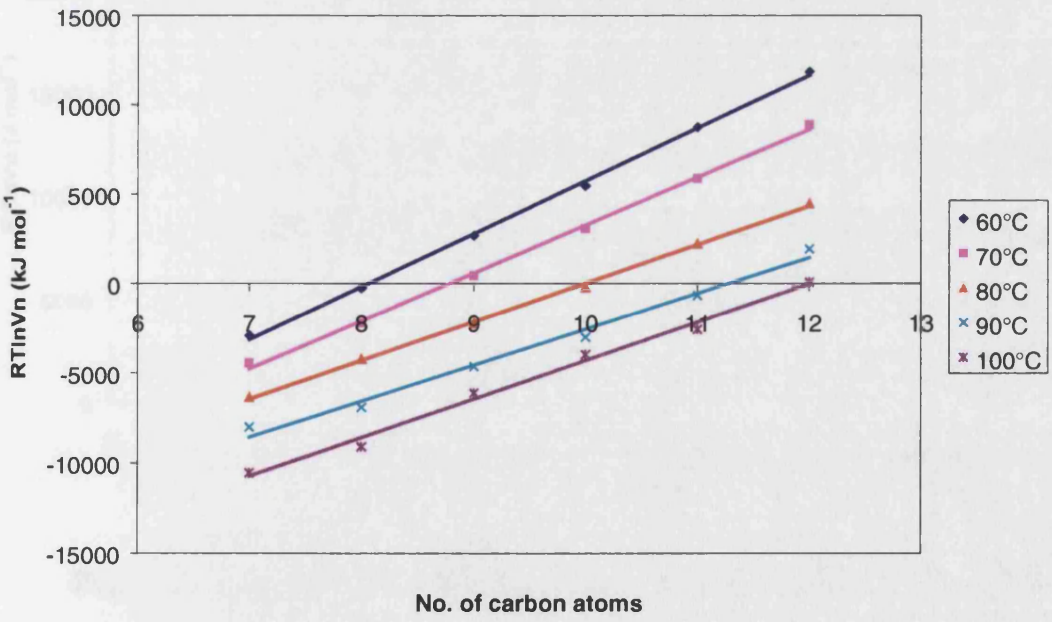

Figure 7.4 Plot of $RTlnV_n$ versus number of carbon atoms for PA.

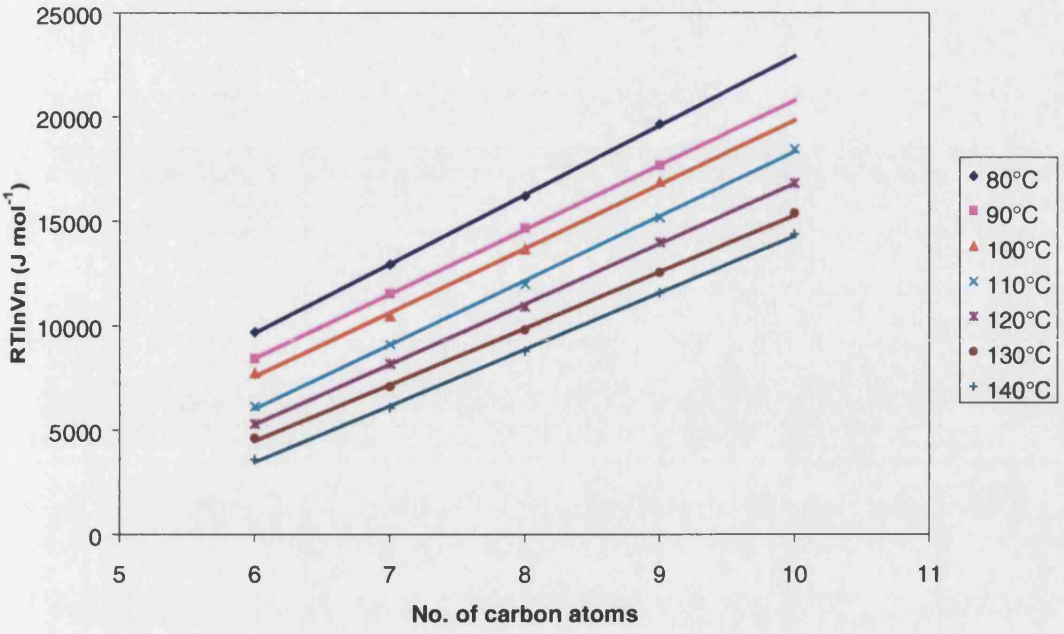

Figure 7.5 Plot of RTlnV$_n$ versus number of carbon atoms for CAM1.

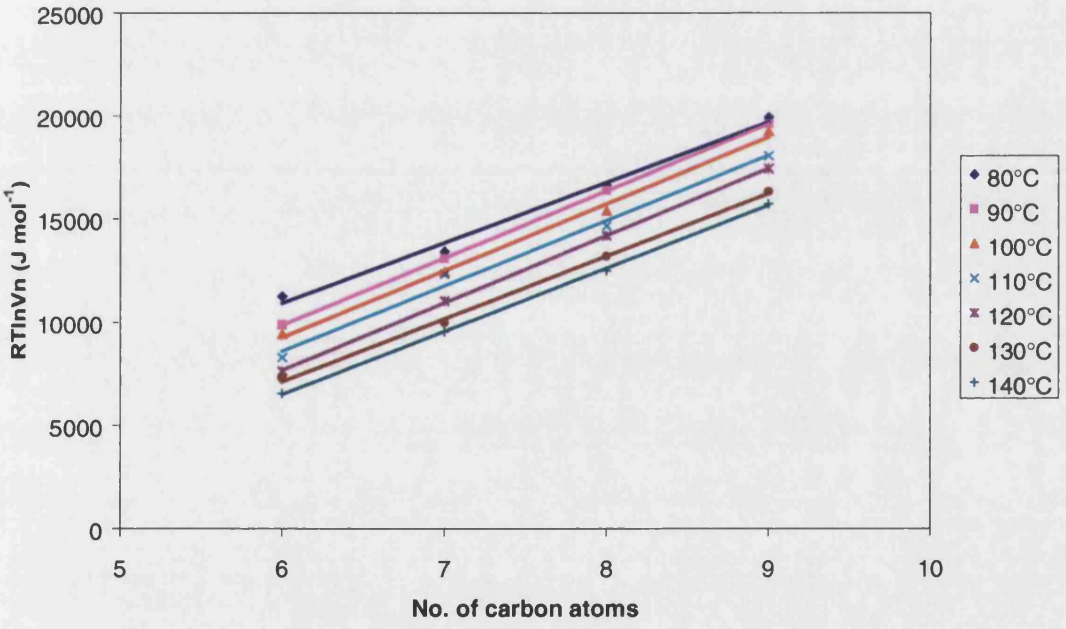

Figure 7.6 Plot of RTlnV$_n$ versus number of carbon atoms for CAM2.

Table 7.4 Dispersive component of surface free energy data for PA, CAM1 and CAM2.

	Dispersive component of surface free energy ($mJ\ m^{-2}$)		
Temperature (°C)	**PA**	**CAM1**	**CAM2**
60	41 ± 3		
70	40 ± 3		
80	42 ± 2	64 ± 2	58 ± 5
90	42 ± 3	58 ± 2	65 ± 2
100	45 ± 3	63 ± 3	65 ± 4
110		65 ± 3	66 ± 4
120		58 ± 2	70 ± 2
130		56 ± 2	67 ± 3
140		56 ± 3	69 ± 2

Retention times for the elution of decane, undecane and dodecane were not collected for CAM1 or CAM2 due to the excessive retention times predicted from the lower alkane results. Retention times for pentane and hexane on PA were not used, as the retention times were too short to be sufficiently accurate for the calculations.

Enthalpy of adsorption data (Table 7.3) for CAM2 were approximately 2 kJ mol^{-1} lower than CAM1. PA results were approximately 2 kJ mol^{-1} higher than CAM1 for heptane to nonane. Balard et al. evaluated the degree of surface modification of silicas by IGC[255]. They found a strong correlation between degree of coating and adsorption enthalpy. As CAM1 and CAM2 gave similar results, the surface modification of the two was considered to be equivalent. The comparable adsorption enthalpies for PA and the surface-modified minerals indicated that the interactions between the two materials would also be similar.

Surface free energy results of 40 – 45 mJ m^{-2} for PA (Table 7.4) were statistically equivalent at all measured temperatures. These are in good agreement with a literature value for nylon of 46 mJ m^{-2} [256].

Results of 58 to 66 mJ m^{-2} for CAM1 and CAM2 were comparable between 60 to 110 ° C, but higher than PA. Above this temperature marked differences were seen with results for CAM2 of 67 – 70 mJ m^{-2} compared with 56 – 58 mJ m^{-2} for CAM1. These results were significantly lower than those obtained for the unmodified calcined clay (CAC1, chapter 6). Tsutsumi and Ohsuga evaluated the effect of silane coupling agents on glass fibres[257]. They observed a reduction of 20 – 50 % on the dispersive component of surface energy with surface modification. The addition of the silane coupling agent therefore lowered the surface free energy of the surface. For mineral-polymer composites, this gives greater compatibility within the matrix.

To determine any acceptor-donor differences between PA, CAM1 and CAM2, polar probes were injected at 100 °C. Specific interactions were calculated as detailed in chapter 5, by plotting ΔG_a versus log P_0 (Figures 7.7 to 7.9). Results are summarised in Table 7.5.

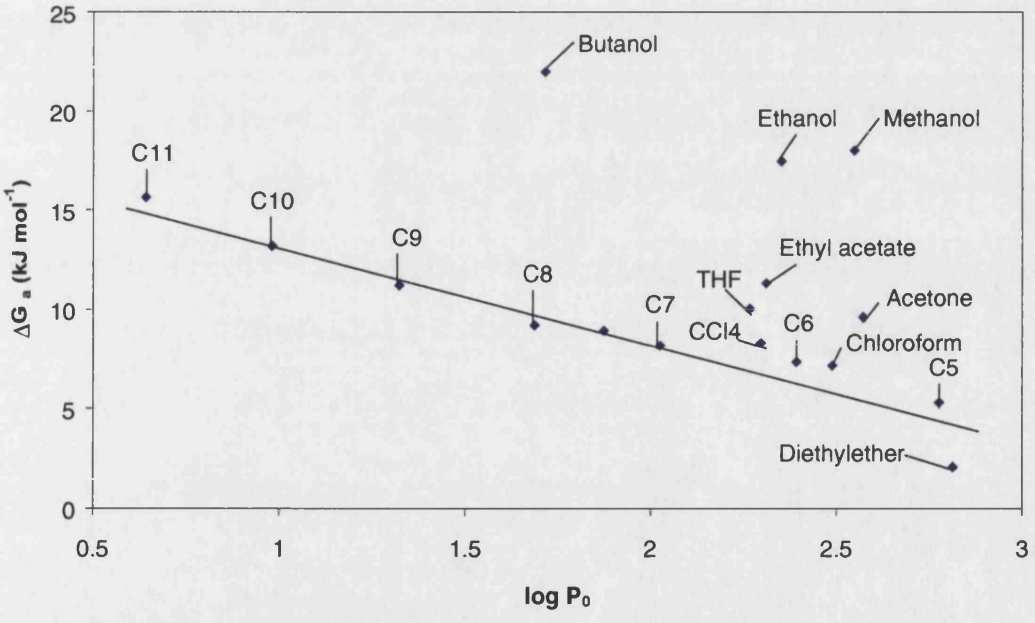

Figure 7.7 Plot of ΔG_a versus log P_0 for PA.

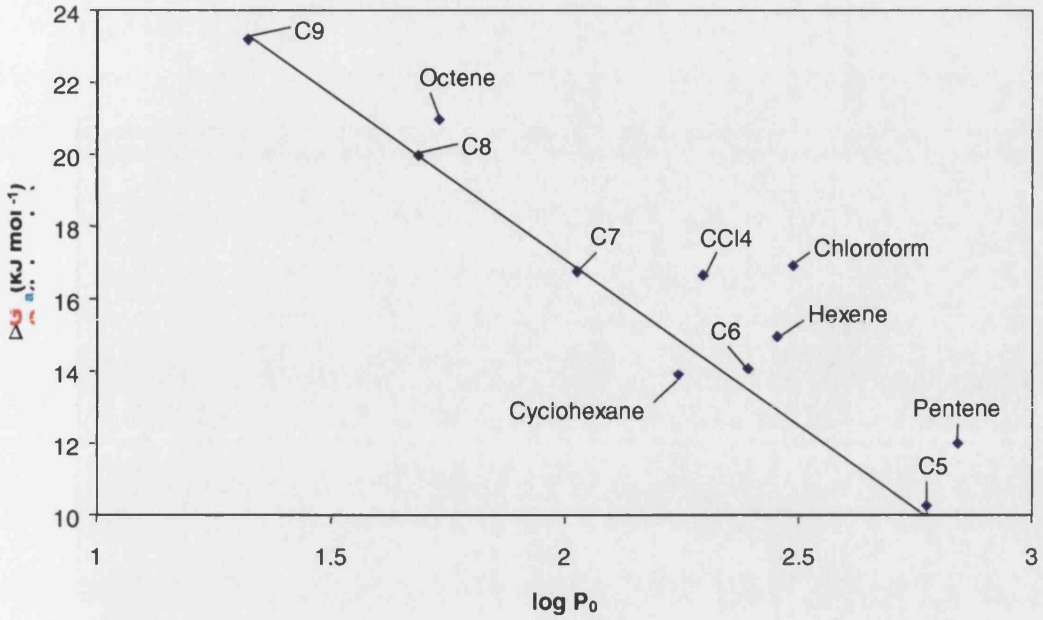

Figure 7.8 Plot of ΔG_a versus log P_o for CAM1.

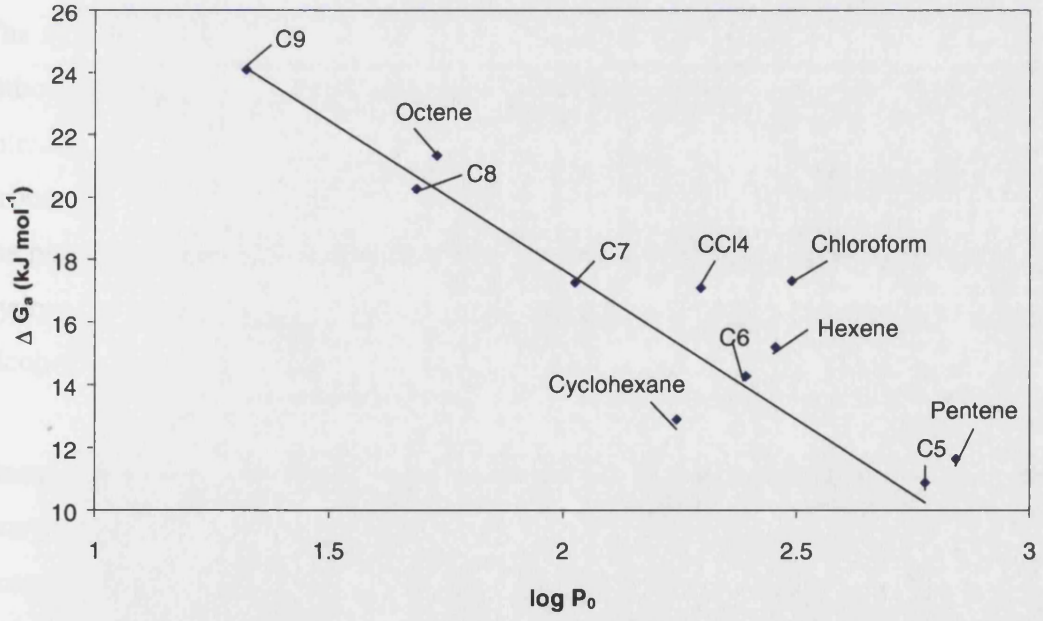

Figure 7.9 Plot of ΔG_a versus log P_o for CAM2.

Table 7.5 Details of specific interactions with polar probes for PA, CAM1 and CAM2.

	Specific interaction $-\Delta G_{specific}$ (kJ mol^{-1})			
Probe	**PA**	**CAM1**	**CAM2**	**CAC***
Methanol	12.4	n/m	n/m	
Ethanol	10.9	n/m	n/m	
Butanol	12.0	n/m	n/m	
Carbon tetrachloride	1.5	2.2	2.0	-2.7
Chloroform	n/m	4.1	4.0	-1.8
Cyclohexane	n/m	-1.0	-2.5	-4.3
Acetone	4.0	n/m	n/m	NPD
Ethyl acetate	4.4	n/m	n/m	NPD
Diethyl ether	-2.4	n/m	n/m	NPD
Pentene	n/m	2.2	1.8	4.9
Hexene	n/m	1.8	1.8	4.0
Octene	n/m	1.4	1.8	3.8
THF	3.1	n/m	n/m	n/m

n/m = not measured * results from chapter 6.

The strongly acidic alcohols gave large specific interactions with the PA surface, although results for carbon tetrachloride, a weaker acid, showed only minimal interactions. The amphoteric probes interacted weakly, as did THF, the strongly basic probe. The result for the predominantly basic diethyl ether was negative compared with the non-polar alkanes. Polyamides are basic and undergo hydrogen bonding with hydroxyl groups. This is indicated by the large specific interaction energies for the alcohol probes.

Results for CAM1 and CAM2 were similar, with no strong interactions observed. A marginally higher specific interaction was, however, seen for cyclohexane on CAM2 compared with CAM1, indicating a slightly higher surface accessibility to a bulky probe. Comparing these results with those for CAC (the unmodified precursor to CAM1) the changes to surface polarity can be clearly described. On silane treatment specific interactions change from acidic, electron acceptor-type to those of basic, electron donor-type. Thus specific interaction results for the acids, carbon tetrachloride and chloroform were negative for CAC and positive for CAM1 and CAM2.

Results for the alkenes showed the opposite effect, with a reduction in specific interaction energy on surface modification. These data are indicative of the presence of the functional amine group at the mineral surface.

To assess the effect of surface modification on the polymer-mineral interactions, the physical properties of the composites were measured. Results are detailed in Table 7.6.

7.3.2 *Physical testing of polyamide injection mouldings*

Table 7.6 Physical properties of injection mouldings.

		PA + 30 wt.% CAC (uncoated CAM1)	**PA + 20 wt.% CAM1**	**PA + 20 wt.% CAM2**
Gloss	**20 °**	n/m	63 (2)	74 (5)
	60 °	n/m	81 (2)	89 (1)
	85 °	n/m	98 (1)	99 (3)
Falling weight impact strength	**Peak force (N)**	n/m	3455 (395)	3490 (374)
	Fail Energy (J)	n/m	25.8 (2.1)	25.8 (6.1)
Izod strength	**Notched (kJ m^{-2})**	3.8 (0.4)	32.8 (20.5)	24.2 (2.6)
	Un-notched (kJ m^{-2})	87 (6)	249 (39)	302 (17)
Flexural properties	**Modulus (MPa)**	2094 (33)	1765 (35)	1573 (140)
	Yield strength (MPa)	74 (1)	64.0 (0.3)	61.4 (1.1)
Tensile properties	**Peak stress (MPa)**	68 (1)	65 (3)	64 (3)
	Break strain (MPa)	66 (1)	63 (2)	61 (2)

Standard deviations given in parenthesis. Archive data were only available for CAC at 30 wt.% loading[258].

Gloss results for the mouldings containing CAM1 were lower than those with CAM2. CAM2, being finer, gave a lower light scattering compared with CAM1, and thus higher gloss (the mechanism of which is discussed in chapter 4). Falling weight impact strength for mouldings containing CAM1 and CAM2 were equivalent. Izod impact strength results showed the same trend, although the un-notched Izod strength for CAM2 was higher than the result for the CAM1-based mouldings. Results for the CAC-based specimens gave significantly lower results than either of the silane-coated samples. Tensile strengths of all the polyamide mouldings were similar.

Flexural modulus results for the CAM1 mouldings were greater than the CAM2 mouldings. Modulus is dependent on particle size and anisotropy. As the particle shape of the two calcined clays is equivalent, flexural modulus differences were due to particle size effects, with the finer material giving a lower result. Flexural modulus for the CAC-based system compared with that for CAM1 was greater due to the higher filler volume fraction.

Silane coupling agents are considered as adhesion promoters between a mineral and a polymer matrix. The filler surface interacts with the polymer through orientation and modification in polymer morphology at the boundary or interphase. Surface modification also affects the rheology of the polymer by altering wetting behaviour, dispersion and flow.

Dispersion of a mineral in a molten polymer involves three steps, these being: wetting of the mineral surface; separation of the individual mineral particles; and stabilisation of the dispersion (to prevent reagglomeration). The addition of an amino-functional group to the calcined clay reduced the dispersive component of the surface free energy, increasing the wetting potential within the polymer matrix. Some importance has been attributed to the significance of acid-base reactions in filler dispersion, orientation and, to a lesser extent, adhesion. Acid-base reactions are not considered, however, to be of primary importance in interface region[259].

Adsorbed water on the mineral surface will serve to aggregate individual particles. The silane coupling agent interacts with any residual surface water, reducing the tendency to aggregate[260]. Once these particles are separated in a high shear environment, such as that encountered during compounding, they are stabilised in the polymer matrix. As the adsorption enthalpies results for CAM1 and CAM2 were similar, their stability within the polymer matrix should also be equivalent. The physical properties of the composites support these findings.

Silane treatment modifies the interphase region of the polymer-mineral composite. The mechanical strengths of the composites containing CAM1 and CAM2 were greater than that based on CAC. The silane region at the mineral surface may increase the crystallinity in the interphase[261]. Additionally, it is assumed that there is a formation of an interpenetrating polymer network of siloxanes with the polymer at the mineral interface. These effects result in a toughening of the composite. However, the system is complex, and there is still considerable debate as to the exact nature of the interphase and its role in toughening of composites.

7.4 **Further discussion**

The mechanism of silane interactions with inorganic substrates has been characterised by a number of techniques, including FTIR[262], Raman spectroscopy[263] and XPS[264]. Aminopropyl triethoxysilane forms two regions on a reactive substrate comprising chemisorbed and physisorbed layers[265]. A compositional gradient is believed to exist at the interface. Physically adsorbed silanes also exist on the substrate surface. This layer comprises predominantly small oligomeric siloxanes. These act as lubricating agents in a polymer melt and also inhibit any preferred interactions between the functional groups at the surface and specific sites on the polymer chain.

Although the exact nature of the interphase region is still unclear, the widely accepted explanation is one in which both covalent bonding and chain entanglement occurs[266,267]. Jenneskens et al. studied the interphase between glass beads with surface-bound 3-aminopropyltrisiloxane and PA6[268]. They showed evidence for the occurrence of physical entanglements between the siloxane and the PA6 by the use of ^{13}C labelling.

A two component structure for the surface-bound siloxane was found, consisting of a rigid and a mobile phase. Additionally they found evidence for amide formation between the carboxylic acid end groups of the PA and the amine groups from the siloxane.

IGC has also been used to explain the interactions in the interphase. Schultz and Lavielle characterised the surfaces of reinforcing fibres to predict the adhesion of the fibres in polymer matrices[111]. They attribute adhesion to acid-base interactions, as described by the specific interaction parameter. These interactions were correlated with shear stress at the fibre-polymer interface during mechanical testing.

In this study, the mechanisms of wetting and dispersion of the mineral during compounding and moulding were considered to be influential on ultimate physical properties, as well as adhesion at the interface. Thermodynamic data for both CAM1 and CAM2 were similar. PA composites produced from these two materials had comparable strength properties, indicating good dispersion. When compared with IGC data for unmodified calcined clay (CAC) the effect of silane-modification was demonstrated. The silane lowered the net surface free energy of the matrix, promoting wetting and improving particulate stabilisation. The formation of siloxanes may also increase the surface stability, as described above, reducing interfacial stresses.

The use of polar probes allowed the acid-base characterisation of the modified surface and the polymer. The calcined clay surface was found to alter from a predominantly acidic one, to one predominantly basic, supporting the evidence for the presence of an exposed amide group. This permitted the formation of covalent bonds with the carboxylic end groups of the polyamide, resulting in a stronger composite than one containing unmodified calcined clay.

7.5 Conclusions

1. The enthalpy of adsorption results for PA, CAM1 and CAM2 were similar.

2. For PA, the dispersive component of surface free energy results did not alter with measurement temperature. They were found to be in good agreement with literature values.

3. The dispersive component of surface free energy data for both CAM1 and CAM2 were marginally higher than those calculated for PA. Results were significantly lower when compared with the unmodified calcined clay, CAC1. Silane modification therefore lowered the surface free energy, increasing their compatibility in the polymer matrix.

4. PA was found to have a basic surface, as the specific interactions for the acidic probes were large. Silane treatment of calcined clay also resulted in a predominantly basic surface.

5. Composites comprising CAM1 and CAM2 in a PA matrix had similar physical properties. Their addition increased the toughness of the systems compared with a composite with unmodified calcined clay. These differences were attributed to wetting, coupling and dispersive effects within the matrix.

The data obtained from IGC could thus be used to describe the thermodynamic character of the polymer and mineral surfaces, fulfilling objective 8 of the thesis. This gave a better understanding of the interphase region, and should permit better optimisation of surface modifiers for these materials in the future.

8 FURTHER WORK

The work included in this report has merely scratched the surface of the use of IGC in thermodynamic characterisation. During research as many questions were raised as were answered. Suggestions for further work could therefore extend to almost any area within the thesis scope of polymers and minerals. To limit this, recommendations have been restricted to areas directly within the scope of the main research areas of calcium carbonates, clays and their modifications and the influence of both of these on polymer composites.

8.1 **The study of PCC polymorphs by IGC and their effects in polymer films.**

Precipitated calcium carbonates are found as the different crystal forms of calcite, vaterite and aragonite, depending on their production history. The surface thermodynamic differences of these have not been characterised by IGC, although some limited work has been published. PCCs are used in polyethylene and polyethylene terephthalate polymer films to improve their antiblocking properties and (at higher loadings) alter their physical properties. Poor wetting and adhesion of the PCCs in the polymer matrix have restricted their use in certain areas. The reasons for these behaviours are not clearly understood. IGC could be used to study the different crystal structures, and predict the effect of surface modifications on these to optimise surface compatibility.

8.2 **The effect of stabilisers on Infrared barrier clays.**

An initial study into the weathering stability of polyethylene films containing calcined clays revealed some differences in non-stabilised systems. To predict accurately the results for agricultural films in-situ, lengthy outdoor weathering trials are necessary. The stabiliser systems are often chosen empirically, based on previous findings in similar applications. The possible adsorption and interaction effects between these stabilisers, and other components, such as slip additives, have not been documented.

IGC may be used to monitor the possible interactions of one or more components of agricultural films. The interactions of each component can be evaluated by injecting these directly, or in solution, into the calcined clay GC column. Results may be used to predict potential synergies for certain types of stabilisers.

The interaction mechanisms with different fillers could be considered. Adsorption differences are suggested to be due to surface area effects. However, surface porosity and chemical reactivity must also contribute. These complex and probably interdependent mechanisms have not been resolved. The studies so far have been restricted to analysis in the infinite dilution region. If probes are applied in the finite dilution range, then additional surface information can be obtained. Adsorption isotherms can be constructed, as with more conventional adsorption studies. Different adsorption sites may also be selected for specific study. Infinite dilution methods are unable to distinguish these sites, but using finite concentration data, areas of specific surface activity may be identified. These could then be related to interactions with additives and stabilisers.

If more data are available regarding the contribution of specific mineral sites to additive efficiency, a more accurate method of designing the correct stabiliser system should be made available. Additionally, the effects of different fillers could be understood more readily.

8.3 The optimisation of silane-modified minerals

IGC was used to characterise unmodified and silane-modified calcined clays for use in polyamide mouldings. The silane was added at theoretical monolayer coverage. This is often greater than the required level for good adhesion and wetting at the interface. Calcined clays could be modified with different levels of silanes, and characterised by IGC. The optimum coating level should be predicted from the surface free energy results. Polyamide composites could be prepared containing the surface modified clays, and the physical properties measured. The physical properties could then be compared with the results predicted for optimum silane coverage of the filler.

The initial study only measured the effect of surface modification with an aminosilane. Many different grades and chemical compositions are available. These are used for a wide variety of applications, such as filler modifications for rubbers and sealants.
As was clearly demonstrated, IGC data are useful in determining the compatibility and polarity of surfaces. By using model probes different silane modifications may be evaluated for a particular matrix.

9 CONCLUSIONS

The aim of the study was to apply IGC to polymers, minerals and their composites in order to predict physical properties for selected applications. A standard gas chromatograph was modified for use as an IGC instrument. Its validity in determining phase transition temperatures was confirmed by the study of polystyrene.

From this initial study, a second polymer, polypropylene, was evaluated using IGC. The scope was also extended to include a precipitated calcium carbonate (PCC). This was surface-modified with stearic acid, and the thermodynamic data collected. Composites were prepared and their physical properties were measured.

The thermodynamic data for the PCCs were in good agreement with literature values. Reproducibility between injections was good. Small changes in net retention volume with prolonged heating were observed. A standard conditioning time was therefore recommended for all future work. In addition, if the experiment continued over an extended period, it was advised that new columns should be prepared to ensure the data obtained was reproducible and reliable.

IGC at infinite dilution was found to be a suitable technique for the characterisation of both specific and non-specific interactions of the surfaces of mineral fillers. Enthalpy of adsorption data obtained for uncoated and surface-modified PCCs revealed an increase in enthalpy with surface modification. The polar contributions of these interactions were, however, reduced.

Surface free energy data showed subtle, but significant differences in the high-energy sites on these materials. These data were related to interaction energy differences at the polymer-filler interface. The mechanical properties of composites are related to the adhesion energy between the components. The study showed that a stearate-modified PCC with lower surface free energy resulted in a composite with greater toughness than those with higher surface free energies. The technique was thus considered useful in predicting the efficiency of surface modification, and optimising processing routes.

No data comparing PCCs with these types of surface modification have been published previously. The study was then extended to kaolinite systems, to ensure it was more widely applicable.

The study of a high-purity, non-chemical clay demonstrated the variation in kaolinite surface chemistry with processing history and source. Good agreement was achieved between literature values for a specific kaolinite, and the locally-sourced clay. The values obtained were considered to be indicative of heterogeneity and surface activity, rather than a true representation of surface free energy.

IGC was used to measure the thermodynamic nature of kaolinite after heat treatment by calcination. Results showed a reduction in surface activity on calcination. These results were higher than expected, assuming that the interactive forces were halved because of structural rearrangements. This was attributed to the probes being adsorbed onto the remaining high-energy sites. Although these were fewer in number they were shown to have a significant effect on retention times.

Specific interaction enthalpies were measured. The polarities of surface sites on the calcined clay were significantly lower than those on the hydrous clay. However, the relatively small difference in specific free energy of adsorption after calcination was less than predicted. The greatest effect was attributed to a change in specific surface polarity, rather than accessibility of the probes.

Comparative results between clays and calcined clays have not been published previously. The results of the study were therefore considered to be the first record of such thermodynamic data. The research was then extended to consider the expression of specific interaction parameters by two techniques. The first technique utilised surface tension data. The second technique expressed specific interaction parameters in terms of saturated vapour pressure. The latter data are readily obtained from literature across a broad temperature range. The two sets of results for the hydrous clay correlate well. As the two measurement methods were comparable, and the saturated vapour pressure data are readily available, the latter technique was adopted for all further studies.

After calculating thermodynamic data for clays altered significantly by heat treatment, the research was continued to evaluate the use of IGC for measuring more subtle differences. Two calcined clays from the same ore source were evaluated. The clays were then used in the preparation of polyethylene (PE) composites to see if the surface chemistry data could be correlated with physical differences. The PE and the composites were also studied by IGC.

Surface energy results for PE, as defined by the free energy of adsorption, were comparable with those from the literature. Adsorption enthalpies of the calcined clays and the composites were higher than those determined for PE. The contribution to adsorption enthalpy was also found to be disproportionately greater for the calcined clay component than the PE component in the composites. Some differences were seen in the thermodynamic properties of the two calcined clays.

PE blown films were then prepared from the composites, along with an unfilled PE film. UV stability was assessed by accelerated weathering, and measured by incremental tensile and FTIR analyses. Both methods revealed differences between the unfilled PE, and films containing the calcined clays, with the unfilled PE being more UV stable than either of the filled films. For the two films containing calcined clays, the second calcined clay was more UV stable than the first. This was attributed to their surface free energy differences. The technique has not previously been used in studying degradation, and the value of using IGC for predicting differences in composite behaviour was clearly demonstrated.

The final study looked at the use of IGC for assessing the thermodynamic characteristics of polyamides (PA). Calcined clays, including those measured previously, were modified with an aminosilane coupling agent and were also included. Again, composites of the calcined clays and polymer were prepared, and the physical properties of these were measured. The mechanisms of wetting and dispersion of the mineral during composite preparation were considered to be of greatest influence on ultimate physical properties. Thermodynamic data for the two silane-treated calcined clays were similar. PA composites produced from these two materials had comparable strength properties, indicative of good dispersion.

When compared with IGC data for unmodified calcined clay, the effect of silane-modification was demonstrated. The silane lowered the net surface free energy of the matrix, promoting wetting and improving particulate stabilisation.

The use of polar probes allowed the acid-base characterisation of the modified surface and the polymer. The calcined clay surface was found to alter from a predominantly acidic one, to one predominantly basic. The net effect within the more basic PA was, however, considered to be less influential than the dispersive effects. The data obtained from IGC could thus be used to describe the thermodynamic character of the polymer and mineral surfaces.

This research has demonstrated clearly the value of IGC in obtaining reliable and reproducible thermodynamic data for polymer and minerals systems. Surface modifications can be characterised in terms of non-specific and specific interactions. These data can then be used to predict the performance of the two components when combined in a composite system. The information for non-specific interactions is, however, limited by its representation of sites of higher activity, rather than the bulk contribution. This effect can be used advantageously in assessing surface heterogeneity. If the technique is used in combination with other surface characterisation methods, such as FTIR and XPS, then a more thorough understanding of the nature of these surfaces will result. IGC will thus continue to be used in an ever-wider range of applications wherever a need for such fundamental data exists.

10 REFERENCES

1 Baker R.A., TAPPI Polymers, Laminations and Coatings Conference, **1**, 17-27 (Aug. 24-28, 1997).

2 Good R.J., Surface and Colloid Science, (Good R.J. and Stomberg R.R. Eds.), **11**, Plenum, New York (1979).

3 Lloyd D.R., Ward T.C. and Schreiber H.P. (Eds.), Inverse Gas Chromatography. Characterization of Polymers and Other Materials. ACS Symposium Series 391, ACS, Washington DC (1989).

4 Sheldon R.P., Composite Polymeric Materials, Applied Science Publishers Ltd., England (1982).

5 Furnas C.C., Industrial and Engineering Chemistry, **23**, 9, 1052 (1931).

6 Pukanszky B. and Voros G., Polym. Composites, **17**, 3, 384-392 (1996).

7 Poiseuille J.L.M., Comptes Rendus, **11**, 961-1041, **12**, 112 (1840).

8 Market Survey, Maack Business Services (1998).

9 Haggstrom B., Rubber Handbook, SGF, Swedish Institution of Technology, 208-209 (2000).

10 Manufacturing, Properties & Applications – Aerosil. Degussa, Frankfurt-am-Main, W. Germany.

11 Riegel E.R., Industrial Chemistry, Van Nostrand Reinhold Co., N.Y. (1975).

12 Dalton J., Private communication to Imerys Central Research (2000).

13 European Symposium on Particle Technology: Description of Comminution, Amsterdam, June (1980).

14 Grim R.E., Clay Mineralogy, McGraw-Hill. (1968).

15 Bundy W.M., Keller '90 Symposium, Columbus, USA. (1990).

16 Katz H.S. and Milewski J.V., Handbook of Fillers and Reinforcements for Plastics, Van Nostrand Reinhold Co., N.Y. (1978).

17 ISO 178 (1990) Plastics – Determination of Flexural Properties.

18 Nielsen L.E., Mechanical Properties of Polymers and Composites, **2**, Marcel Dekker, N.Y. (1974).

19 BS 2782 Method 306C. Determination of Impact Strength (Falling Weight Method).

20 BS 2782 Method 515B. Determination of Gloss of Plastic Sheets.

21 Willard H.H., Merritt L.L., Dean J.A. and Settle F.A., Instrumental Methods of Analysis, Wadsworth Publishing, **13**, 13.8 (1988).

22 Navroj S., Koenig J.L. and Ishida H., J. Adhesion, **18**, 93 (1985).

23 Packham D.E. (Ed.), Handbook of Adhesion, Longman Scientific and Technical, UK (1992).

24 Paddy J.F., Surface and Coll. Science, **1**, 39-251, (E. Matejevic Ed.), Wiley Interscience, New York (1969).

25 Fox H.W. and Zisman W.A., J. Coll. Science, **5**, 514, (1950).

26 ASTM D-2578-67.

27 Girifalco L.A. and Good R.J., J. Physical Chemistry, **61**, 904 (1957).

28 Fowkes M., Treatise on Adhesion and Adhesives, I, **9**, (Patrick R.L. Ed.) Marcel Dekker, New York (1966).

29 Schultz J., Tsutsumi K. and Donnet J.B., J. Coll. Inter. Science, **59**, 272 (1977).

30 Washburn E.W., Phys Review, **17**, 272-374 (1921).

31 Van Oss C.J., Giese R.F., Li Z., Murphy K., Norris J., Chaudhury M.K. and Good R.J., J. Adhesion Science and Technology, **6**, 4, 413-428 (1992).

32 Ashton D.P. and Rothan R.N., Controlled Interfaces in Composite Materials, (Ishida H. Ed.), 295, Elsevier, Amsterdam (1990).

33 Joslin S.T. and Fowkes F.M., Ind. Eng. Chem. Prod. Res. Dev., **24**, 3, 369 (1985).

34 Lipson J.E.G. and Guillet J.E., Developments in Polymer Characterisation, **3**, (Dawkins J.V. Ed.), Applied Science Publishers, Barking (1982).

28 Hinshaw J.W., LC-GC Int., **8**, 3, 137-142 (1995).

36 DeBoer J.H., The Dynamic Character of Adsorption, Clarendon Press, Oxford, Chap. VIII. (1953).

37 Guillet J.E., Romansky M., Price G.J. and van der Mark R., ACS Symposium Series 391, (Lloyd D.R., Ward T.C. and Schreiber H.P., Eds.) **3**, 20-32 (1989).

38 Fowkes F.M., Relevance to Adhesion Science and Technology, (Mittal K.L. and Anderson H.R. Eds.), VSP, Ultrecht (1991).

39 Saint-Flour C. and Papirer E., Ind. Chem. Prod. Res. Dev., **21**, 337-341 (1982).

40 Saint-Flour C. and Papirer E., Ind. Chem. Prod. Res. Dev., **21**, 666-669 (1982).

41 Gutmann V., The Donor-Acceptor Approach to Molecular Interactions, Plenum Press, New York (1983).

42 Voelkel A., Szymanowski J., Beger J. and Ebert K., J. Chromatography, **398**, 31 (1987).

43 Szymanowski J., CRC Rev. Anal. Chem., **21**, 407 (1990).

44 Matveichuk L.S., Bakhtizina R.Z., Kudasheva F.K. and Berg G.A., Khim. Tverd. Topl., **2**, 95 (1989).

45 Papirer E., Kuczynski E. and Siffert B., Chromatographia, **23**, 401 (1987).

46 Ticehurst M.D., Rowe R.C. and York P., Int. J. Pharmaceuticals, **11**, 241-249 (1994).

47 Finlayson M.F. and Shah B.A., J. Adhesion Sci. Technol., **4**, 431 (1990).

48 Condor J.R. and Young C.L., Physicochemical Measurement by Gas Chromatography, Wiley and Sons, Chichester (1979).

49 Kieslev A.V. and Yashin Y.I., Gas Adsorption Chromatography, Plenum, New York (1969).

50 Williams D.R., Chromatography and Analysis, **2**, 9-11 (1991).

51 Voelkel A., Critical Reviews in Analytical Chemistry, **22**, 5, 411-439 (1991).

52 Lloyd D.R. and Ward T.C., Inverse Gas Chromatography Characterization of Polymers and Other Materials (Lloyd D.R., Ward T.C. and Schreiber H.P. Eds.), ACS Symposium Series 391, ACS, **1**, 1-11Washington DC, (1989).

53 Literature search by the author: RAPRA database (April 2000).

54 Schreiber H.P., Proceedings from Antec 95, Boston, USA, May 7-11, **2**, 106-109 (1995).

55 Al-Saigh Z.Y., Inter. J. Polym. Anal. and Charact., **3**, 3, 249-91 (1997).

56 Mohlin U-B. and Gray D.G., J. Coll. Inter. Sci., **47**, 747 (1974).

57 Bolvari A., Master's Thesis, Virginia Polym. Inst. and State Univ., VA (1988).

58 Dorris G.M. and Gray D.G., J. Coll. Inter. Sci., **77**, 353 (1980).

59 Katz S. and Gray D.G., J. Coll. Inter. Sci., **82**, 2, 326-338 (1981).

60 Katz S. and Gray D.G., J. Coll. Inter. Sci., **82**, 2, 318-325 (1981).

61 Brunauer S., Emmett P.H. and Teller E., J. Am. Chem. Soc., **60**, 309 (1938).

62 Anhang J. and Gray D.G., J. Appl. Polym. Sci., **27**, 71 (1982).

63 Al-Saigh Z. Y., Polymer, **40**, 12, 3479-85 (1999).

64 Guo Y., Gu B., Zhixiang L. and Qiangguo D., J. Appl. Polym. Sci., **71**, 5, 693-8 (1999).

65 Aucejo S., Pozo M.J. and Gavara R., J. Appl. Polym. Sci., 70, 4, 711-6 (1998).

66 Muralidharan V., Tihminlioglu A., Antelmann O., Duda J.L., Danner R.P. and de Haan A., J. Polym. Sci., Polym. Phys., **36**, 10, 1713-9 (1998).

67 Yampolskii Y.P. and Bondarenko G.N., Polymer, **39**, 11, 2241-5 (1998).

68 Andrzejewska E., Voelkel A., Maga R. and Andrzejewska M., Polymer, **39**, 15, 3499-506 (1998).

69 Di-Paola Baranyi G. and Guillet J.E., Macromolecules, **11**, 228 (1978).

70 Cankurtaran O. and Yilmaz F., Polymer, **37**, 14, 3019-23 (1996).

71 Sakellariou P., Abs. of ACS, 207, **2**, 407-408 (1994).

72 Kaya I. and Demirelli K., J. Polym. Eng., **19**,1, 61-73 (1999).

73 Kaya I., Polym. Plastics Tech. and Eng., **38**, 2, 385-96 (1999).

74 Tihminlioglu F., Surana R.K., Danner R.P. and Duda J.L., J. Polym. Sci., Polym. Phys., **35**,8, 1279-90 (1997).

75 Choi P., Kavassalis T. and Rudlin A., Abs. of ACS, 207, **2**, 472-473 (1994).

76 Voelkel A. and Janas J., Abs. of ACS, 207, **2**, 422-427 (1994).

77 Munk P. and Tian M., Abs. of ACS, 207, **2**, 460-461 (1994).

78 Shiyao B., Sourirayon S., Talbot F.D.F. and Matsusura T., Abs. of ACS, 207, **2**, (1994).

79 Qin R., Schreiber H.P. and Rudin A., J. Appl. Polym. Sci., **56**, 51-56 (1995).

80 Jackson P.L., Huglin M.B. and Cervenka A., Polymer International, **35**, 119-133 (1994).

81 Jackson P.L., Huglin M.B. and Cervenka A., Polymer International **35**, 135-143 (1994).

82 Yilmaz F. and Cankurtaran O., Polymer, **38**, 14, 3539-43 (1997).

83 Price G.J. and Guillet J.E., Abs. of ACS, 207, **2**, 421-422 (1994).

84 Vrentas J.S. and Vrentas C.M., Macromolecules, **31**, 16, 5539-41 (1998).

85 Wohlfarth C., Macromolecular Chem. and Phys., **198**, 9, 6122-714 (1997).

86 Di-Paola-Baranyi G., Hwang C.J., Hsiao C.K. and Listigovers N., Abs. of ACS, 207, **2**, 414-415 (1994).

87 Di-Paola-Baranyi G., ACS Symposium Series 391, (Lloyd D.R., Ward T.C. and Schreiber H.P., Eds.) **9**, 108-120 (1989).

88 Klotz S., Grater H. and Cantow H-J., ACS Symposium Series 391, (Lloyd D.R., Ward T.C. and Schreiber H.P., Eds.) **11**, 135-154 (1989).

89 Habi A. and Djadoun S., Europ. Polym. J., **35**, 3, 483-9 (1999).

90 Seong-Uk H. and Pretel E.J., Polym. International, 45, 1, 55-9 (1998).

91 Sheng J., Li F-K. and Hu J., J. Appl. Polym. Sci., 67, 7, 1199-204 (1998).

92 Lezcano E.G., de Arellano D.R., Prolongo M.G., and Coll. C.S., Polymer, **39**, 8-9, 1583-9 (1998).

93 Lezcanzo E.G., Coll. C.S. and Prolongo M.G., Polymer, **37**, 16, 3603-9 (1996).

94 Su A.C. and Fried J.R., ACS Symposium Series 391, (Lloyd D.R., Ward T.C. and Schreiber H.P., Eds.) **12,** 155-165 (1989).

95 Qiangguo D., Wenjie C. and Munk P., Macromolecules, **32**, 5, 1514-8 (1999).

96 Hadj-Hamou A.S., Habi A. and Djadoun S., Europ. Polym. J., **33**, 7, 1105-11 (1997).

97 Gorbunova I.Y., Kerber M.L., Avdeev N.N., Stepanova A.V. and Vladimirova S.I., Polym. Sci. Series B., **38**, 5-6, 247-50 (1996).

98 Ljundqvist N. and Hjertberg T., Abs. of ACS, 207, **2**, 505-506 (1994).

99 Seong U-H. and Barbari T.A., Polym. International, **48**, 9, 901-8 (1999).

100 Faridi N., Duda J.L. and Danner R.P., Rubber Chem. and Tech., **69**, 2, 234-44 (1996).

101 Gavara R., Catala R., Aucejo S., Cabedo D. and Hernandez R., J. Polym. Sci. Polym. Phys., **34**, 11, 1907-15 (1996).

102 Etxeberria A., Unanue A., Uriarte C. and Iruin J.J., Polymer, **38**, 16, 4085-90 (1997).

103 El-Himbri M.J., Cheng W., Hattam P. and Munk P., ACS Symposium Series 391 (Lloyd D.R., Ward T.C. and Schreiber H.P., Eds.) **10**, 121-134 (1989).

104 Al-Saigh Z-Y. and Munk P., Macromolecules, **17**, 803 (1984).

105 Shi Z.H. and Schreiber H.P., Macromolecules, **24**, 3522-3527 (1991).

106 Shi Z.H. and Shreiber H.P., J. Appl. Polym. Sci., 46, 796-797 (1992).

107 Xing K.C., Wang W. and Schreiber H.P., Antec 97, Conf. Proc. 27 April-2 May, **1**, 53-8 (1997).

108 Tripathy V.S., Lal D., Aggarwal S.K. and Sen A.K., J. Appl. Polym. Sci., 66, 8, 1613-9 (1997).

109 Dieckmann F., Pospiech D., Uhlmann P. and Boehme F., Polymer, **38**, 23, 5887-92 (1997).

110 Panda S., Bu Q., Huang B., Edwards R.R., Liao Q., Yun K.S. and Parcher J.F., Anal. Chem., **69**, 13, 2485-95 (1997).

111 Schulz J. and Lavielle L., ACS Symposium Series 391, (Lloyd D.R., Ward T.C. and Schreiber H.P., Eds.) **14,** 185-202 (1989).

112 Bolvari A.E. and Ward T.C., ACS Symposium Series 391, (Lloyd D.R., Ward T.C. and Schreiber H.P., Eds.) **16,** 217-229 (1989).

113 Xu R., Schreiber H.P., Huang M. and Ishida H., J. Polym. Sci., Polym. Phys., 37, 13, 1441-7 (1999).

114 Panzer U. and Schreiber H.P., Macromolecules, **25,** 3633-3637 (1992).

115 Mukhopadhyay P. and Schreiber H.P., J. Polym. Sci. Part B: Polym Phy., **32,** 1653-1656 (1994).

116 Bosse F., Eisenberg A., El-Kindi M., Deng Z. and Schreiber H.P., J. Adhes. Sci. and Tech., **6,** 4, 455-465 (1992).

117 Qin R-Y. and Schreiber H.P., Langmuir, **10,** 4153-4156 (1994).

118 Mikhopadhyay P. and Schreiber H.P., Macromolecules, **26,** 6391-6396 (1993).

119 Pinchuk I.A., Sokolava G.A., Vakhnenko V.V, and Onishchenko Z.V., Int. Polym. Sci. Tech., 25, 9, 34-6 (1998).

120 Schuster R.H., Schaper J. and Hallensleben M.L., 151st Rubber Division Meeting, 6-9 May, Conf. Proc. XII, 29- (1997).

121 Liang H., Ruijian X., Favis B.D., and Schreiber H.P., Polymer, **40,** 15, 4419-23 (1999).

122 Mukhopadhyay P. and Schreiber H.P., Colloids and Surfaces A: Physicochemical and Engineering Aspects, 100, 47-71 (1995).

123 Chehimi M.M. and Pigois-Landureau E., J. Mater. Chem., **4,** 741-745 (1994).

124 Chehimi M.M., Abel M.L., Perruchot C., Delamar M., Lascelles S.F. and Armes S.P., Synthetic Metals, **104,** 1, 51-9 (1999).

125 Dieckmann F., Pospiech D., Uhlmann P., Boehme F. and Kricheldorf H.R., Polymer, **40,** 4, 983-7 (1999).

126 Bailey R.A. and Persaud K.C., Analytica Chima Acta, **363,** 2-3, 147-56 (1998).

127 Thomas P.S. and Williams D.R., Abs. of ACS, 207, **2,** 416-418 (1994).

128 Rebouillat S., Escoubes M., Gauthier R. and Vigier A., Polymer, **36,** 23, 4521-3 (1995).

129 Price G.J. and Shillcock I.M., Abs. of ACS, 207, **2,** 419-420 (1994).

130 Tovar G., Carreau P. and Schreiber H.P., J. Adhesion, **63**, 1-3, 215-30 (1997).

131 Tan Z. and Vasco G.J., Macromolecules, **30**, 16, 4665-73 (1997).

132 Papirer E., Schultz J. and Turchi C., Europ. Polym. J., **20**, 12, 1155-1158 (1984).

133 Schmitt P., Koerper E., Schultz J. and Papirer E., Chromatographia, **25**, 9, 786-790 (1988).

134 Okonkwo J.O., Colenutt B.A. and Theocharis C.R., Chemically Modified Surfaces (Mottola H.A. and Steinmetz J.R. Eds.), Elsevier, 119-129 (1992).

135 Ahsan T. and Taylor D.A., J. Adhesion, **67**, 1-4, 69-79 (1998).

136 Keller D.S. and Luner P., TAPPI Polymers, Laminations and Coatings Conference Proceedings, 346-359 (1992).

137 Balard H., Papirer E., Sarraf T., Antoine H., Croutxe C. and Reiss G., Eurofillers 95 Conference Proceedings, 79-82 (1995).

138 Zaborski M., Lipinska M., Kosmalska A. and Slusarski L., Chemia. Analitica., **44**, 3B, 505-521 (1999).

139 Steinberg S.M. and Kreamer D.K., Environ. Sci. and Tech., **27**, 883-888 (1993).

140 Zumbrum M.A., Abs. of ACS, **207**, 2, 500-501 (1994).

141 Bandoza T.J., Jagiello J., Andersen B. and Schwartz J., Clays and Clay Minerals, **40**, 3, 306-310 (1992).

142 Bandoza T.J., Jagiello J., Amankwah K.A.G. and Schwartz J., Clay Minerals, **27**, 435-444 (1992).

143 Putyera K., Bandoza T.J., Jagiello J. and Schwartz J., Clays and Clay Minerals, **42**, 1, 1-6 (1994).

144 Hamdi B., Kessaissia Z., Donnet J.B. and Wang T.K., Annales de Chimie-Science des Materiaux, **24**, 1, 63-73 (1999).

145 Jagiello J. and Papirer E., J. Coll. Inter. Sci., **142**, 1, 232-242 (1991).

146 Saada A., Papirer E., Ballard H. and Siffert B., J. Coll. Inter. Sci., **175**, 212-218 (1995).

147 Balard H., Saada A., Siffert B. and Papirer E., Clays and Clay Minerals, **45**, 4, 489-95 (1997).

148 Balard H. and Aouadji O., Eurofillers 95 Conference Proceedings, 49-52 (1995).

149 Balard H., Aouadji O., Clauss F., Baeza R. and Papirer E., Eurofillers 95 Conference Proceedings, 9-12 (1995).

150 Lee Y-J. and Manas-Zloczower I., Powder Technology, **73**, 139-146 (1992).

151 Ruijian X., and Schreiber H.P., J. Appl. Polym. Sci., **70**, 8, 1597-604 (1998).

152 Mukhopadhyay P., Desbaumes L., Schreiber H.P., Hor A.M. and Dipaola-Baranyi G., J. Appl. Polym. Sci., **67**, 2, 245-53 (1998).

153 Weidong W., Schreiber H.P., Yisong Y. and Eisenberg A., J. Polym. Sci., Polym. Phys., **35**, 11, 1793-805.

154 Lara J. and Schreiber H.P., J. Polym. Sci. Polym. Phys., **34**, 10, 1733-40 (1996).

155 Osmont E. and Schreiber H.P., ACS Symposium Series 391, (Lloyd D.R., Ward T.C. and Schreiber H.P., Eds.) **17**, 230-247 (1989).

156 Osmont E. and Schreiber H.P., Polym. Mat. Sci. Eng., **58**, 730-734 (1988).

157 Papirer E., Balard H. and Vidal A., Eur. Polym. J., **24**, 8, 783-790 (1988).

158 Grenier-Loustalot M-F. and Grenier P., Abs. of ACS, **207**, 2, 511-512 (1994).

159 Baustista M.C., Rubio J. and Oteo J.L., J. Mat. Sci., **30**, 1595-1600 (1995).

160 Uhlman P., Grundke K., Simon F. and Jacobasch H-J., Eurofillers 95 Conference Proceedings, 179-182 (1995).

161 Pogue R.T, Ye J., Klosterman D.A., Glass A.S. and Chartoff R.P., Composites Part A; Appl. Sci. and Manufacturing, **29A**, 9-10, 1273-81 (1998).

162 Allington R.D., Attwood D., Hamerton I., Hay J.N. and Howlin B.J., Composites Part A; Appl. Sci. and Manufacturing, **29A**, 9-10, 1283-90 (1998).

163 Bledzki A.K., Lieser J., Wacker G. and Frenzel H., Composite Interfaces, **5**, 1, 41-53 (1997).

164 Jacobasch H.J., Grundke K., Uhlmann P., Simon F. and Maeder E., Composite Interfaces, **3**, 4, 293-320 (1996).

165 Hadjar H., Balard H. and Papirer E., Colloids and Surfaces A: Physicochemical and Engineering Aspects 99, 45-51 (1995).

166 Papirer E., Vidal A. and Balard H., Polym. Mat. Sci. Eng., **58**, 88, 727-29 (1988).

167 Papirer E., Balard H. and Sidiqi M., J. Coll. Inter. Sci., **159**, 238-242 (1993).

168 Balard H., Papirer E., Khalfi A. and Barthel H., Composite Interfaces, **6**, 1, 19-25 (1999).

169 Voelkel A.and Krysztafkiewicz A., Eurofillers 95 Conference Proceedings, 139-142 (1995).

170 Vergelati C., Eurofillers 95 Conference Proceedings, 151-155 (1995).

171 Jagiello J., Ligner G. and Papirer E., J. Inter. Coll. Sci., **137**, 1, 128-136 (1990).

172 Putyera K., Bandoza T.J., Jagiello J. and Schwartz J., Clay and Clay Minerals, **27**, 435-444 (1994).

173 Balard H., Wang W.D. and Papirer E., Abs. of ACS, **207**, 2, 468-469 (1994).

174 Balgacem M.N., Blayo A. and Gandini A., Eurofillers 95 Conference Proceedings, 147-150 (1995).

175 Garnier G. and Glasser W.G., Abs. of ACS, **207**, 2, 507-508 (1994).

176 Chtourou H. and Riedl B., Abs. of ACS, **207**, 2, 509-510 (1994).

177 Wesson S.P., Jen J.S. and Nishioka G.M., J. Adhes. Sci. Tech., **6**,1, 151-169 (1992).

178 Tiburcio A.C. and Manson J.A., J. Appl. Polym. Sci., **42**, 2, 427-438 (1991).

179 Jacob P.N. and Berg J.C., Langmuir, **10**, 3086-3993 (1994).

180 Donnet J.B., Park S.J. and Balard H., Chromatographia, **31**, 9/10, (1991).

181 Shen W., Sheng Y.J. and Parker I.H., J. Adhesion Sci. and Tech., **13**, 8, 887-901 (1999).

182 Schreiber H.P., Adv. Org. Coating Sci. Tech. Series., **11**, 192-204 (1989).

183 Schreiber H.P., Wertheimer M.R. and Lambla M., J. Appl. Polym. Sci., **27**, 2269-2280 (1982).

184 Ulkem I., Bataille P. and Schreiber H.P., JMS: Pure Appl. Chem., **31**, 3, 291-303 (1994).

185 Bosse F., Eisenberg A., Deng Z. and Schreiber H.P., J. Adhes. Sci. Tech., **7**, 11, 1139-1152 (1993).

186 Morales E., Herrero C.R. and Acosta J.L., Polymer Bulletin, **29**, 401-406 (1992).

187 Murakami Y., Poly. J., **26**, 5, 607-612 (1994).

188 Murakami Y., Enoki R., Ogoma Y. and Kondo Y., Polymer J. (Japan), **30**, 6, 520-5 (1998).

189 Tan E-H., Wolff S., Haddeman M., Grewatta H.P. and Wang M-J., Rubber Chem. and Tech., **66**, 594-604 (1993).

190 Papirer E., Balard H., Khalfi H. and Barthel H., IRC 98 Conf. Proc., Paris, 12-14 May, 105-6 (1998).

191 Vansco G.J., Tan Z. and Vansco-Szmeresanyi I., Abs. of ACS, **207**, 2, 409-410 (1994).

192 Felix J.M., Gatenholm P. and Schreiber H.P., Polymer Composites, **14**, 6, 449-457 (1993).

193 Matuana L.M., Woodhams R.T., Park C.B. and Balatinez J.J., Antec 98, III, Conf. Proc., 26-30 April, 3313-8 (1998).

194 Gauthier H., Coupas A.C., Villemagne P. and Gauthier R., J. Appl. Polym. Sci., 69, 11, 2195-203 (1998).

195 Allred R.E. and Schimpf W.C., J. Adhes. Sci. Tech., **8**, 4, 383-394 (1994).

196 Wesson S.P. and Tate M.L., Abs. of ACS, **207**, 2, 465-466 (1994).

197 Gutierrez M.C., Santa S., Rodriguez O., Rubio F., Rubio J. and Oteo J.L., Fourth European Conference on Composites, Testing and Standardisation, Conf. Proc., 31 August- 2 September, 627-951 (1998).

198 Farad M., El-Kindi M. and Schreiber H.P., Abs. of ACS, **207**, 2, 470-471 (1994).

199 Borsch J., J. Adhes. Sci. Tech., **5**, 7, 523-541 (1991).

200 Lundqvist A., Odberg L. and Berg J.C., TAPPI Journal, **78**, 5, 139-142 (1994).

201 Balard H. and Papirer E., Prog. Org. Coatings, **22**, 1-17 (1993).

202 Ziani A., Xu R., Schreiber H.P. and Kobayashi T., J. Coatings Tech., **71**, 893, 53-60 (1999).

203 Guthrie J.T. and Munavar M., Surface Coatings International, **80**, 9, 427-34 (1997).

204 Pogue R.T., Ye J., Klosterman D.A., Glass A.S. and Chartoff R.P., Composites Part A, Appl. Sci. and Manufacturing, 29A, 9-10, 1273-81 (1998).

205 Burness J.H. and Dillard J.G., Langmuir 1994, **10**, 1894-1897 (1994).

206 Balard H. and Papirer E., Prog. In Org. Coatings, **22**, 1-17 (1993).

207 Schmitt P., Koerper E., Schultz J., Papirer E., Chromatographia, **25**, 9, 786-790 (1988).

208 Turov V.V., Bolgillo V.I. and Leboda R., Conference Proceedings Eurofillers 95, 131-134 (1995).

209 Chen C-T. and Al-Saigh Z.Y., Macromolecules, **22**, 2974 (1989).

210 Wang J-Y. and Charlet G., Macromolecules, **22**, 3781 (1989).

211 Chappell P.J. and Williams D.R., J. Coll. Inter. Sci., **128**, 450-457 (1988).

212 Kontominas M.G., Gavara R. and Giacin J.R., Europ. Polym. J. **30**, 2, 265-269 (1994).

213 Sohnel O. and Garside J., Precipitation. Basic Principles and Industrial Applications. Butterworth, Heinemann (1989).

214 Brunauer S., The Adsorption of Gases and Vapours: 1, Oxford University Press (1945).

215 Taylor D.A., and Paynter C.D., Conf. Proc. Eurofillers '95, Mulhouse, France, 361 (1995).

216 Private communication C.D. Paynter to D.M. Ansari.

217 ISO 180 (1982) Plastics – Determination of Izod Impact Strength of Rigid Materials.

218 ISO 178 (1990) Plastics – Determination of Flexural Properties.

219 ICI technical datasheet (1995).

220 Keller D.S. and Luner P., Colloids and Surfaces A, **161**, 401-415 (2000).

221 Ahsan T., Colenutt B.A., and Sing K.S.W., J. Chromatography, **464**, 416 - 421, (1989).

222 Roe R.J., J. Phys. Chem., **72**, 2013 (1968).

223 Gammage R.B., Holmes H.F., Fuller E.L. and Glasson D.R., J. Coll. Inter. Sci., **47**, 350 (1974).

224 Hancock M., ECCI Internal Communication (1972).

225 Packham D.E., Handbook of Adhesion, 458- 461, Longman Scientific and Technical, (1992).

226 Papirer E., Schultz J. and Turchi C., Eur. Polym. J., **20**, 1155 (1984).

227 Adamson A.W., Physical Chemistry of Surfaces, John Wiley and Sons, New York (1990).

228 Nielsen L.E., J. Appl. Phys., **41**, 4726 (1970).

229 Chow T.S., J. Mat. Sci., **15**, 1873 (1980).

230 McGenity P., Paynter C.D., Adams J.M. and Riley A.H., Plastics Rubber Process Appl. **14**: 85 (1990).

231 Pukanszky B., Makromol. Chem. Macromol. Symp,. **70/71**, 213 – 223 (1993).

232 Ciganek M. and Dressler M., Polymer Composites, **10**, 3, 194 - 198 (1989).

233 Saada A., Papirer E., Balard H. and Siffert B., Conf. Proc., 143 – 146, Eurofillers 95, Mulhouse, France, Sept. 11-14 (1995).

234 Grim R.E. and Bradley W.F., J. Am. Ceram. Soc., **23**, 8, 242-248 (1940).

235 Brindley G.W. and Moroney D.M., J. Amer. Ceram. Soc., **43**, 511 (1960).

236 Adams J.A., ECCI Internal Communication (1989).

237 Brindley G.W. and Yamananaka S., Amer. Miner., **64**, 830-835 (1979).

238 Hancock M., Plasticulture, **79**, 3, 4-14 (1998).

239 Achimsky L., Audouin L. and Verdu J., Polym. Degradation and Stability, **57**, 231 – 240 (1997).

240 Tooley P.A. and Khan Le Q., SPE Antec Conference Proceedings, **3**, 235 – 240 (1986).

241 Borealis technical datasheet.

242 Kaelble D.H., Physical Chemistry of Adhesion, Wiley Interscience, New York, 152 (1971).

243 ASTM D4329-92, Standard Practice for Operating Light and Water Apparatus (Fluorescent UV and Condensation Type) for Exposure of Plastics, Cycle A (1992).

244 Davis A. and Sims D. Weathering of Polymers, Elsevier, London, (1986).

245 Al-Madfa H., Mohamed Z. and Kassem M.E., Polym. Degradation and Stability, **62**, 105 – 109 (1998).

246 ASTM D882-91, Standard Test Methods for Tensile Properties of Thin Plastic Sheeting (1991).

247 Halliwell S.M., RAPRA Review Report 53, Weathering of Polymers, 8-11 (1992).

248 Dilara P.A. and Briassoulis D., Polym. Test. 17, 549-585 (1998).

249 Hancock M., Marsh J.E. and Lee R.L., Mineral Catalysed Photodegradable Film, Filplas '92, Manchester (1992).

250 Allen N.S., Edge M., Corrales T., Childs A., Liaw C.M., Catalina F., Peinado C., Minihan A. and Aldcroft D., Polym. Degradation and Stability, **61**, 183 –199 (1998).

251 Titov W.V. and Lanham B.J., Reinforced Thermoplastics, Applied Science Publishers, London (1975).

252 Mack H., Tailoring Filler Surface with Silanes, Technical Publication, Degussa-Hüls AG, Germany (1999).

253 Plueddemann E.P., Silane Coupling Agents, 127, Plenum Press, New York (1982).

254 BASF technical datasheet for Durethan-grade polyamides.

255 Balard H., Papirer E., Khalfi A. and Barthel H., Eurofillers 97, Conf. Proc., 81-84, Sep. 8-11 (1997).

256 Kaelble D.H., Physical Chemistry of Adhesion, Wiley Interscience, **5**, (1970).

257 Tsutsumi K. and Ohsuga T., Coll. Polym. Sci., **268**, 38 (1990).

258 Private communication D.A. Greenhill to D.M. Ansari.

259 Plueddemann E.P. and Stark G.L., SPI 28th Ann. Tech. Conf. Reinf. Plast., **21-E** (1973).

260 Plueddemann E.P. and Stark G.L., Mod. Plast., **54**, 102 (1997).

261 Gahde J., Plast. u Kauttschuk, **22** (8), 626 (1975).

262 Bascom W.D., Macromolecules, **5**, 792 (1972).

263 Shih P.T.K. and Koening J.L., Mater. Sci. Eng., **20**, 145 (1975).

264 Anderson H.R., Fowkes F.M. and Hielscher F.H., J. Polym. Sci. Phys., **14**, 879 (1976).

265 Naviroj S., Koening J.L. and Ishida H., Prog. in Sci. Eng. Comp., 227 – 234 (1982).

266 Plueddemann E.P. and Stark G.C., SPI 35th Ann. Tech. Conf. Reinf. Plast., **20B**, 264 (1980).

267 Rosen T.P., J. Coatings Tech., **50**, 70 (1978).

268 Jenneskens L.W., Venema A., Van Veenndaal N. and Huysmans W.G.B., J. Polym. Sci., A, **30**, 133-136(1992).